DELIVERABLE REPORT

Deliverable:	D3.3 Report on characterization of aged MNMs
Work Package:	WP3: Lifecycle evolution of MNMs
Lead Beneficiary:	Commissariat à l'Energie Atomique et aux Energies Alternatives (CEA)
Nature of Deliverable:	Report
Dissemination Level:	Public (PU)
Delivery Date:	
Submitted By:	Sylvie Motellier, Sophie Briffa, Brice Fiorentino, Jean-Gabriel Mattei, Denise Mitrano, Bernd Nowack, Olena Oriekhova, Nathalie Pelissier, Isabella Romer, Olivier Sicardy, Serge Stoll, Eva Valsami-Jones
Revised By:	U. Schöbinger (eurofins), K. Dawson (UCD)
Approved By:	

Project full title: " Engineered nanomaterial mechanisms of interactions with living systems and the environment: a universal framework for safe nanotechnology"

Grant agreement no: NMP4-LA-2013-310451

Table of contents

Glossary

AF4: asymmetric flow field flow fractionation

BET: specific surface area according to the Brunauer–Emmett–Teller (BET) theory

CCC: critical coagulation concentration

Dh: hydrodynamic diameter (Z-average)

DLS: dynamic light scattering

EDX: energy dispersive X-ray analysis

EELS: electron energy loss spectroscopy

HRTEM: high-resolution transmission electron microscopy

ICP-MS: inductively coupled plasma-mass spectrometry

IEP: isoelectric point

MALLS: multi angle laser light scattering

MNM: manufactured nano material

NP: nanoparticle

NTA: nanoparticle tracking analysis

PDI: polydispersity index

PZC: point of zero charge

SEM: scanning electron microscopy

spICP-MS: single particle-inductively coupled plasma-mass spectrometry

STEM: scanning transmission electron microscopy

TEM: transmission electron microscopy

US: ultra-sound/ultra-sonication

UV/Vis: ultra-violet / visible

XANES: X-ray absorption near edge structure

XRD: X-ray diffraction

ZP: zeta potential

Goals of the NanoMILE report on characterization of aged MNMs

The NanoMILE project aims to establish a fundamental understanding of the mechanisms of manufactured nanomaterial (MNM) interactions with living systems and the environment, across the entire life cycle of MNMs and in a wide range of target species. To establish an understanding of changes in the nature of MNMs as they undergo transformations within products and biological or environmental compartments across their life cycle and critically to feed this information into subsequent research to ensure that these "aged" and transformed MNMs are tested for their biological/environmental role. WP3 of NanoMILE has investigated and quantified the alteration and transformation of MNMs in products and during their use and release into the environment or biota. Exposure to MNMs in occupational, consumer or environmental settings may either be to the original, parent MNMs or to MNMs that has been incorporated into products and subsequently released, either in their original form or in an altered form due to industrial or natural processes. To date, few studies have tried to establish the changes that MNMs undergo when incorporated into, and released from, products. As a result there is major uncertainty as to the state of many MNMs following their release.

WP3 has exposed relevant MNMs selected from the libraries of WP2 to different processes, different bio-physico-chemical conditions, in order to characterize the changes in the MNM, and either delivered altered MNMs or provided detailed protocols on how to induce these alterations, to alternative WPs.

The deliverable report D3.2 "*Alteration of MNMs"* submitted in month 24 described the experimental methods concerning air and water exposures that have been developed for a selection of ENMs from the NanoMILE library as well as the aging methods used to provide aged materials to the other project partners as specified in Milestone 6. In this D3.3 report, we will focus on the results from task 3.3. "*Characterization of altered MNMs*". In this task, the selected ENMs provided by WP2 and exposed to different aging processes identified in task 3.1 have been characterized using various complementary techniques including microscopy techniques (TEM / SEM), XRD, dynamic light scattering, zeta potential, BET, and FFF-ICPMS / SP-ICPMS.

Summary

In its first part (Part A), this deliverable reports on the characterization of MNMs selected from the NanoMILE particle library, and that have been aged by WP3 partners to study the aging process in end-of-life-cycle-relevant conditions. These are on the one side the aging in air under UV/Vis-light and the aging in aqueous suspensions. It was shown that TiO_2 and CeO_2 are highly resistant to UV/Vis aging in air, even under prolonged exposure (1000h). Ag NPs, on the contrary, displayed severe alteration when exposed to sunshine-enhanced irradiation in suspension: newly-formed nanoprisms of triangular shape could be observed, depending on the size and capping agent of the pristine particles.

Ag MNMs were also aged with washing liquids and the detergent chemistry, dominated by oxidizing agents and secondarily by the physical presence/absence of non-dissolvable solids, was a major factor in particle dissolution, surface chemistry change(s) and new particle precipitation/formation. However, in the case of nano-enhanced fabrics, degradation of Ag NPs is negligible compared to those suspended in these same detergents, which is most likely due to the protection offered by the incorporation into the fabrics themselves. Besides, based on leaching tests, the release of NPs from landfills into the environment due to disposal of nano-enabled textiles is likely small.

CeO_2 showed severe alteration of morphology when in contact with phosphate solution: structures resembling sea urchins or needles were observed. The transformation rate depends on the pH, with an optimum at pH = 5. Zr substitution in ceria NPs decreased the extent of alteration of the particles as a result of ZrO_2 resistance to transformation. Increased temperature led to partial dissolution of CeO_2 NPs but the PVP type of capping (chain length) plays a role in the changes in size at different temperatures. The role of NOM (fulvic acids, FAs) on the stability of CeO_2 MNMs was also investigated. It was shown that once formed, FAs-CeO_2 complexes are very stable and resist dilution and pH changes as a result of strong electrostatic interactions. NOM-coated CeO_2 MNMs will also better resist to aggregation when ionic strength is increasing (passing for example from fresh to estuarine or marine waters).

The second part (Part B) describes physico-chemical properties of the aged MNMs that have been delivered to the NanoMILE partners that requested them for toxicology studies. Sulfidation of Ag NPs and phosphatization of CeO_2 NPs led to highly altered particles. “Sea urchin”/needle-like structural transformations could be observed with CeO_2 NPs as they chemically evolve to $CePO_3$.

On the contrary, TiO_2 and ZnO MNMs did not show evidence of alteration under prolonged UV aging in air.

Overview of the aging processes

Two main aging protocols have been assayed in task 3.2 that are relevant of the life-cycle processes undergone by the different MNM types. The first one is aqueous aging and concerns mainly CeO_2 and Ag NPs. Water and washing liquids have been assayed for Ag NPs while phosphate and natural organic matter (NOM) were tested for CeO_2. The NPs provided to the partners of WP 4-8 were aged either by sulfidation (Ag NPs) or by phosphatization (CeO_2). The second protocol is air exposure with the use of accelerated weathering testers and concerns only TiO_2 and ZnO NPs in powdered form.

This report contains two parts. Part A is dedicated to the characterization of the MNMs selected from the NanoMILE library by WP3 partners and aged according to the protocols described above. Part B refers to the characterization of the MNMs listed in Milestone 6 that have been aged and provided to the NanoMILE partners upon request for further toxicological tests. The table below summarizes the MNMs that were used and their associated aging protocols.

Summary of the aging experiments achieved in WP3

Part A

MNM	Reference (supplier)	Aging reaction	MNM form for aging	Work done by
CeO_2	CeO_2 NM 212 (JRC)	Aqueous with NOM	Suspension	UoGe
	CeO_2 NM 211 (JRC)	Aqueous with phosphate	Suspension	UoB
	CeO_2 NM 212 (JRC)	Aqueous with phosphate		
	$Ce_xZr_{(1-x)}O_2$ (PROM)	Aqueous with phosphate	Suspension	
	ZrO_2 (PROM)	Aqueous with phosphate		
	CeO_2 PVP10 (UoB)	Aqueous with phosphate/T°		
	CeO_2 PVP40 (UoB)	T°		
	CeO_2 PVP360 (UoB)	T°		
	CeO2 NM 211 (JRC)	UV/T°	Suspension	CEA
	CeO2 NM 212 (JRC)			
TiO_2	TiO_2 UN (PROM)	UV/T°	Suspension and powder	CEA
	TiO_2 AA4040 (PROM)			
	TiO_2 F127 (PROM)			
	TiO_2 PVP (PROM)			
Ag	Ag NPs 60 nm (Aldrich)	Aqueous in washing liquids	Suspension	EMPA
	Ag NPs 100 nm (Aldrich)		Embedded in fabrics	
	Ag NPs Citrate (UoB)			
	Ag NPs PEG (UoB)			
	Ag NPs 20 nm (Aldrich)	UV/T°	Suspension	CEA
	Ag NPs 60nm (Aldrich)			
	Ag NPs 100nm (Aldrich)			
	Ag NPs Citrate (UoB)			
	Ag NPs PEG (UoB)			

Part B

MNM	Reference (supplier)	Aging reaction	MNM form for aging	Work done by
CeO_2	CeO_2 undoped (PROM)	Aqueous with phosphate/T°	Suspension	UoB
TiO_2	TiO_2 PVP (PROM)	UV/T°	Powder	CEA
ZnO	ZnO NM 110 (JRC)	UV/T°	Powder	CEA
	ZnO NM 111 (JRC) TECS			
Ag	Ag NM300K (JRC)	Aqueous with Na_2S	Suspension	EMPA

Part A: Characterization of the MNMs from the NanoMILE library

A.1 TiO_2 - Aging with UV/Temperature (CEA)

A.1.1 Summary of the aging experiments

Stock suspensions (1 g L^{-1} Ti) of the TiO_2 NPs with different coatings (from Promethean Particles Ltd., see D3.2) were prepared. For the one week (168h-170h) aging experiments in the QSUN test chamber, they were either diluted to 0.5 g L^{-1} Ti or dried in a thermal chamber to yield liquid or powder samples, respectively. These were "soft aging conditions" with an irradiance of 1.44 W m^{-2} at 420 nm, $T_{black\ panel}$ = 70 °C, T_{air} = 40 °C, and a relative humidity of 50%. Longer aging experiments of 42 days (1000h) proceeded directly with the commercial stock suspensions (ca. 1.7% w/w) in the QUV test chamber. These denoted "severe aging conditions" were characterized by an irradiance of 0.68 W m^{-2} at 310 nm and $T_{black\ panel}$ = 70 °C.

A.1.2 Characterization methods

Size and zeta potential

Size (Dh) and zeta potential (ZP) were acquired as a function of pH using DLS with a Zetasizer NanoZSP (Malvern) equipped with an automatic titrator (MPT2 with pH electrode MV114-SC, Malvern). Size measurements were done at an angle of 173° (backscatter) while zeta potential measurements were done at 13° with reference to the 633nm-laser beam. The temperature was set at 25 °C. Size measurement accuracy was checked by the analysis of calibrated 60 nm-polystyrene latex beads (Magsphere) while zeta potential accuracy was ensured by regular analysis of a ZP transfer standard of -42 mV (Malvern). A three-point pH calibration was carried out prior to each titration experiment and the suspensions were homogenized throughout titration by magnetic stirring. The titrating solutions were either 0.1 M HNO_3 or 0.01 M N_2-degassed NaOH.

For titrations, a minimum sample volume of 10 mL was required. Pristine or aged stock suspensions were treated for 5 min in an ultrasonic cleaner (Branson) prior to dilution to the target sample concentration in UP water or in sodium nitrate.

TEM

The NPs were observed with a TEM/STEM apparatus (Tecnai Osiris, FEI) equipped with a HAADF (High Angle Annular Dark Field) detector and an EDX (Energy Dispersive Spectroscopy) microanalysis system (Esprit, Bruker Nano GmbH) connected to four quadrant SDD detectors (ChemiStem technology, FEI). The acceleration voltage was 200 kV and line resolution was 1.02 Å (point to point resolution of 2.5 Å).

The samples were deposited on a grid (copper w or w/o C film) as 3µL droplets. The droplets were left for a few minutes in order for the particles to settle, and the liquid was drawn off by using absorbing paper. The grid was then immediately transferred to a vacuum chamber to avoid any subsequent alteration in air.

XRD

The primary crystallite size was estimated using a 2-circles Advance diffractometer (Bruker) equipped with a Cu-Kα source and a LynxEye linear detector. Diffraction patterns were acquired in θ-2θ mode. The liquid samples were deposited on glass microscope slides and dried prior to their analysis.

A.1.3 Results

Remark: In the results given below, all concentrations refer to the metal content of the considered suspension (i.e. Ti for TiO_2 NPs).

Size and ZP by DLS

a) Preliminary experiments

Ionic strength, scan direction for titration, and NP concentration were investigated in preliminary experiments.

Figure A.1-1 shows an example of the titration curves of Dh and ZP of TiO_2 UNi in UP water.

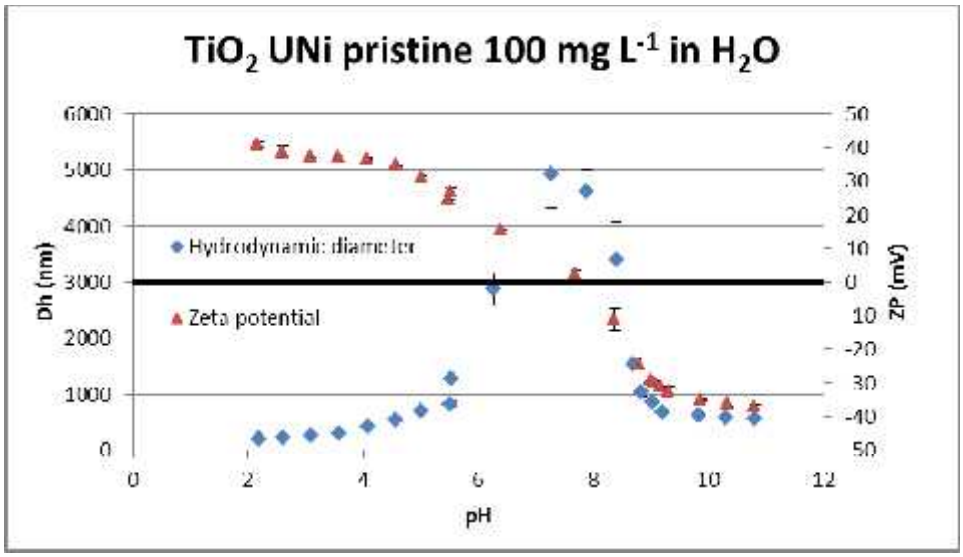

Figure A.1-1: Titration curves of Dh and ZP as a function of pH. Experimental conditions: [TiO_2 NPs] = 100 mg L^{-1} (metal basis) in UP H_2O.

It is observed that the PZC corresponds to the maximum of Dh, i.e., to the pH at which agglomeration is at its maximum because of minimum inter-particle electrostatic repulsion. Below and above this pH, de-agglomeration occurs and the size of the clusters decreases.

Dh and PZC are known to depend on the ionic strength of the medium (Parks and de Bruyn, 1962, Blok and de Bruyn, 1970). So, in order to investigate the extent of influence of this parameter here, similar experiments were also conducted in $NaNO_3$ 1 mM and 10 mM (Table A.1-1).

Table A.1-1: Evolution of Dh and PZC with the ionic strength of the medium

[$NaNO_3$] (mM)	Dh max (nm)	PZC
0	5000	7.70
1	1700	6.78
10	**8000**	**6.53**

A decrease of ca. one pH unit of the PZC is observed when the ionic strength is increased to 1 mM, and another slight decrease occurs when the concentration of $NaNO_3$ is raised from 1 mM to 10 mM. This shift may be ascribed to the specific adsorption of the anionic species NO_3^- onto the surface of the NPs and/or to the existence of permanent surface charges (Zhang and Zhao, 1997). The Dh decreases first and re-increases with ionic strength because of the compression of the double layer.

The scan direction for titration was also investigated. For this purpose, the pH was first increased to alkaline values (pH_{max} = 9) and then decreased to acidic pHs (pH_{min} = 4). The whole process was done in $NaNO_3$ 1mM, which keeps a constant ionic strength over the investigated pH range. Figure A.1-2 gives an example of the curves obtained with this procedure.

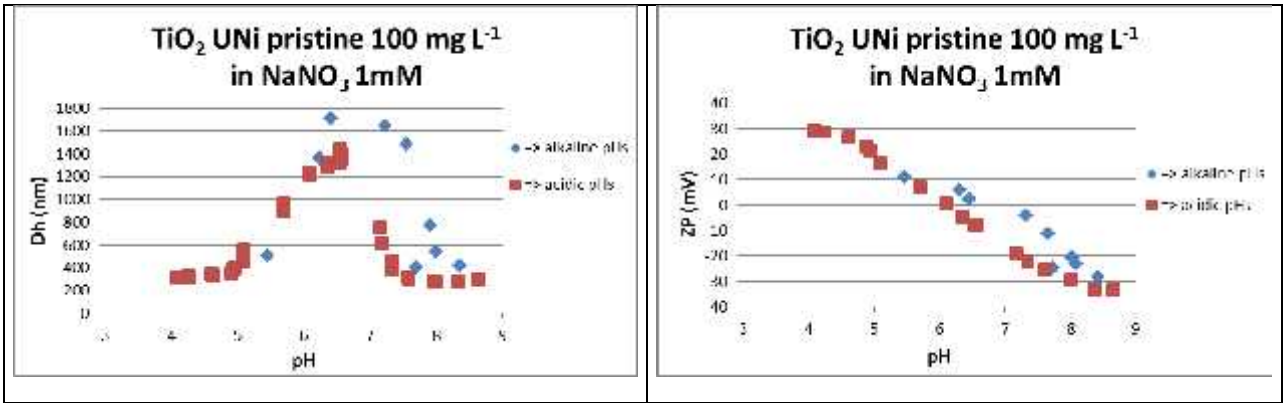

a b

Figure A.1-2: Influence of the scan direction on the pH titration profile of Dh and ZP. Experimental conditions: [TiO_2 NPs] = 100 mg L^{-1} (metal basis) in $NaNO_3$ 1 mM.

A shift can be observed both for Dh and ZP: the scan towards alkaline pHs returns significantly higher PZC that coincide with a shift of maximum Dh. Such behavior has already been observed in soils and minerals and was ascribed to the higher ionic strength in the second pass or to dissolution/precipitation phenomena (Appel, 2003). The first bias was minimized here, though, and dissolution is not likely to occur in the pH range investigated. The choice was made to perform all the titrations by one single scan from pH = 9 to pH = 4.

The last parameter investigated in this series of preliminary experiments is NP concentration. Figure A.1-3 gives an example of the behavior of a TiO_2 suspension during pH titration at different NP concentrations.

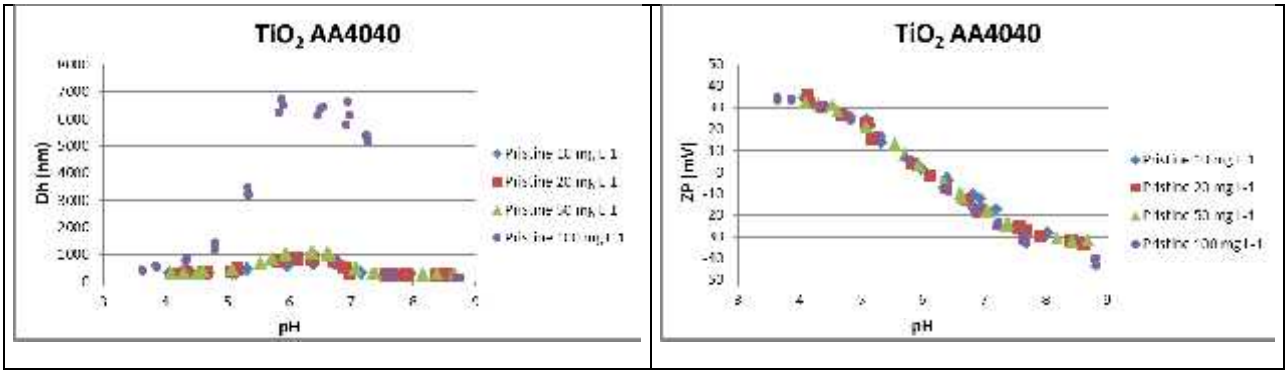

a b

Figure A.1-3: Influence of the NP concentration in suspension on the pH titration profile of Dh and ZP. Experimental conditions: suspensions in $NaNO_3$ 1 mM, pH scan from 8 to 4.

Good dispersion is observed up to a concentration of 50 mg L^{-1}. Above this concentration, clusters formed in the vicinity of the PZC are very large, even though de-agglomeration occurs on either side as with lower concentrations. Contrary to Dh, the effect of NP concentration on ZP is negligible. Finally, the NP concentration of the suspension was adjusted to a value of 20 mg L^{-1} which ensures a satisfactory dispersion and allows for tolerance on the concentration of NP.

b) Characterization of pristine and aged NPs using DLS

It can be observed in Figure A.1-4 that only severe conditions of aging may alter the titration profile of both the size and the zeta potential of the TiO_2 NPs. Concerning PZC, initially equal to ca.6.0, a small shift towards acidic pHs occurs only for aging protocols of the powder form with UV irradiation for 1000h, and is concomitant with a de-agglomeration process of lesser magnitude. In any other "softer" aging protocols, no significant alteration of the titration data can be seen.

The same conclusion can be drawn with all types of TiO_2 NPs, whatever their coating (examples of titration curves of TiO_2 F127 in Figure A.1-4). It confirms that, in all instances, a decrease in PZC is observed when the particles are aged in the powder form for 1000h in the QUV (average δ(PZC) = -0.3 pH unit) simultaneously to an increase in the minimum size (away from the PZC, in the favorable pH range for dispersion).

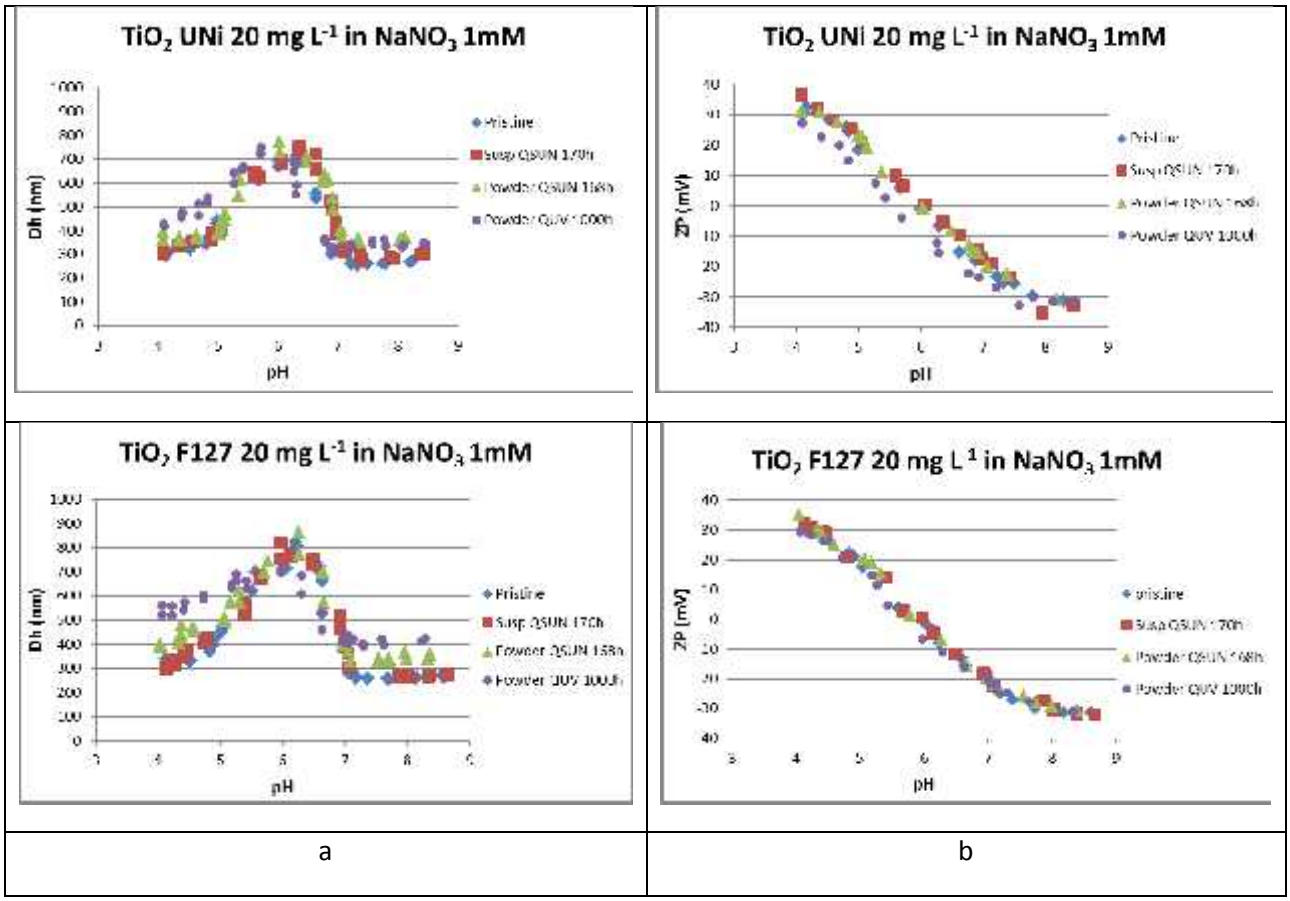

Figure A.1-4: Evolution of Dh (a) and ZP (b) as a function of pH for TiO_2 NPs after different aging protocols: examples of uncoated TiO_2 UNi and Pluronic F-127-coated TiO_2 F127. Experimental conditions: [TiO_2 NPs] = 20 mg L^{-1} (metal basis) in $NaNO_3$ 1 mM, pH scan from 9 to 4.

This may appear somewhat surprising as a more significant effect on the polymer-coated NPs was expected from UV / sunlight exposure due to the likely degradation of the capping agents. However, the PZCs of the three coated TiO_2 NPs and that of the uncoated ones are quite identical, with values between 5.9 and 6.0 (Figure A.1-5).

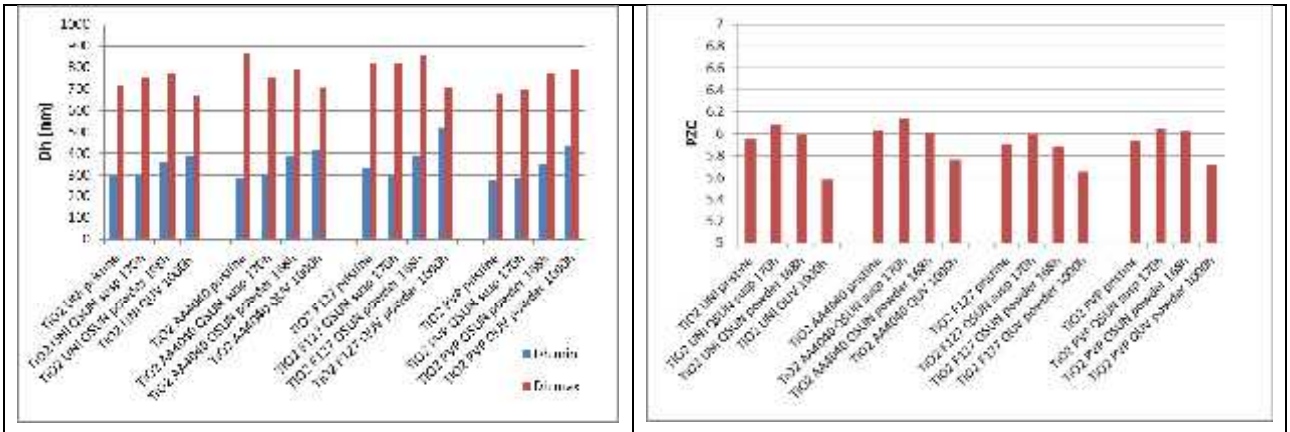

a b

Figure A.1-5: Influence of the aging protocol on the size of the agglomerates (Dh min: minimum size for optimum dispersion conditions, and Dh max: maximum size for optimum agglomeration conditions) (a) and on the value of PZC (b) for the different TiO_2 NPs. Experimental conditions: see Figure A.1-4.

This result suggests that the coating has no influence on the surface charge of the particles, which is obviously the case for neutral polymers such as PVP or pluronic F127 but is rather unexpected for Dispex AA4040, the ammonium salt of a low molecular weight polyacrylic acid (pKa = 4.5).

TEM

A first approach of the TiO2 NPs observation by TEM (Figure A.1-6) shows that the primary particles are small (less than 10 nm) but they are agglomerated/aggregated in large clusters of several hundreds of nanometers up to a few micrometers. There is no visible single particle.

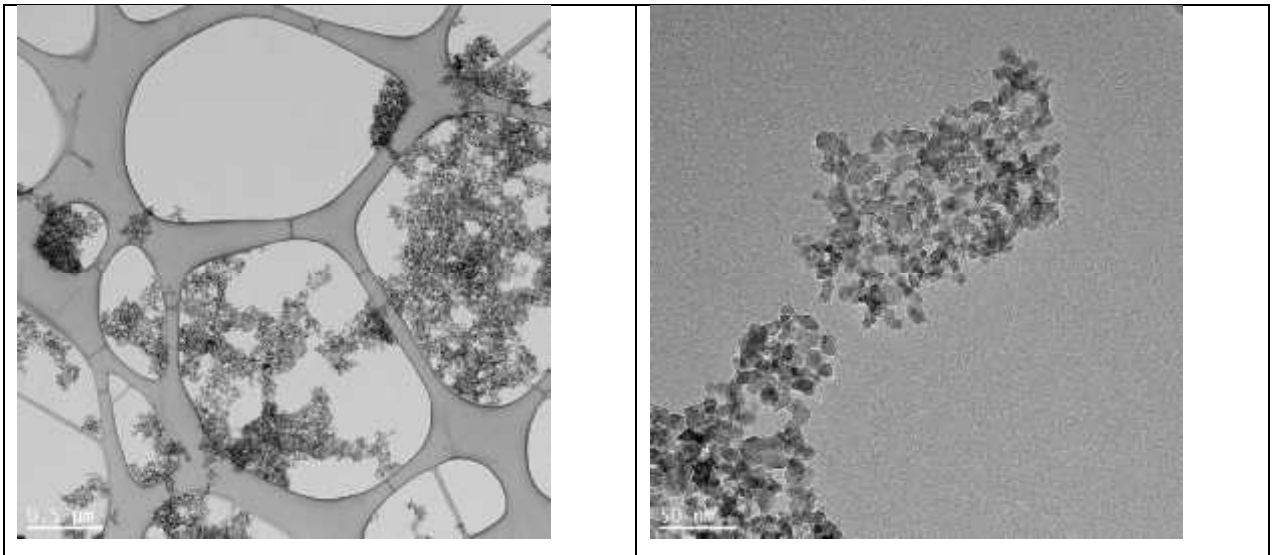

Figure A.1-6: TEM images of the pristine uncoated TiO_2 UNi NPs: overview at low magnification.

TEM observations confirmed the durability of TiO_2 NPs under UV/thermal treatment, whatever their initial capping. Figure A.1-7 gives two examples of TEM investigations of pristine and aged particles under “severe aging conditions” for comparison.

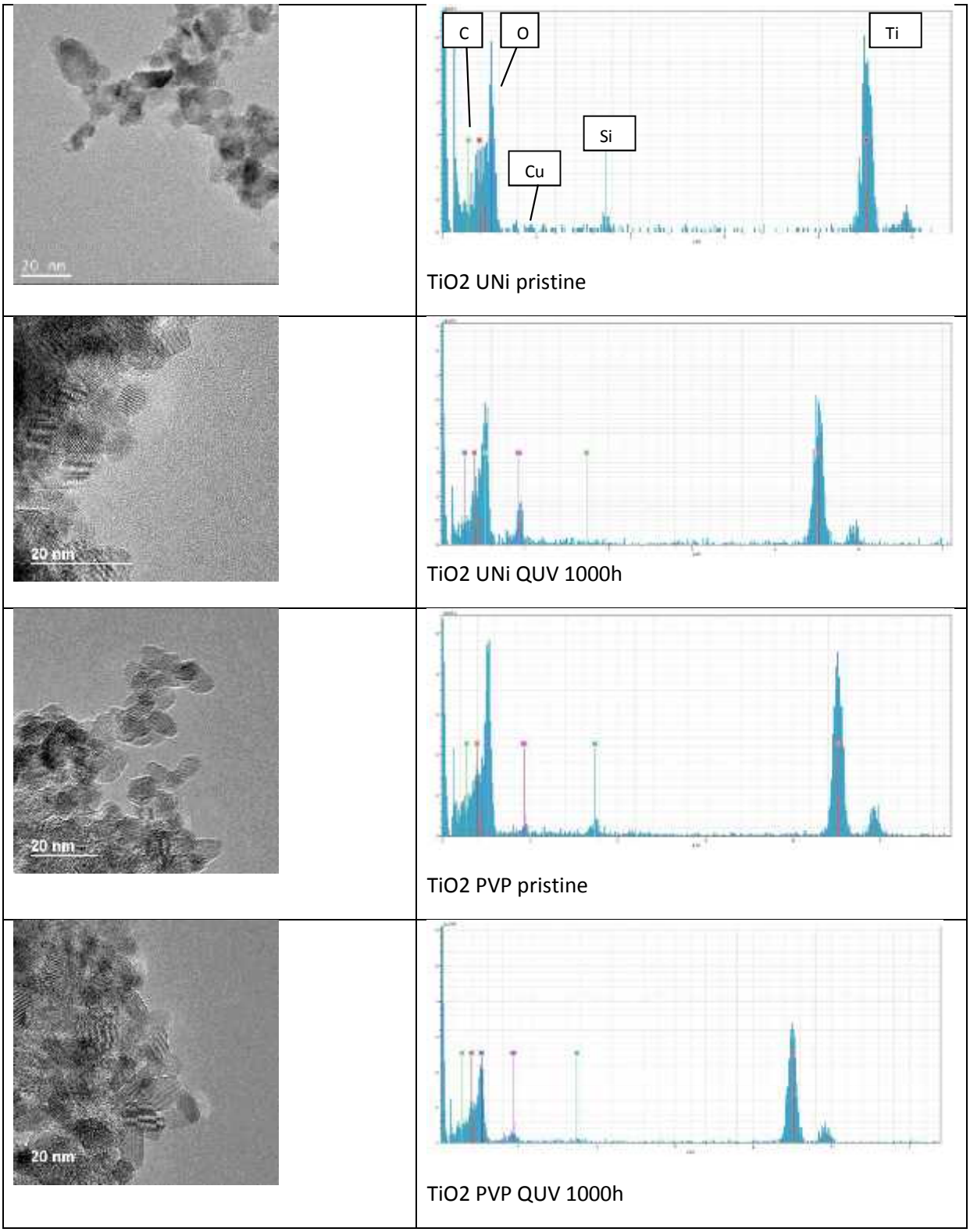

Figure A.1-7: TEM images and EDX spectra of pristine and 1000h QUV-aged TiO2 NPs. Examples of uncoated TiO_2 UNi and polyvinylpyrrolidone-coated TiO_2 PVP.

No visible alteration of the morphology of the grains neither significant modification of the EDX spectrum is observed. Due to the very small size of the particles, characterization of the polymeric coating is quite difficult. It was not investigated in the scope of this experiment.

XRD

Figure A.1-8 shows the XRD scans of the pristine NPs and those of the same particles aged 168h in the QSUN in the powder form. They are representative of the anatase form of TiO_2, whether pristine or aged. The characteristic lines are significantly broader than expected for bulk TiO_2 and reflects the "nano" form of the particles. The crystallite sizes derived from the line widths are summarized in Table A.1-2. They all lie between 7.2 and 7.6 nm, with no specific trend as to the aging process.

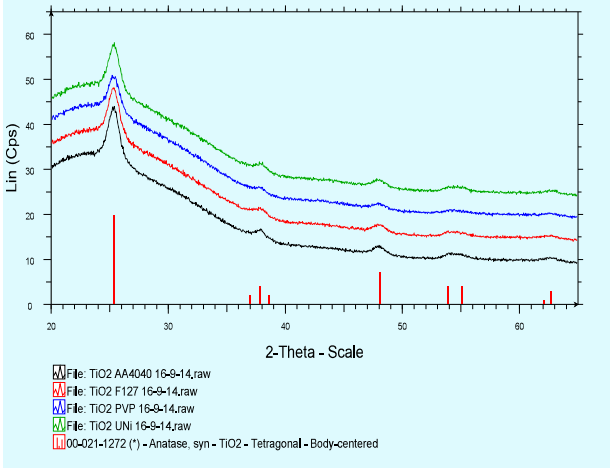

a

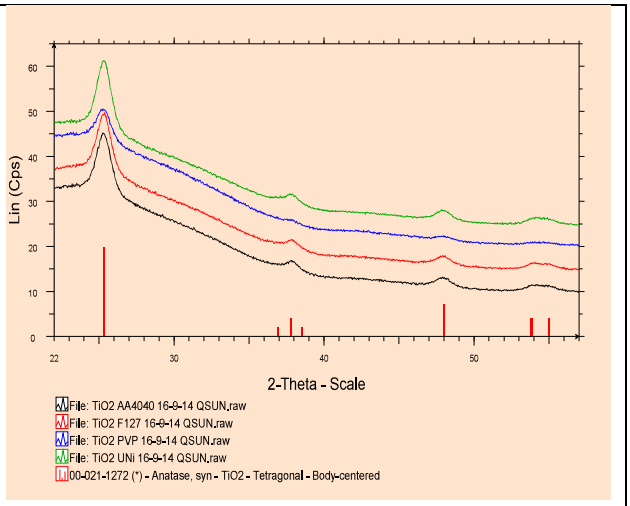

b

Figure A.1-8: XRD diffraction patterns of TiO_2 NPs either pristine (a) or aged one week as powder in the QSUN (b).

Table A.1-2: Crystallite size of the TiO_2 NPs

TiO_2 NP	**Crystallite size (nm)**
TiO_2 UNi	7.2
TiO_2 UNi QSUN powder 168h	7.2
TiO_2 PVP	7.3
TiO_2 PVP QSUN powder 168h	7.6
TiO_2 F127	7.3
TiO_2 F127 QSUN powder 168h	7.2
TiO_2 AA4040	7.3
TiO_2 AA4040 QSUN powder 168h	7.2

A.2 CeO_2

A.2.1 Aging of CeO_2 with NOM (UoGe)

A.2.1.1 Summary of the aging experiments

Environmental physicochemical processes controlling the fate and behavior of MNMs such as dissolution, aggregation, surface coating have been widely investigated in the literature and the importance of natural organic matter was often highlighted (Loosli et al., 2015; Mohd Omar et al., 2014; Oriekhova and Stoll, 2016). To get an insight into NOM impact on CeO_2 MNMs in a first time the characterization of pristine CeO_2 particles (NM212) in changing pH conditions was done using DLS, NTA, SEM, and acid-base titration methods. In the second time, interaction between CeO_2 MNMs and natural organic matter (NOM) was investigated. We considered fulvic acids (FAs) as NOM surrogate (Suwannee River Fulvic acid Standard II, 2S101F, International Humic Substance Society, USA). FAs concentration, pH variation and stability of FAs-CeO_2 complexes with time were considered as key parameters that influence MNMs behavior and aging in aquatic systems. Experimental protocols, suspension preparation and aging procedures have been presented in the deliverable report D3.2. In this part, we focus on the characterization of CeO_2 and FAs-CeO_2 complexes in altered and changing conditions. We concentrated on three parameters such as pH variation, dilution effect and variation of ionic strength on the stability of uncoated and coated particles as well as NOM coating stability (Figure A.2.1-1). To assess the influence of ionic strength we chose NaCl and $CaCl_2$ as electrolytes and performed aggregation kinetics experiments that are described below. The dilution effect was investigated on already formed FAs-CeO_2 MNMs by changing the concentration of components but with constant ratio between them. The influence of pH changing effect was also investigated on CeO_2 and FAs-CeO_2 complexes.

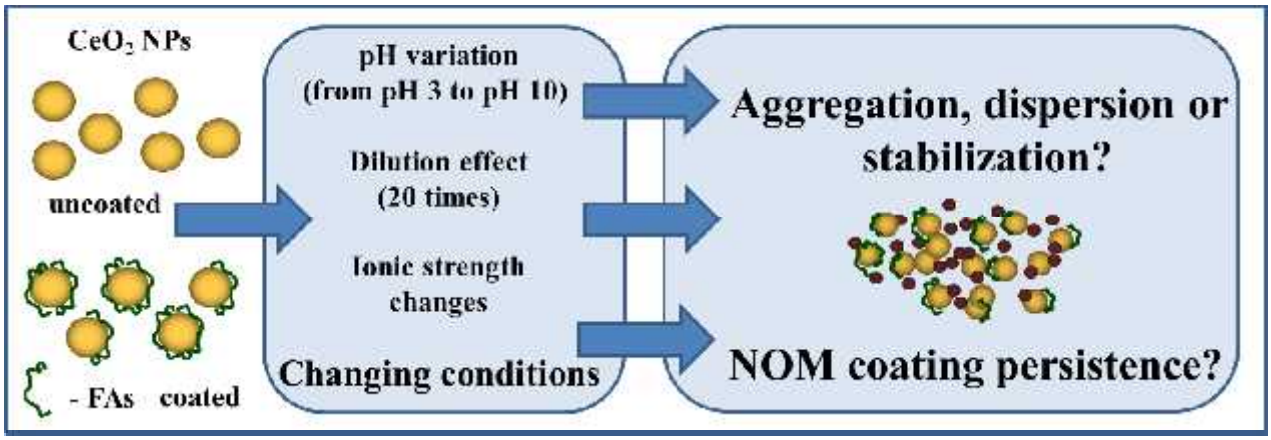

Figure A.2.1-1: Schematic representation of the key parameters that influence the CeO_2 MNMs behavior in natural water conditions.

A.2.1.2 Characterization methods

pH changing effect

To characterize the uncoated CeO_2 MNMs, 100 mL of the 50 mg L^{-1} suspension were prepared at pH 3.0 ± 0.1 with 0.001 M NaCl as a background electrolyte. The pH was increased from pH 3.0 to 10.0 using 0.01 M NaOH. Dh and ZP were systematically measured 15 min after pH adjustment. The control of pH was done during all experiments with a HACH LANGE HQ40d portable meter and a pH probe PHC101 (Hach Lange, Switzerland). Suspension homogenization was achieved in all experiments by using a magnet vortex with rotational speed equal to 200 rpm. The same procedure was used for coated CeO_2 MNMs. 50 mg L^{-1} CeO_2 MNMs suspensions

with 2 mg L^{-1} FAs were prepared at pH 3.0 so as to obtain NOM-coated MNMs. DLS measurements were performed after each increase of pH.

Dilution impact

The suspension stability versus decrease of compounds concentration was investigated at two different pH values corresponding to pH 3.0 ± 0.1 and pH 8.0 ± 0.1. First, a suspension with concentrations of 100 mg L^{-1} CeO_2 MNMs and 4 mg L^{-1} FAs was prepared. The solution was then diluted by factors of 2, 4, 10, and 20. The corresponding concentrations are provided in Table A.2.1-1.

Table A.2.1-1: Component concentration in dilution experiments

Component	**Component concentration, mg L^{-1}**				
Dilution factor	1:1	1:2	1:4	1:10	1:20
CeO_2	100	50	25	10	5
FAs	4	2	1	0.4	0.2

Aggregation kinetics experiments

The influence of increasing ionic strength (using a monovalent electrolyte NaCl and divalent electrolyte $CaCl_2$) on the stability of uncoated and coated MNMs was evaluated using aggregation kinetics experiments. The experiments were conducted at pH 3.0 and 8.0. We gradually increased the concentration of NaCl added to the suspension containing uncoated and coated CeO_2. The corresponding values of concentrations used were in the range from 0.05 to 0.75 M for NaCl and from 0.25 to 50 mM for $CaCl_2$. The concentration of CeO_2 MNMs and FAs was the same for all samples and corresponded to 50 mg L^{-1} and 2 mg L^{-1}, accordingly. It should be noted that the order of components that were added to the solution was important to successfully disperse the MNMs and avoid aggregation. First, the relevant volume of FAs was added into a tube and then was diluted with ultrapure water. Next, we adjusted the pH and added the appropriate concentration of CeO_2 MNMs. The last step was the addition of the relevant concentrations of electrolyte. Measurement of z-average hydrodynamic diameter (Dh) was done directly after mixing all components.
The MNMs aggregation rate was investigated by dynamic light scattering methods (DLS) using a Malvern Zetasizer Nano ZS (Malvern Instruments Ltd, UK). The Dh diameters were recorded during 60 min with 30 sec time interval, starting immediately after adjustment of ionic strength. The experimental data were fitted with linear function to obtain the slope of Dh versus time. This value represents the aggregation rate constant (k). To obtain the attachment efficiency we normalized aggregation rate constant for different electrolyte concentrations to the rate constant in the fast aggregation regime (k_{fast}):

$$\alpha = \frac{k}{k_{fast}} \quad (1)$$

Using the dependence of attachment efficiency on electrolyte concentration we determined the critical coagulation concentration (CCC). CCC is the minimal concentration of electrolyte that is needed to achieve a fast aggregation regime. This value corresponds to the transition between the slow and fast aggregation regime and is an important characteristic that defines the quantity of electrolyte needed to effectively induce the coagulation and elimination of particles from suspension.
To obtain zeta potential (ZP) electrophoretic mobility was measured using the Doppler technique with a Malvern Zetasizer Nano ZS and then Smoluchowsky equation (Gregory, 2005) was used:

$$U_E = \frac{\varepsilon \xi}{\eta} \quad (2)$$

A.2.1.3 Results

pH changing effect

Uncoated MNMs.

Point of zero charge (PZC) is one of the important parameters that characterize the stability domain of nanoparticles. To define the pH_{PZC} we performed electrophoretic mobility and size distribution measurements in a range of pH from 3 to 10. The titration procedure was made in presence of sodium chloride as background electrolyte (0.001 M). Titration was performed from acid to basic environment. As shown in Figure A.2.1-2a, when pH < 4.5 ± 0.1 the surface of CeO_2 MNMs is found strongly positively charged (ZP was equal to +51.3 ± 1.3 mV at pH 3.0). MNMs are stable in this domain which is also confirmed by the size distribution with Dh equal to 185 ± 75 nm. Further increase of pH leads to the decrease of surface charge until the PZC is reached and then to charge inversion. The surface of CeO_2 MNMs is found strongly negatively charged at pH > 8.0 ± 0.1. In the PZC region nanoparticle aggregation occurred and Dh diameters are found in the range between 800 and 1500 nm. As illustrated in Figure A.2.1-2a further pH increase after the PZC does not result in a significant decrease of the Dh diameters (disaggregation). We found the value of pH_{PZC} equal to 6.8 ± 0.1. This result is close to the theoretical value of pH_{PZC} = 7 (Jolivet et al., 2000) and to the experimental result obtained by Buettner et al., (2010), in pure water with pH_{PZC} = 6.5.

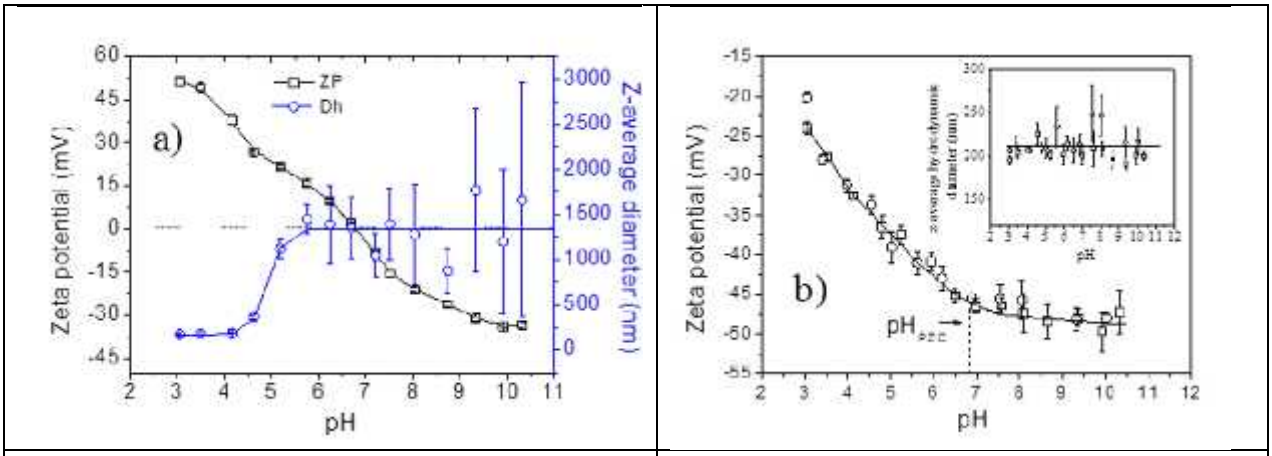

a b

Figure A.2.1-2: ZP and Dh of CeO_2 MNMs in pH changing conditions: a) uncoated CeO_2 MNMs; b) FAs-CeO_2 MNMs complexes.

Coated MNMs.

ZP and Dh variations as a function of pH for FAs coated CeO_2 MNMs are presented in Figure A.2.1-2b. First, it should be noted that the ZP is negative in all pH range and is decreasing from –24.0 ± 0.9 to –49.7±2.5 mV. Two different domains are obtained. In the first domain, the values of ZP rapidly decrease with increase of pH from –24.0 ± 0.9 to –45.2 ± 0.9 mV until the pH corresponding to the CeO_2 PZC. Then, above the pH_{PZC} the increase of pH does not significantly influence ZP that is now in the range from –45.2 ± 0.9 to –49.7±2.5 mV. Meanwhile, we observed a constant Dh that was equal to 220 ± 40 nm in all pH range. Such variations can be explained by the electrostatic properties of the FAs-CeO_2 complexes and in particularly by the modification of the acid-base properties of CeO_2 MNMs in presence of FAs. At pH 3 nanoparticles are positively charged. Consequently, addition of negatively charged FAs leads to the rapid adsorption of FAs on the nanoparticle surface. A 2 mg L^{-1} FAs concentration induces a rapid and significant charge inversion of CeO_2 MNMs. After formation of FAs-CeO_2 complexes ZP is negative, but the particle size did not change due to the long-range electrostatic repulsive forces between the complexes. Then increase of pH leads to the decrease of the value

of ZP due to the neutralization of the positively charged surface sites of CeO_2 MNMs by hydroxyl ions (Jolivet et al., 2000) according to the equation (1):

$$M\text{-}OH_2^+ + OH^- \rightarrow M\text{-}OH + H_2O \quad (1)$$

The neutralization of CeO_2 surface charge occurs at a pH value which is close to the pH_{PZC} (as shown in Figure A.2.1-2b). Then by increasing further the pH, since zeta potential is stable, the second deprotonation step (2):

$$M\text{-}OH + OH^- \leftrightarrow M\text{-}O^- + H_2O \quad (2)$$

is found more difficult to achieve. Further surface deprotonation above pH_{PZC} is not significant enough because of the increase of repulsive electrostatic interactions due to the presence of negatively charged FAs at the nanoparticle surface. This is an important point indicating that FAs adsorption at the nanoparticle surface can significantly change their surface acid-base properties. Also these results indicate that NOM coating on MNMs is likely to persist in pH changing conditions in natural environments.

Dilution effect

We imitated one of the possible aging processes of CeO_2 MNMs that were coated with FAs by decreasing the concentration of components by successive dilution. ZP and Dh of FAs-CeO_2 complexes in concentration changing conditions are presented in Figure A.2.1-3. At pH 3.0 one can see that no big difference is recorded regarding the 20 times dilution factors. ZP is stable and is equal to –29.7 ± 1.7mV. Dh does not exceed 325 nm. In the same time, at environmentally relevant pH 8.0 we observed the slight increase of Dh and ZP (ZP becomes less negative) with decrease of component concentration. Dh does not exceed 300 nm, but ZP is changing from –46.6 ± 1.1 to –41.6 ± 2.3 mV. However, we suppose that such increase in ZP values is also not significant. Our results confirm that electrostatic interactions between positively charged MNMs and negatively charged FAs are high enough so that FAs-CeO_2 complexes once formed are able to resist to a strong dilution effect. This is also an important point indicating that FAs coating around CeO_2 MNMs is one of the key factors that will control, even in changing conditions, transformation and toxicity of MNMs in aquatic systems.

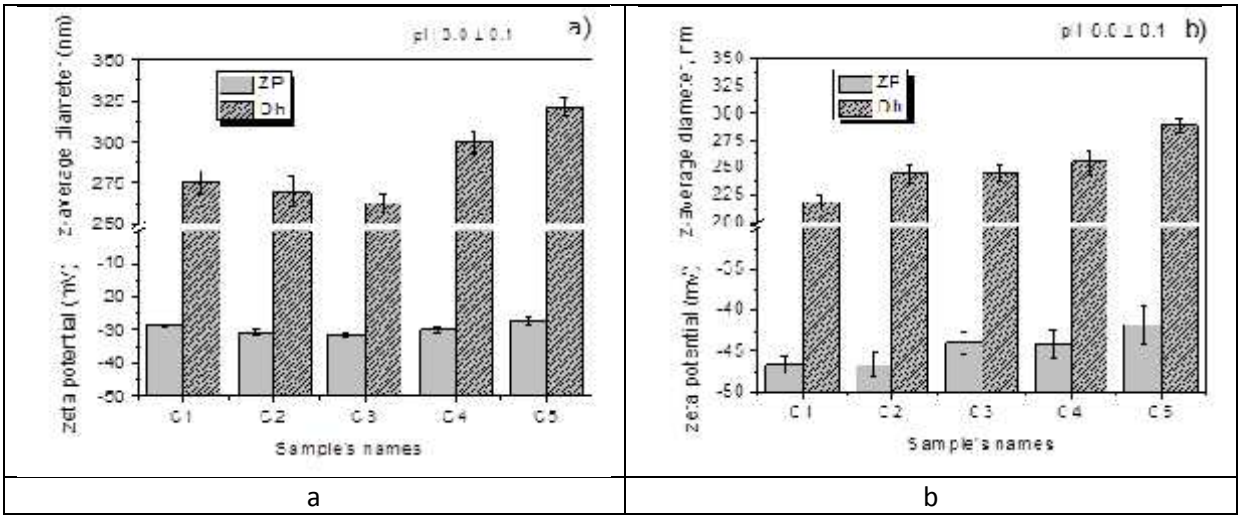

a b

Figure A.2.1-3: ZP and Dh of CeO_2 MNMs in concentration changing conditions: a) pH 3.0 b) pH 8.0. C1 – CeO_2 MNMs concentration is equal to 100 mgL^{-1}, FAs concentration is 4 mg L^{-1}; C2 – [CeO_2] = 50 mg L^{-1} with [FAs] = 2 mg L^{-1}; C3 – [CeO_2] = 25 mg L^{-1} with [FAs] = 1 mg L^{-1}; C4 – [CeO_2] = 10 mg L^{-1} with [FAs] = 0.4 mg L^{-1}; C5 – [CeO_2] = 5 mg L^{-1} with [FAs] = 0.2 mg L^{-1}.

Influence of ionic strength

To understand the effect of ion valency and concentration on the behavior of uncoated and coated CeO_2 MNMs we investigated the influence of mono- and divalent electrolyte using NaCl and $CaCl_2$. Two situations were considered: i) at pH < pH_{PZC}, when MNMs are stable and ii) at environmentally relevant pH = 8.0 when MNMs have been previously stabilized due to the coating.

Uncoated CeO_2 MNMs.

The influence of monovalent electrolyte (NaCl) on the stability of the uncoated CeO_2 MNMs was investigated at pH < pH_{PZC}. In this pH condition MNMs are stable with high positive surface charges. In the presence of NaCl (Figure A.2.1-4a) ZP decreases rapidly until 0.1 M, and then reaches plateau at higher electrolyte concentrations (> 0.1 M). Increase of NaCl concentrations leads to the decrease of ZP from +55 to +25 mV, due to the decrease of the thickness of diffuse layer when the ionic strength is higher than the CCC. Particles can approach closer to each other and van der Waals attraction become sufficient to outweigh the double layer repulsion, hence leading to the particle destabilization. Consequently Dh diameters are increasing with increase of salt concentration from base line value less than 200 nm to 2500 nm (Figure A.2.1-4b). Using the procedure previously described we calculated the attachment efficiencies between uncoated CeO_2 MNMs in increasing NaCl concentrations. As shown in Figure A.2.1-4 the aggregation behavior of MNMs in monovalent electrolyte follows the DLVO theory (Buettner et al., 2010; Li et al., 2011). We distinguish two aggregation regimes: diffusion limited and reaction limited. When the aggregation is diffusion limited attachment efficiency approaches to 1. The CCC was determined and equal to 0.11 ± 0.02 M (Figure A.2.1-5) giving the minimal concentration of NaCl that is necessary to destabilize 50 mg L^{-1} of uncoated CeO_2 MNMs for their further elimination from suspension.

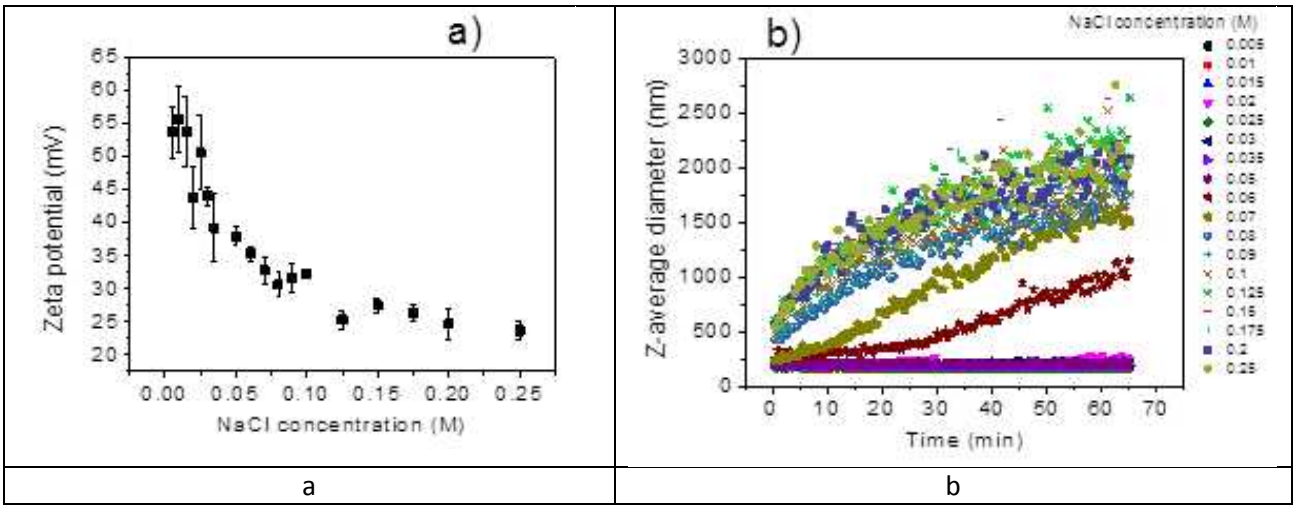

a b

Figure A.2.1-4: a) ZP of uncoated CeO_2 MNMs as a function of sodium chloride concentration. ZP decreases with increase of ionic strength; b) Dh variation of uncoated CeO_2 MNMs as a function of salt concentration. Kinetics of aggregation is enhanced by increasing the ionic strength of the CeO_2 dispersion. Experimental condition: [CeO_2] = 50 mg L^{-1}, pH < pH_{PZC}. Dh diameters increase with time and with increase of NaCl concentrations.

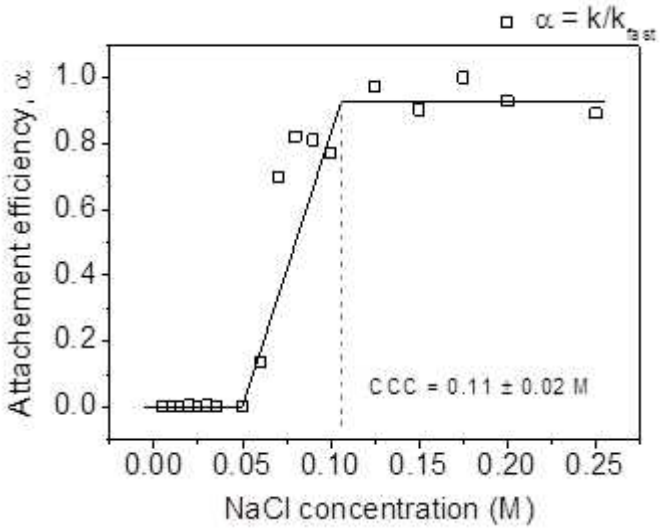

Figure A.2.1-5: Attachment efficiency between uncoated CeO_2 MNMs as a function of NaCl concentration. Critical coagulation concentration (CCC) is found equal to 0.11 ± 0.02 M. Experimental condition: [CeO_2] = 50 mg L^{-1}, pH < pH_{PZC}.

FAs coated CeO_2 MNMs

To understand the behavior of CeO_2 coated with FAs by increasing the ionic strength two electrolytes were used; NaCl and $CaCl_2$. First, the suspension of FAs-CeO_2 electrostatic complexes was prepared and pH was set to an environmentally relevant value that was equal to 8.0 ± 0.1. Then we sequentially increased the salt concentration from 0.5 to 0.75 M for NaCl and from 0.25 to 50 mM for $CaCl_2$ (Figure A.2.1-6). The attachment efficiencies of coated CeO_2 calculated from the growth of the Dh diameters as a function of electrolyte concentrations are presented in Figure A.2.1-7. The CCC values for two salts have been determined and correspond to 0.39 ± 0.02 M for NaCl and 2.9 ± 0.3 mM for $CaCl_2$. The difference of CCC values, more than 100 times, can be explained by the Schulze-Hardy rule, indicating that the CCC is proportional to the ion charge (CCC ~ $1/z^6$, where z is ion valency) (Gregory, 2005). Divalent ions have a stronger screening effect and a higher affinity to the highly negative surface of FAs-CeO_2 complexes compared with monovalent ions. Thus a less concentrated solution of $CaCl_2$, compared with NaCl, is needed to destabilize coated particles, due to the higher positive charge and specific adsorption of Ca^{2+} ions on the MNMs surface. The ZP values of coated CeO_2 MNMs before addition of electrolyte are equal to –51.1 ± 0.6 mV (Figure A.2.1-8a). The addition of small amount of divalent salt leads to a high response and a change of ZP of about 30 units to the value –21 ± 0.7 mV comparing with NaCl when the addition of higher concentration changes ZP only of 14 units (ζ = –37.3 ± 1.0 mV) (Figure A.2.1-8). The increase of concentrations of both electrolytes leads to the gradual increase of ZP values (ZP becomes less negative) from –37.3 ± 1.0 to –16.8 ± 6.0 mV for NaCl and from –21.9 ± 0.7 to –15.4 ± 0.8 mV for $CaCl_2$.The enhancement of aggregation by Ca^{2+} ions can also be explained by bridging effect through formation of intermolecular complexes between coated MNMs and divalent ions (Li and Chen, 2012). The CCC ratio of NaCl between uncoated and coated CeO_2 MNMs was also assessed and found equal to 3.5. More concentrated solution of NaCl was necessary in order to aggregate coated CeO_2 MNMs as FAs create a stabilizing coating around particles. Such conclusion is also confirmed by the values of ZP. For coated particles ZP is more negative and is equal to –51.1 ± 0.6 mV compared with uncoated particle (ζ = –21.1 ± 0.8 mV). Our results indicate when coated CeO_2 MNMs are present in a system in which ionic strength is increasing (passing for example from fresh to coastal or marine waters) they will better resist to aggregation in particular when monovalent salt are considered.

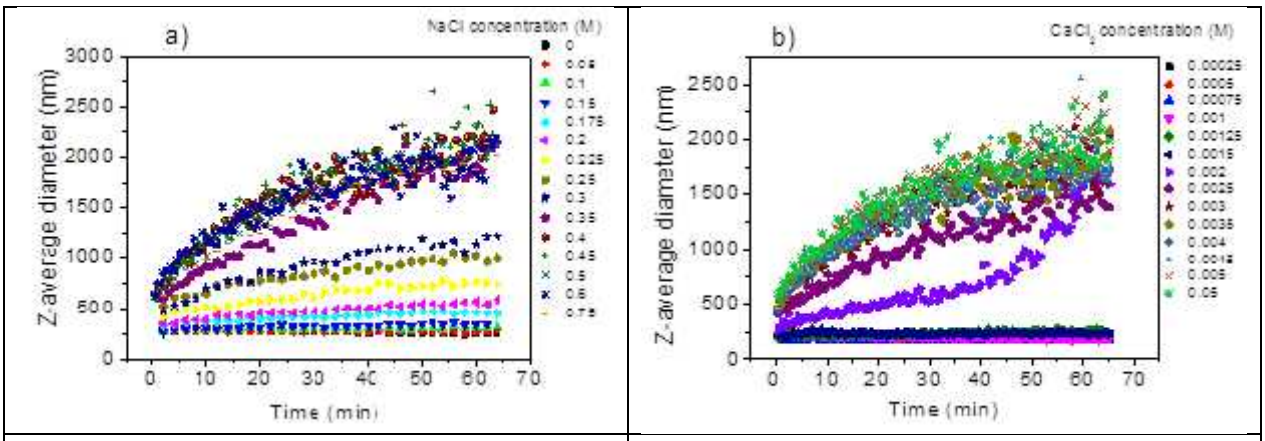

a b

Figure A.2.1-6: Dh variation of coated CeO_2 MNMs as a function of concentration of different electrolytes: a) NaCl; b) $CaCl_2$. Experimental condition: [CeO_2] = 50 mg L^{-1}, [FAs] = 2 mg L^{-1}, pH = 8.0 ± 0.1.

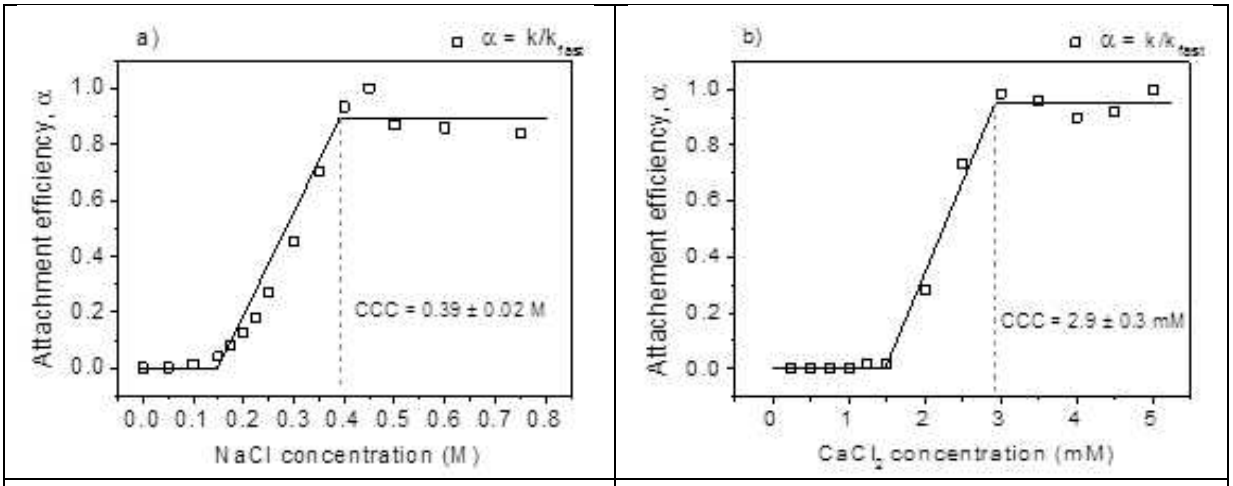

a b

Figure A.2.1-7: Attachment efficiency between coated CeO_2 MNMs as a function of electrolyte concentration: a) NaCl, CCC (NaCl) = 0.39 ± 0.02 M; b) $CaCl_2$, CCC ($CaCl_2$) = 2.9 ± 0.3 mM. Experimental condition: [CeO_2] = 50 mg L^{-1}, [FAs] = 2 mg L^{-1}, pH = 8.0 ± 0.1.

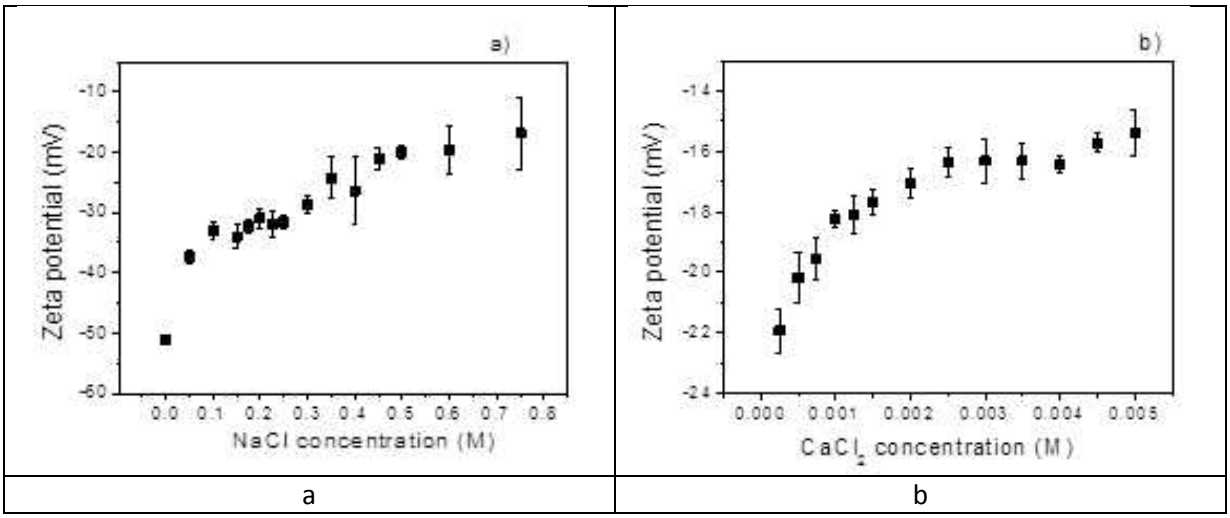

a b

Figure A.2.1-8: ZP of FAs-CeO_2 MNMs complexes as a function of electrolytes concentration: a) NaCl; b) $CaCl_2$. ZP increases with increase of ionic strength.

To resume the behavior of uncoated and FAs coated CeO_2 MNMs was investigated using various altered conditions. Two main parameters (Dh and ZP) were analyzed and we focused on the influence of pH variation, dilution effect and increase of ionic strength on the stability of uncoated and coated CeO_2 MNMs. The first important outcome here is to show that low FAs concentrations, representative of environmental fresh water conditions, are sufficient to coat and stabilize relatively highly concentrated CeO_2 MNMs suspensions against aggregation in changing pH conditions. In addition when $pH < pH_{PZC}$ strong electrostatic complexes are formed between FAs and CeO_2 MNMs and charge inversion is observed. The second important outcome indicates that the FAs-CeO_2 complexes, once formed, are stable regarding dilution effects. The third outcome here is related to the better stability of NOM coated CeO_2 regarding important changes in the ionic strength. We believe our findings constitute important results since, from environmental risk assessment point of view, stabilization of CeO_2 MNMs and persistence of NOM coating in natural changing environment could significantly enhance their mobility and residence time throughout aquatic systems and water treatment processes.

A.2.2 Aging of CeO_2 with phosphate (UoB)

A.2.2.1 Summary of the aging experiments

Four different cerium dioxide particles - CeO_2 PROM (provided by Promethean), JRC CeO_2 NM211, JRC CeO_2 NM212, and CeO_2 PVP10 (capped with 10K PVP) produced at UoB - were added to a solution of 5mM of KH_2PO_4, citric acid and ascorbic acid, 5 times the concentration as the one used by Zhang et al. (2012), and the pH was adjusted to 2.3, 5.5 and 12.3. The final concentrations of the CeO_2 NPs in the suspensions were 496 and 6200 mg L^{-1} in the case of CeO_2 PROM, 160 and 2000 mg L^{-1} for theCeO_2 NM212 and CeO_2 NM211, and 40 mg L^{-1} for the CeO_2 PVP10. After 7 and 21 days of static incubation, the suspensions with the highest concentration were dried out in a 50°C oven for three days and used to measure XRD. The CeO_2 NPs suspensions with lower concentration were used for UV-Vis and zeta potential, at 7 and 21 days, and for TEM observation, after 21 days.

Zirconium doped ceria nanoparticles with various Zr/Ce ratios (PROM A-G, composition of NPs in Table A.2.2-1) were exposed to a c. 5.5 pH corrected 5 mM phosphate solution composed of KH_2PO_4, citric acid and ascorbic acid based on the work of Zhang et al. (2012). Samples were exposed for 21 days of static incubation. DLS, both sizing and zeta potential, XRD and TEM before phosphate solution addition (pristine), immediately after phosphate solution addition, after 7 days of exposure and 21 days of exposure.

Table A.2.2-1: composition of the Zr-doped ceria NPs used for aging

Sample	Composition
A	CeO_2
B	$Ce_{0.86}Zr_{0.14}O_2$
C	$Ce_{0.73}Zr_{0.27}O_2$
D	$Ce_{0.48}Zr_{0.52}O_2$
E	$Ce_{0.22}Zr_{0.78}O_2$
F	$Ce_{0.08}Zr_{0.92}O_2$
G	ZrO_2

CeO_2 PVP10, PVP40 and PVP360 (capped with 10K-, 40K-, or 360K PVP, respectively) nanoparticles prepared according to Merrifield et al. (2013), 10K PVP capped zinc oxide and 10K PVP capped copper oxide prepared

by a modified method as well as commercial ceria (Promethean) were subjected to temperature aging. Nanoparticle samples were placed in closed vials on a shaker set at 80 rpm, the temperature was set (25, 45, 65 or 80 °C) and the aging was carried out for 28 days. Sample characterization took place at various time points by means of DLS – both size and zeta potential, UV/Vis, and TEM imaging.

A.2.2.2 Characterization methods

DLS, UV-Vis, TEM, and XRD experiments were conducted. DLS measurements were conducted with a Malvern Zetasizer 5000 or nano ZS that combined particle sizing and electrophoresis in low volume disposable cuvettes and at least five concordant measurements recorded to calculate a mean z average size and zeta potential at 21°C. The UV-vis was investigated using a Jenway double beam UV-Vis spectrophotometer, with a low volume quartz cuvette. The UV-Vis absorption spectra were collected over a wavelength range of 200-800nm. Suitable blanks and controls were measured. TEM measurements were performed using a JEOL 1200EX (accelerating voltage 80 kV) for imaging. Samples were prepared by partially drying a drop of the particle solution on a cu mesh 400 holey carbon film (Agar scientific) at room temperature, the grid was washed thoroughly with water and re-dried. XRD measurements were performed using a powder diffractometer Bruker D8 autosampler (Haworth 503A).

A.2.2.3 Results

Aging of CeO_2 NPs with phosphate

TEM results are shown in Figure A.2.2-1. It can be observed that particles change shape (all the particles are spherical before the aging process) after a period of 21 days. In most cases, needles or “sea urchins” could be observed at pH = 5, which we believe is the ideal pH for phosphate aging. Zeta potential and UV/Vis results (data not shown) did not show any tendencies in any of the particles studied. They change over time.

Examples for the XRD results are shown in figure A2.2-2. It can be observed that the XRD spectrum changes the most at pH = 5 and after 21 days, where $CePO_3$ peaks were observed. Similar results were obtained for the other particles, but the spectra are less clear.

Particle	pH = 2	pH = 5	pH = 12
Prom	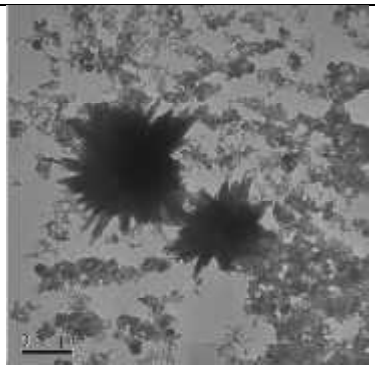	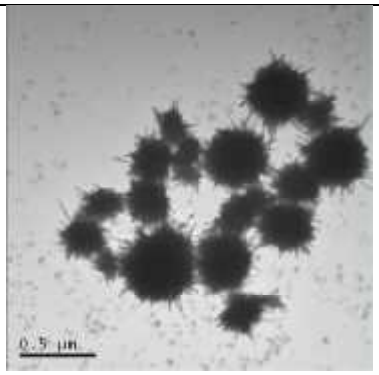	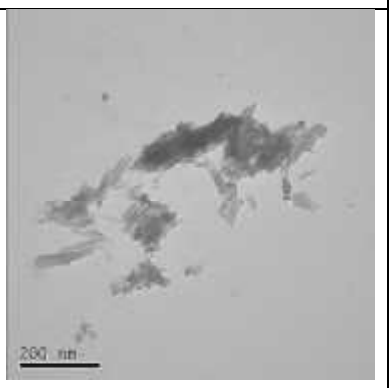
NM211	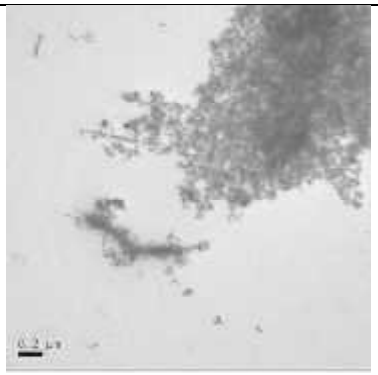	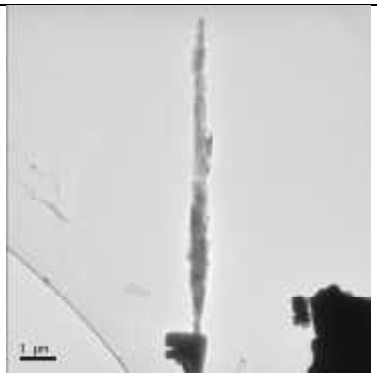	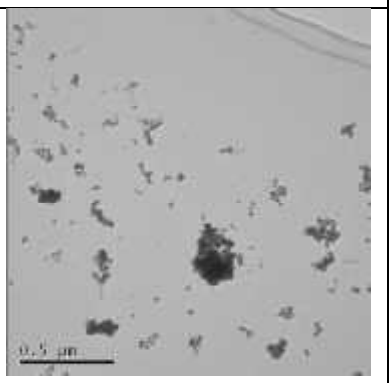
NM212	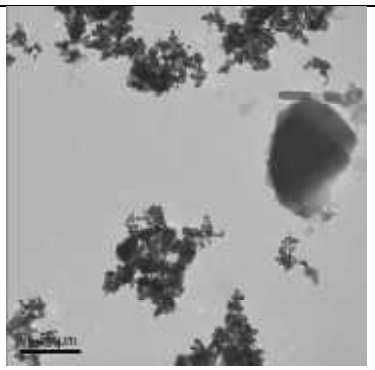	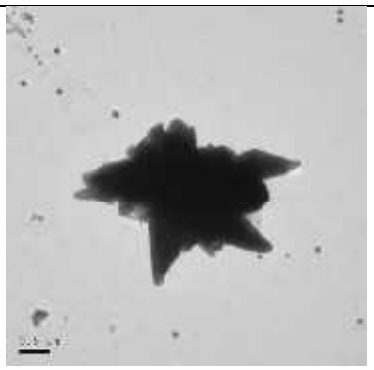	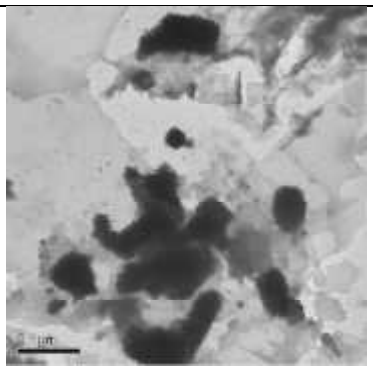
CeO_2 PVP10	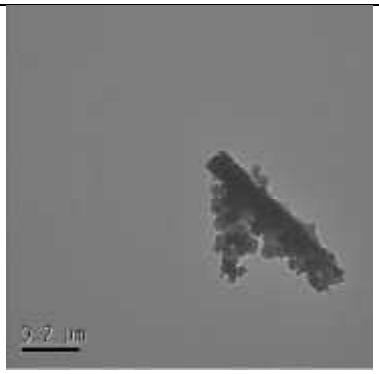	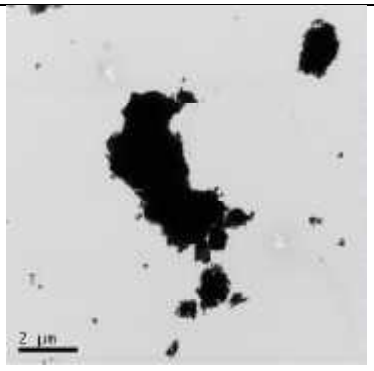	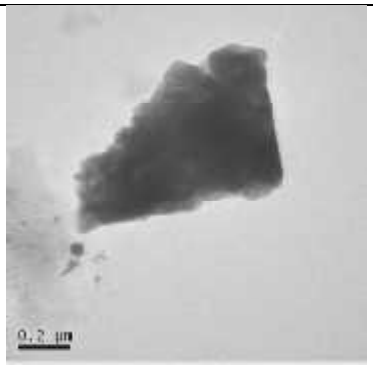

Figure A.2.2-1: TEM results for the different particles at different pH over a period of 21 days of phosphate aging.

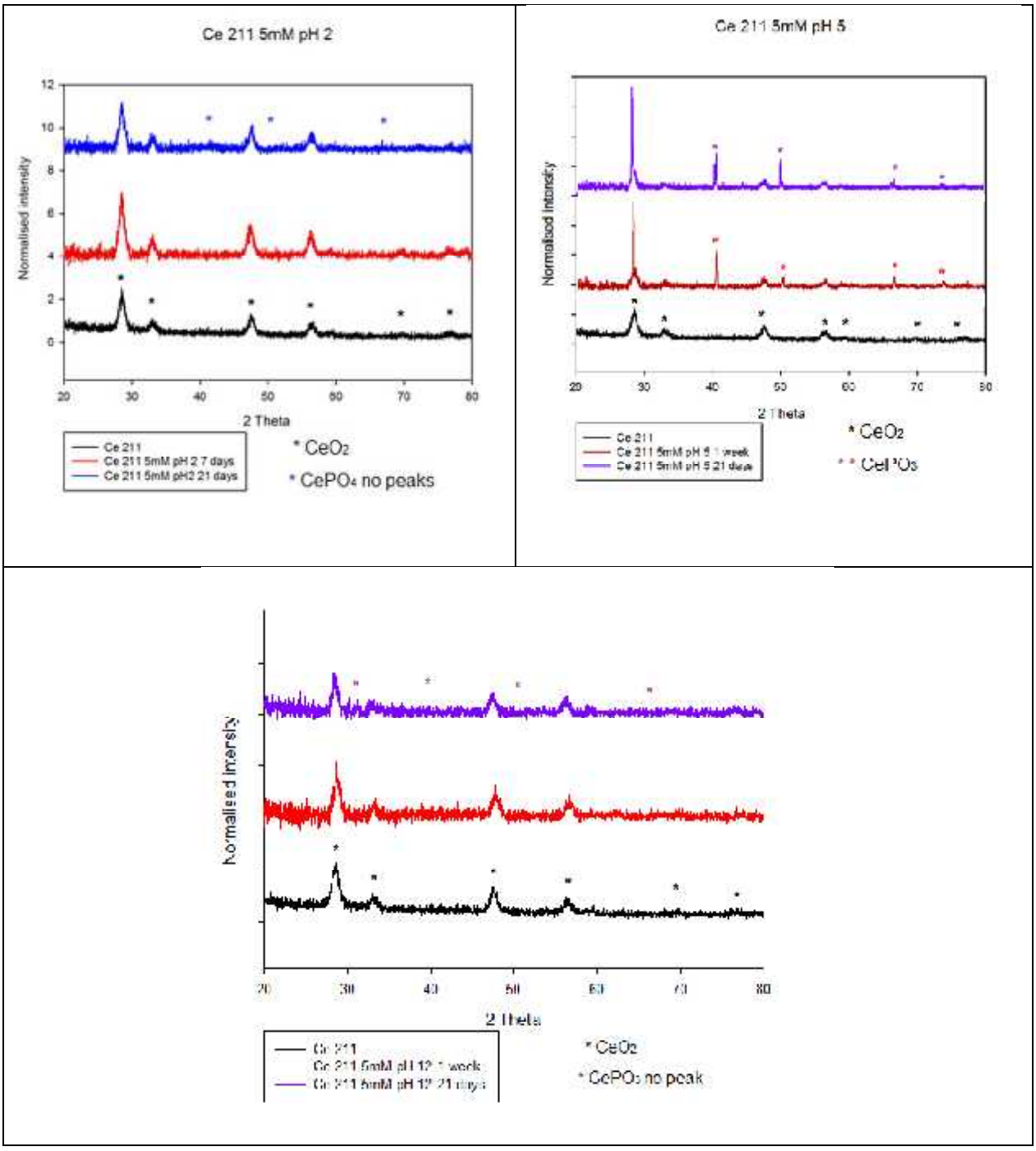

Figure A.2.2-2: XRD results obtained for NM211 after 1 week and 21 days.

Aging of Zr-doped CeO_2 NPs with phosphate

Examples of the DLS measurements are shown in Figure A.2.2-3 and A.2.2-4.

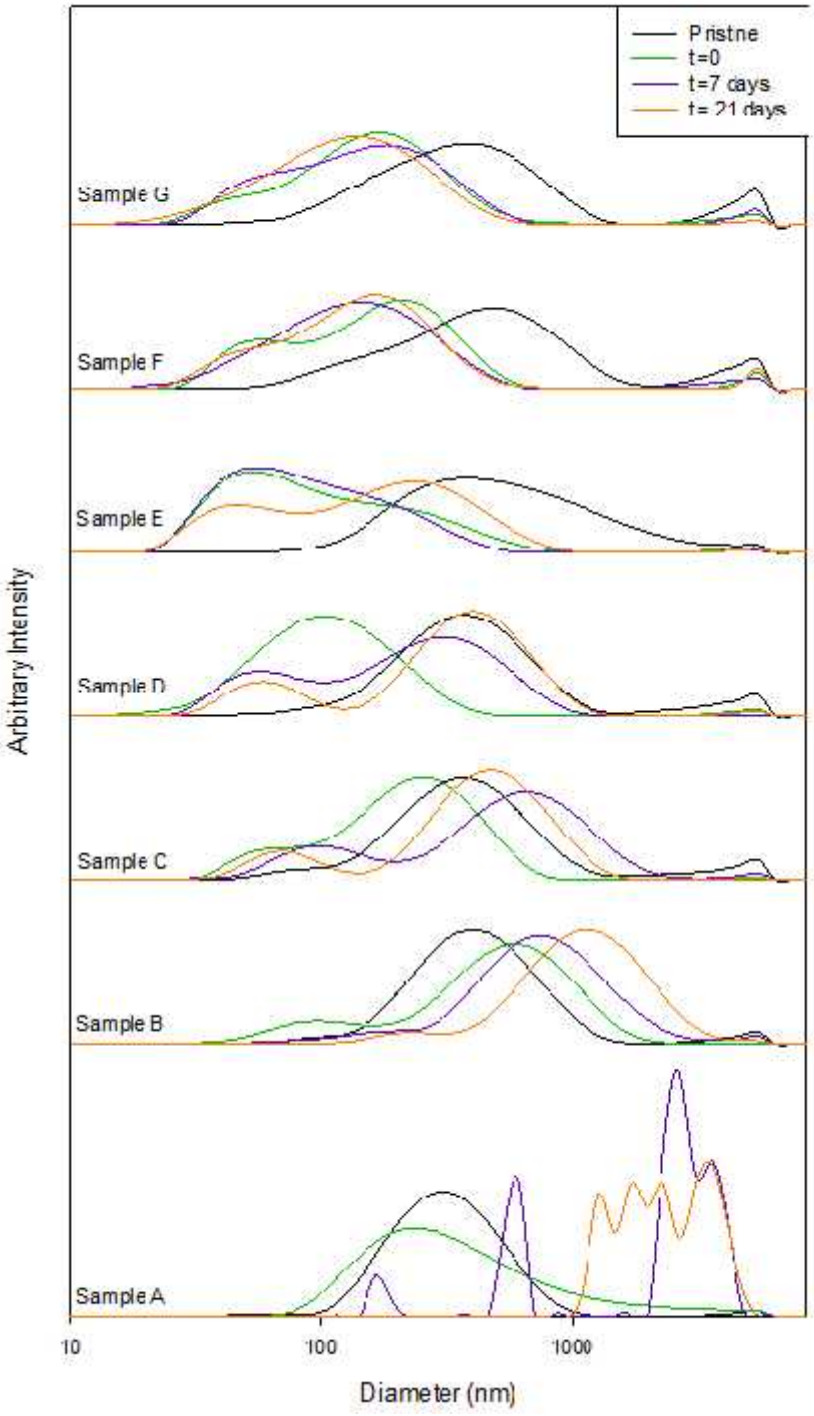

Figure A.2.2-3: DLS size measurements for Samples A-G with 5 mM phosphate solution.

Results show a decrease in diameter for samples A-D with the addition of the phosphate due to the hydrodynamic diameter calculated for the needle-like structures. Samples E and F show an initial decrease and then an increase in diameter reflecting transformation and aggregation. Sample G shows an increase in diameter. In this case only aggregation has occurred and no transformations.

Figure A.2.2-4 shows pristine samples to be stable. On addition of the phosphate solution the zeta values for all the samples decreases to stable negative values. Following this there is an increase in zeta potential values with all samples apart from C and F being unstable with values close to 0.

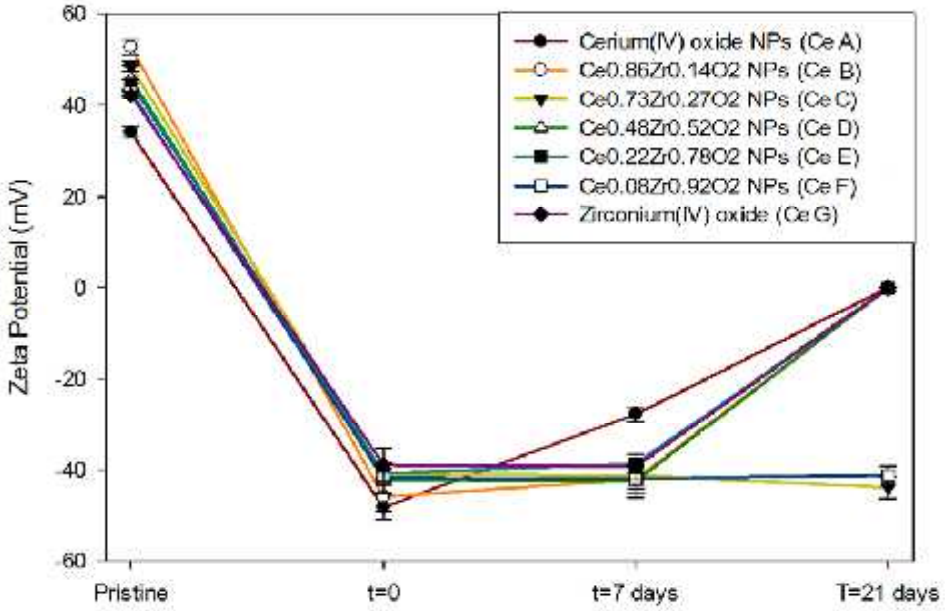

Figure A.2.2-4: Zeta potential values for samples A-G with 5 mM phosphate solution.

XRD spectra are displayed in Figure A.2.2-5. They show the formation of cerium phosphate in all cases except for sample G.

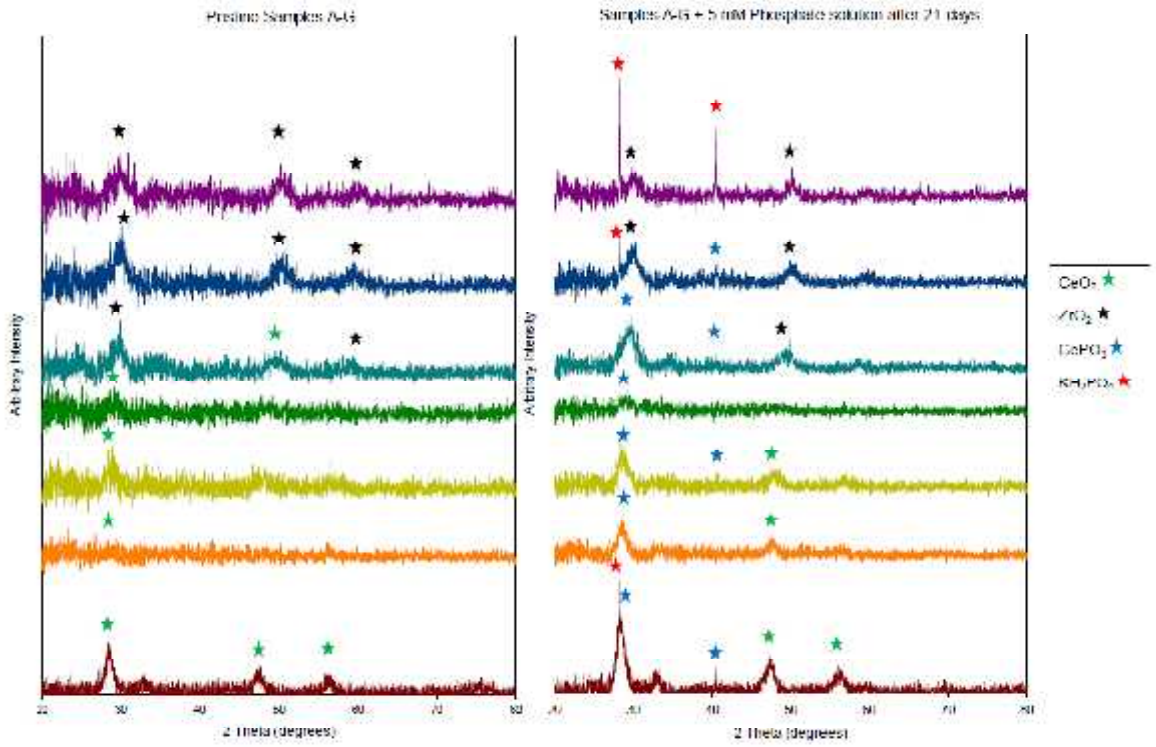

Figure A.2.2-5: XRD Spectra for Samples A-G in their pristine state (left) and after 21 days exposed to a 5 mM phosphate solution (right).

Examples of TEM images of samples A to G are given in Figure A.2.2-6. “Sea urchin”/needle-like structural transformations can be noted. Images show a decrease in transformations with a decrease in ceria presence (i.e. a decrease from A-G). ZrO_2 is not structurally transformed (sample G). Images also show an increase in transformations as a function of time (i.e. from top to bottom).

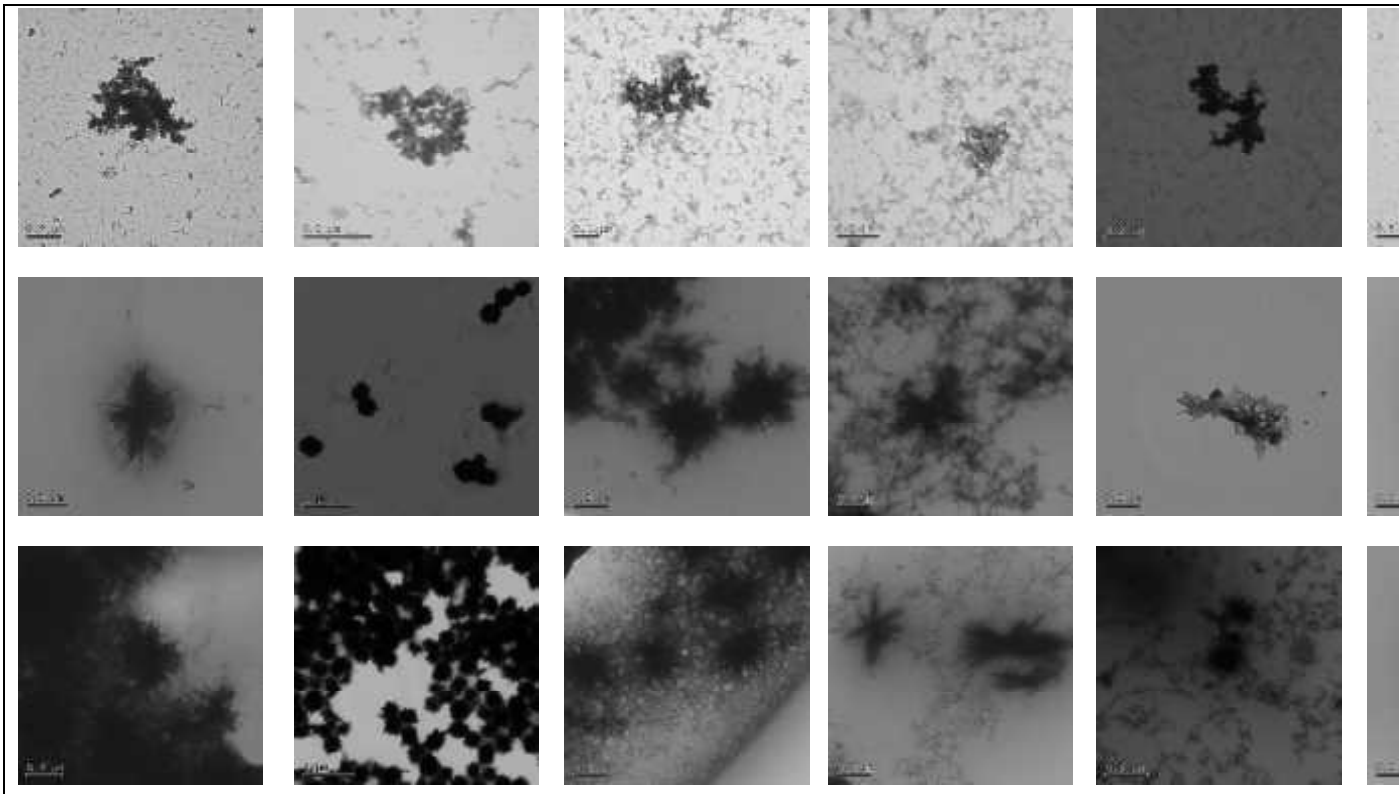

A	B	C	D	E	

Figure A.2.2-6: TEM imaging of Samples A-G before (top), after 7 (center) and 21 (bottom) days exposure to a 5 mM p

Aging of CeO_2 NPs with temperature

The effect of temperature on the evolution of ceria is illustrated in Figures A.2.2-7 to A.2.2-9.

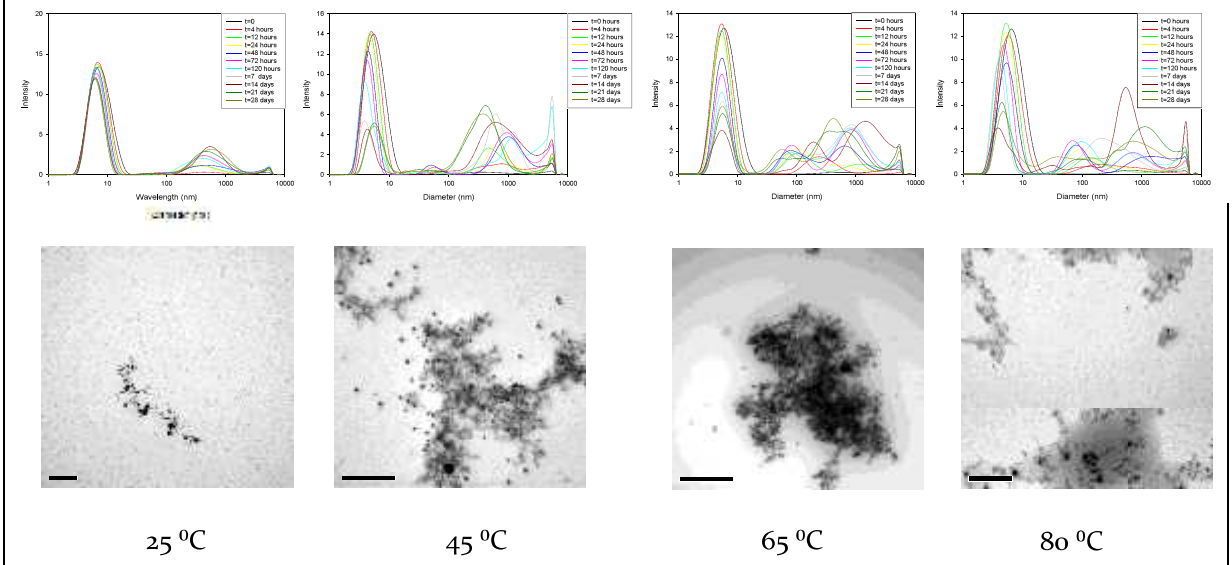

a

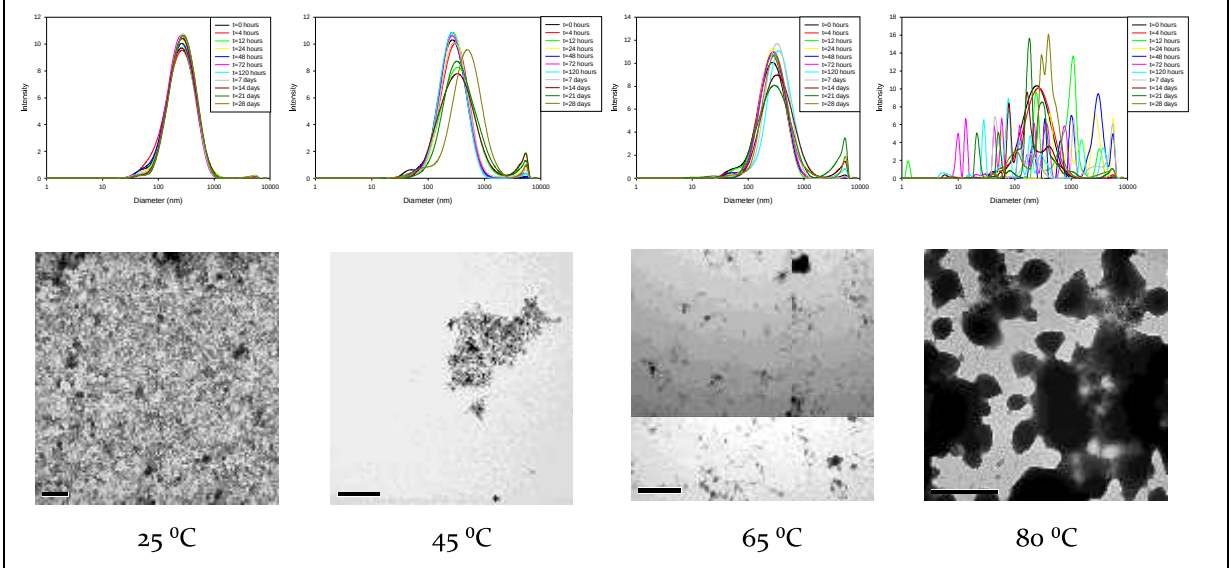

b

Figure A.2.2-7: DLS size distribution as a function of time and TEM images after 28 days on exposure to different temperatures. (a) CeO_2 PVP10 and (b) PROM CeO_2 NPs.

The following conclusions can be drawn:

- As the temperature increases the rate of change in size increases.
- Differences are noticed between reference, capped and uncapped samples.
- The rate of size change varies for the different nanoparticle cores. Ceria > copper oxide > zinc oxide.
- In the case of the ceria samples, as the PVP chain length increases the changes in size at different temperatures look to decrease.

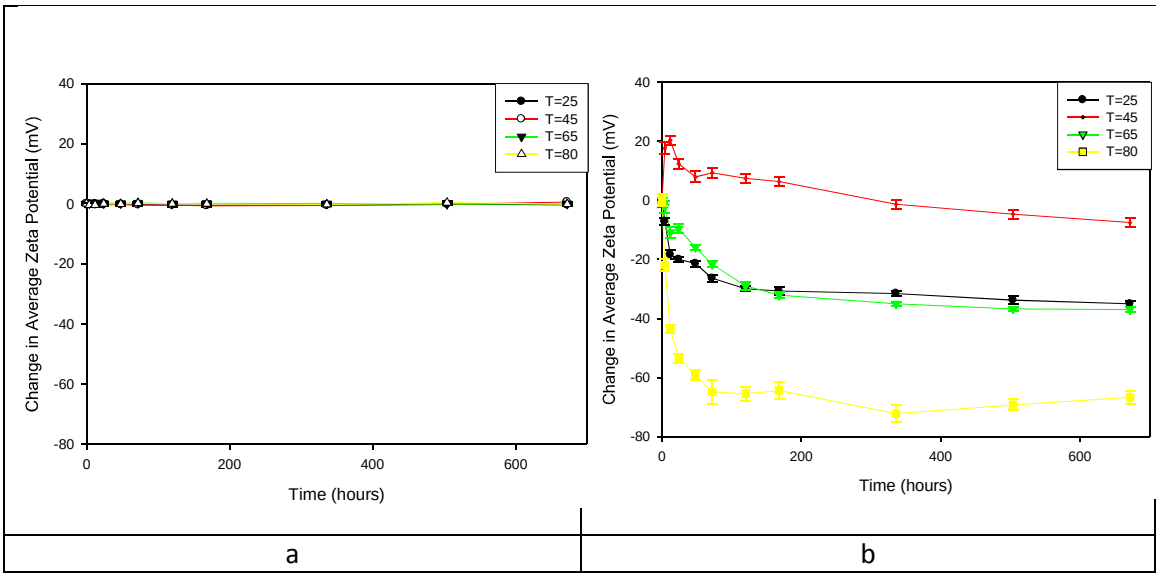

Figure A.2.2-8: Zeta potential graphs of (a) CeO_2 PVP10 and (b) CeO_2 PROM at different temperatures as a function of time.

All PVP zeta potential graphs show the zeta potential to be around zero due to steric stabilization caused by the PVP. All capped particles show very little change in zeta potential as a function of time regardless of the temperature. Yet for the Promethean ceria the zeta potential was significantly affected.

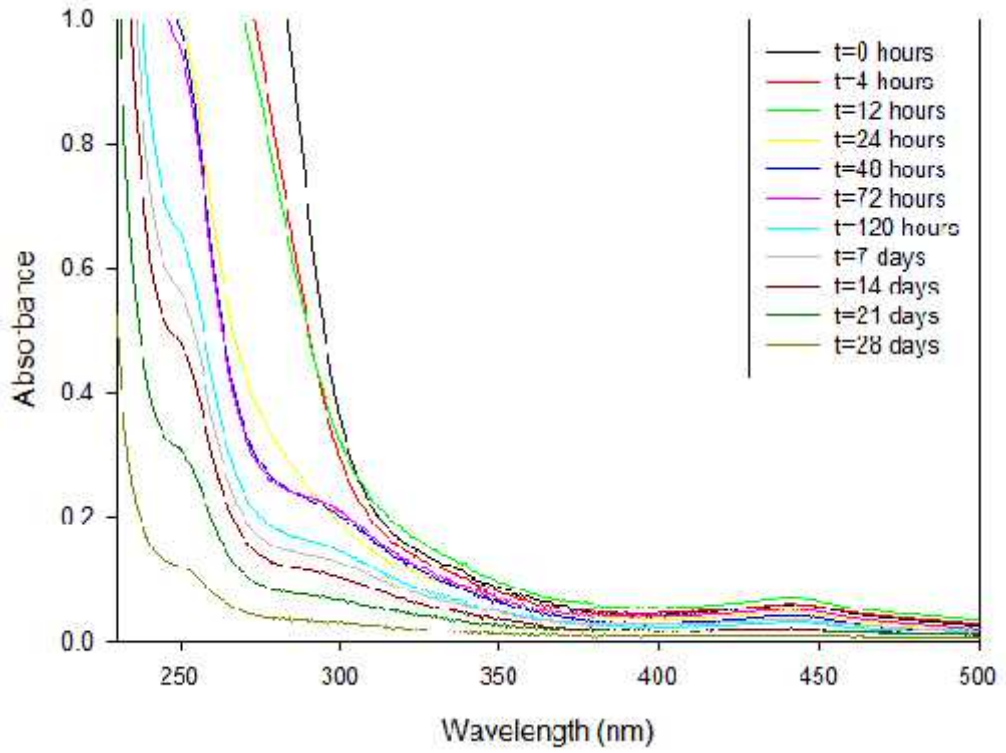

Figure A.2.2-9: Influence of time of exposure on UV/Vis spectrum at T=45°C of CeO_2 PVP10.

UV/Vis spectra showed the probability of dissolution of particles as well as the possibility of the PVP capping becoming less effective as ceria UV peak becomes noticeable however PVP still present in dispersion as zeta potential values are not affected.

A.2.3 Aging of CeO_2 with UV/Temperature (CEA)

A.2.3.1 Summary of the aging experiments

Stock suspensions (1 g L^{-1} Ce) of CeO_2 NM211 and CeO_2 NM212 NPs (provided as powder from JRC, see D3.2) were prepared. They were used for the aging protocols either after dilution to 0.5 g L^{-1} (Ce) or after drying in a thermal chamber to proceed with suspensions or powder, respectively. The aging conditions tested with these NPs were "soft": QSUN for one week with an irradiance of 1.44 W m^{-2} at 420 nm, $T_{black\ panel}$ = 70 °C, T_{air} = 40 °C, and a 50% relative humidity.

A.2.3.2 Characterization methods

DLS, TEM, and XRD experiments were conducted using the same procedures and devices as those described in § A.1.

A.2.3.3 Results

Remark: In the results given below, all concentrations refer to the metal content of the considered suspension (i.e. Ce for CeO_2 NPs).

Size and ZP by DLS

a) Preliminary experiments

Ionic strength and scan direction for titration were identical as those optimized with TiO_2. The NP concentration optimization was carried out in preliminary experiments.

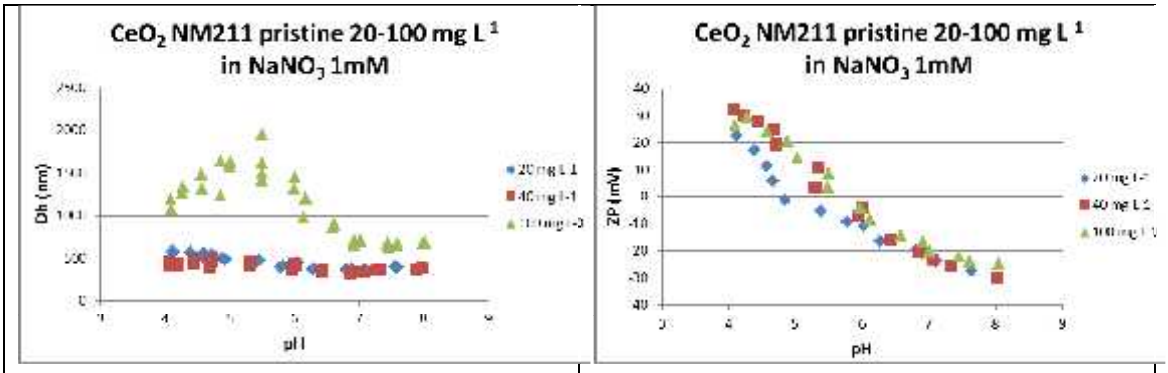

a b

Figure A.2.3-1: Influence of the NP concentration in suspension on the pH titration profile of Dh (a) and ZP(b). Experimental conditions: suspensions in $NaNO_3$ 1 mM, pH scan from 8 to 4.

The same behavior as already experienced with TiO_2 can be observed in Figure A.2.3-1: a marked tendency to agglomerate for concentrations above a certain threshold (>40 mg L^{-1}). However, in the case of CeO_2, zeta potentials also seem to be affected by a decrease in particulate concentration and the final working concentration was set to 40 mg L^{-1} as a good compromise.

b) Characterization of pristine and aged NPs using DLS

The titrations of size and zeta potential of both types of CeO_2 investigated are reported in Figure A.2.3-2 and a summary of the relevant parameters is given in Figure A.2.3-3. The PZC is slightly decreased after one week of aging in the powder form, especially as regards CeO_2 NM211 (δ(PZC)=-0.6 pH unit, see Figure A.2.3-3). This phenomenon is correlated with an absence of de-agglomeration in the acidic zone of the pH range, which is in favor of an aggregation process with stronger binding between particles.

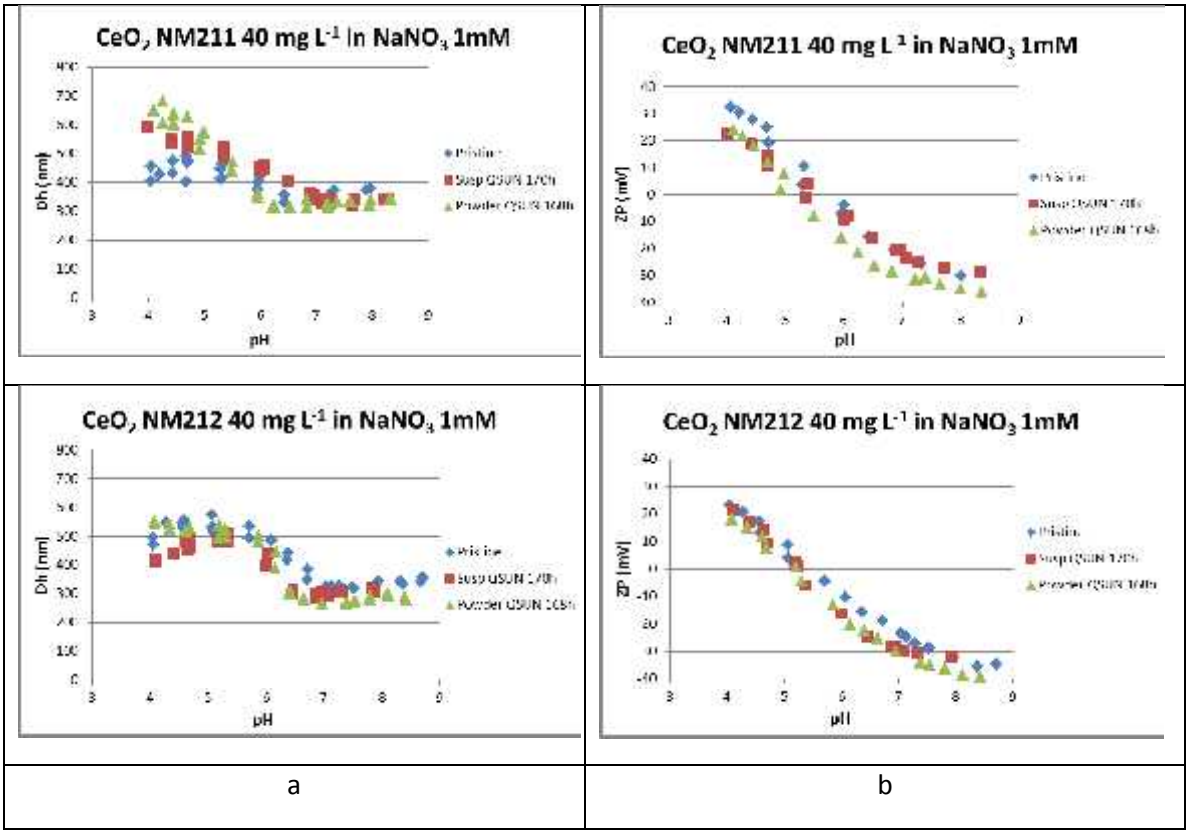

a b

Figure A.2.3-2: Evolution of Dh (a) and ZP (b) as a function of pH for CeO_2 NPs after different aging protocols. Experimental conditions: [CeO_2 NPs] = 40 mg L^{-1} (metal basis) in $NaNO_3$ 1 mM, pH scan from 9 to 4.

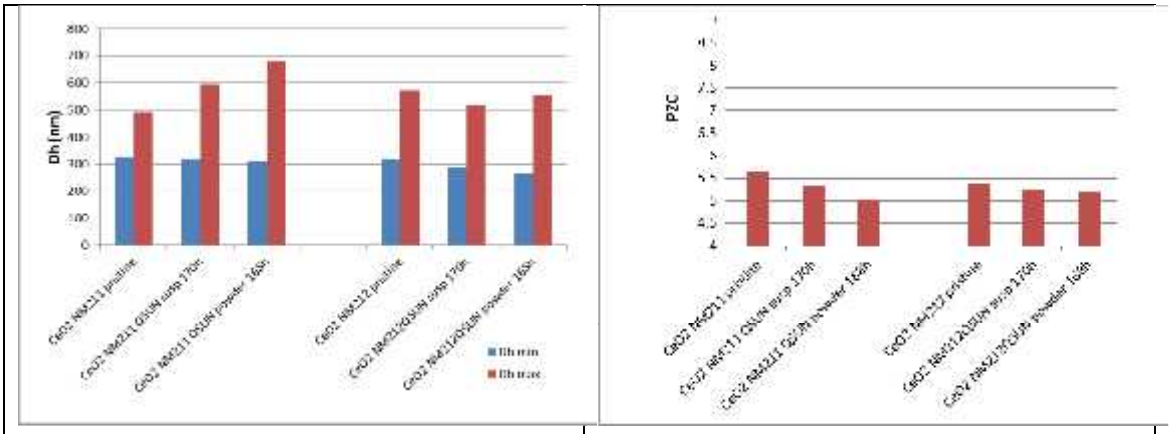

a b

Figure A.2.3-3: Influence of the aging protocol on the size of the agglomerates (Dh min: minimum size for optimum dispersion conditions, and Dh max: maximum size for optimum agglomeration conditions) (a) and on the value of PZC (b) for the different CeO_2 NPs. Experimental conditions: see Figure A.2.3-2.

The values of the average hydrodynamic diameters for pristine CeO_2 NM211 and CeO_2 NM212 are close to those provided by the producer ($Dh_{CeO2\ NM211}$ = 293 nm and $Dh_{CeO2\ NM212}$ = 213 nm, 3 g L^{-1} in UP water (Charanjeet et al., 2014), given the high agglomeration/aggregation state of these materials and, additionally, the high polydispersity of CeO_2 NM212.

TEM

TEM images of pristine CeO_2 NPs and the same NPs aged one week as powder in the QSUN are presented in Figure A.2.3-4.

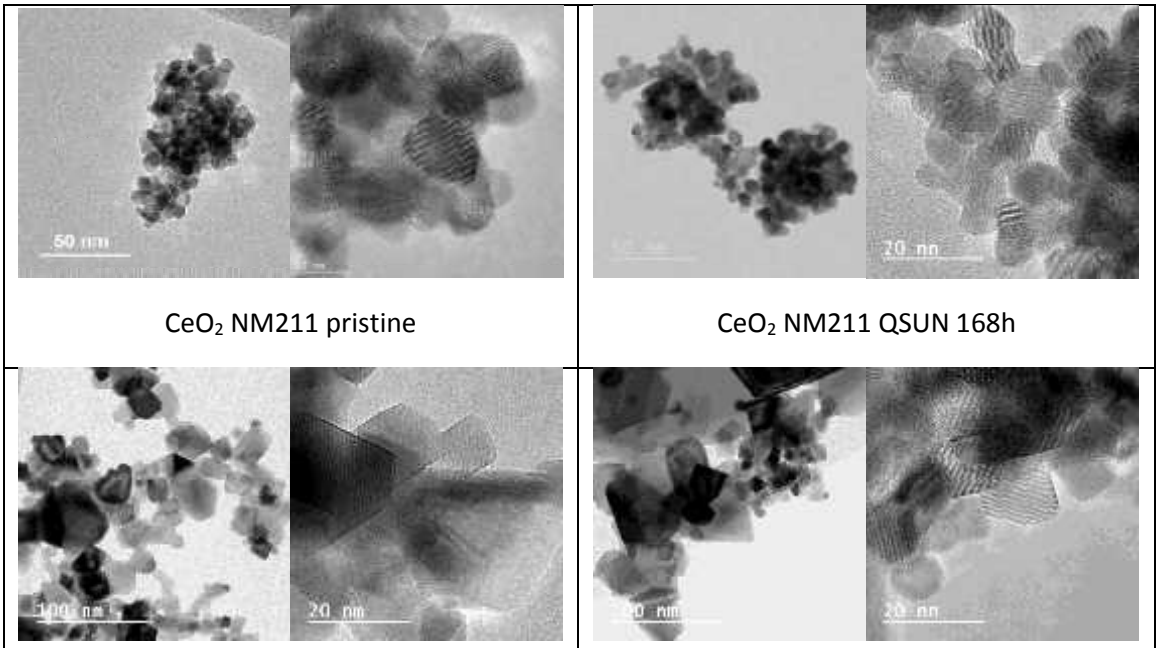

CeO_2 NM211 pristine	CeO_2 NM211 QSUN 168h
CeO_2 NM212 pristine	CeO_2 NM212 QSUN 168h
a	b

Figure A.2.3-4: TEM images of CeO_2 NPs. (a): Pristine (a) and (b): powder aged 168h in the QSUN.

The images of the primary particles compare well with those obtained by JRC (Charanjeet et al., 2014): CeO_2 NM211 shows small (ca. 10 nm), near spherical particles with regular morphology and a relatively homogenous size distribution whereas CeO_2 NM212 look more polyhedral with non-homogenous size distribution, ranging from below 10 nm to well in excess of 100. They both present agglomerated structures.
There is no visible alteration of the particles or change in the aggregation state after the aging process.

XRD

Figure A.2.3-5 shows the XRD patterns of the pristine CeO_2 NPs and those of the same particles aged 168h in the QSUN in the powder form. Crystallite sizes deduced from the line widths are gathered in Table A.2.3-1.

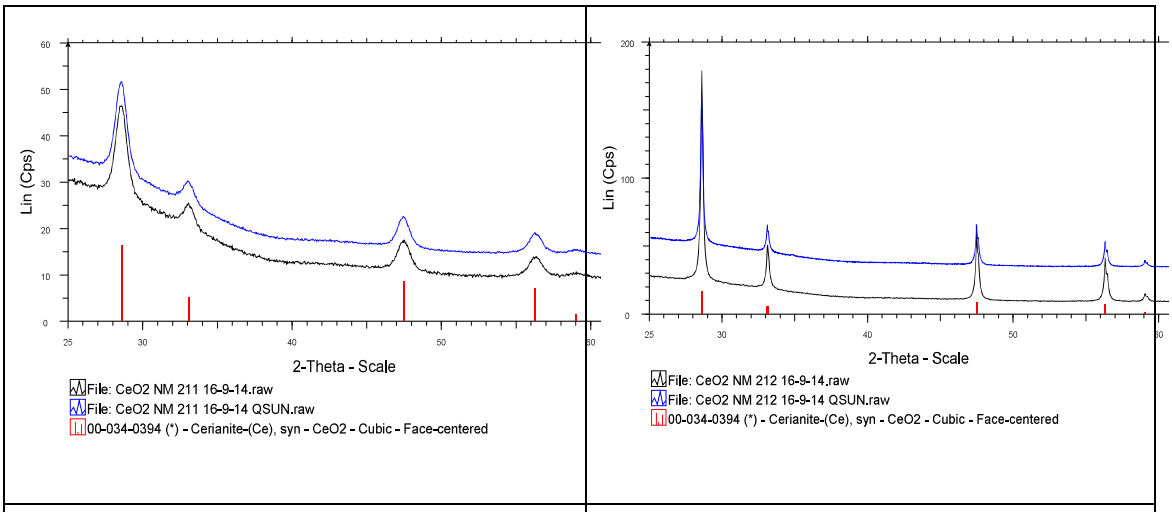

NM211 | NM212

Figure A.2.3-5: XRD diffraction patterns of pristine and one-week-QSUN-aged CeO_2 NPs. CeO_2 NM211 (a) and CeO_2 NM212 (b).

Table A.2.3-1: Crystallite size and lattice parameter of the CeO_2 NPs

CeO_2 NP	**Crystallite size (nm)**	**a (Å)**
CeO_2 NM 211	9.2	5.4126
CeO_2 NM 211 QSUN powder 168h	9.5	5.4136
CeO_2 NM 212	60	5.4098
CeO_2 NM 212 QSUN powder 168h	67	5.4102

The scans show a cubic cerionite phase profile both for pristine and aged particles. The line widths are thinner in the case of CeO_2 NM212, reflecting the larger crystallite size of these NPs. Indeed, the values obtained for CeO_2 NM211 are similar to those determined by the manufacturer whereas those for CeO_2 NM212 are significantly higher (measured crystallite size between 33 and 49 nm), and maybe closer to the accurate value as discussed in Charanjeet et al. (2014). Again, the higher polydispersity together with the uncertainty on the broadening of the lines for larger crystallite sizes may contribute to the lack of consistency in the data.

A.3 Ag NPs

A.3.1 Aging of Ag NPs with washing detergents (EMPA)

A.3.1.1 Summary of the aging experiments

The potential for nanomaterials to be released from consumer goods is not in itself a new topic, but the basis of scientific understanding of released particles and the transformations they may undergo during the products life cycle (*e.g.* during storage, use and disposal) is often hampered by the narrow scope of many research endeavors in terms of both the breadth of variables studied and the completeness of characterization using multiple analytical methods. Additionally, studies of sequential aging of products representing multiple stages of the life cycle are scarce. In order to bridge these gaps for the release of nanomaterials from textiles, we conducted a comprehensive suite of studies that allowed us to suggest some overarching themes for finding important mechanisms and parameters for particle transformations when still adhered to the fabric or when released. This undertaking of a large matrix of variables makes us more confident to suggest broader conclusions since trends can be monitored across more variables than in any other nano-composite release study to date.

Two studies are shown here which describe the transformation of Ag NPs in washing detergents. The first looks at the particles only suspended in a suite of different seven different detergents while the second expands on these results to see the transformations of particles released from nano-enhanced fabrics. Furthermore, the fabrics themselves are studied after washing to determine if there was a change of Ag speciation on the fraction of Ag that remained on the fabric.

Fabrics

Standardized textiles were prepared from liquors composed of Ag or Au NPs and commercial wetting and binding agents. The binder used was Effect SAX (HeiQ Materials AG, Switzerland), which is a blocked r isocyanate with cationic character, which de-blocks above 150^{o}C (i.e. in the curing phase). The textiles were treated using Ag concentrations reflective of application levels used in practice and our previous studies (Windler et al. 2013, Mitrano et al. 2014), approximately 30 - 80 mg metal/kg fabric in all treatments. The NP-containing liquid formulations were impregnated into 30 cm x 40 cm 100% polyester (PET) woven fabric pieces using a dual-roll padder operated at 2 m s^{-1} with 4 bar roll pressure followed by a stenter frame operated at 120 °C for two minutes and 160 °C for three minutes. The application procedure was carried out using a laboratory system that is representative of commercial industrial scale textile treatment systems. An edge zone of 1 ± 0.5 cm from each sheet was discarded and not used in the experiments. Fabric sheets were cut into 1 cm^2 squares and mixed to ensure representative sampling in each wash set, except for the fabrics used for x-ray absorption spectroscopy (XAS) analysis where 1 x 10 cm strips were used.

Laundry Detergent Solutions

Seven washing solutions were investigated, the same as used in Mitrano et al. (2015). Five were “grocery store brand” detergents from a Swiss store, are commercially available and intended for use in private homes. Two liquid detergents (“color” and “all purpose” (CL and APL)) and three powder detergents (“color”, “all purpose”, and “oxi” (CP, APP and OP)) were chosen. Additionally, two detergents (one liquid, one powder) was acquired from a company producing detergents for

industrial-scale laundering, *e.g.* for hospitals, nursing homes, restaurants, *etc.* (labeled industrial detergent; IL and IP). For brevity, detergent formulations are hereafter mentioned only by their abbreviations. In all figures, liquid detergents are highlighted in blue color, powder detergents in green and industrial detergents in orange throughout the manuscript. The detergents are distinguished by the presence/absence of oxidizer, the presence/absence of particulate matter and pH. The industrial detergents are purposefully stronger to increase brightening potential and kill microbial growth. In particular, the industrial liquid detergent can be diluted as a mixture with other detergents or used alone as an intense cleansing step after a normal washing cycle, as done here. For additional annotations regarding detergent compositions and their effects on Ag NPs in solution, see Mitrano et al. (2015).

All detergents were used at 4 g L^{-1} and diluted in DI H_2O and pH was measured using a Metrohm 827 pH meter. All detergents solutions had a pH values between 8.9 and 11.5, except for the commercial liquid detergent measuring 3.1. Chloride is an important ion that leads to precipitation of AgCl and so was measured in the raw (settled) solution by a Metrohm 733 ion chromatograph equipped with a MetroSep A Supp 5 column. Concentrations ranged from 0.5 to 5 mg L^{-1}, except the industrial powder detergent measuring nearly 12 mg L^{-1}.

Fabric Aging Procedure with Sunlight Irradiation (CEA)

Select sheets of fabric were subjected to accelerated aging in the Q-SUN Xe-3 Xenon test chamber (Q-LAB), which is meant to mimic exposure to full spectrum sunlight. Fabrics were exposed for 7 days (168 h; 870.7 kJ m^{-2} total irradiance) in the chamber at 70°C (black panel), 40°C (air, 50% humidity) and 1.44 W m^{-2} at 420 mm. QSUN exposure is represented graphically in all figures by red shading or text throughout the figures and tables.

Simulated Washing Procedures

The washing procedure was carried out as described in previous literature and ISO Standard 105-C06:2010, with some modifications for these specific solutions (Geranio et al., 2009; Lorenz et al., 2012; Windler et al., 2012; Mitrano et al., 2014). A Washtex-P Roaches laboratory washing machine was operated at 40 ± 2 rpm with steel vessels. Temperature was controlled by a thermostat, keeping the washing medium at a constant temperature of 40 °C ± 2 °C. A washing detergent volume of 20 mL was placed into polyethylene bottles (50 mL with a tight fitting cap to withstand the extra pressure created when oxidizing agents were in the solution) with 0.5 g of fabric (approximately 20 individual 1 cm x 1 cm squares) and 5 polyethylene balls (Ø 8 mm). One wash cycle consisted of a washing step (40 min), 2 rinse steps with DI H_2O (5 min each) and fabric drying in an oven at 40°C. Each washing experiment was conducted in triplicate and results are indicative of the average.

Simulated leaching test (TCLP)

One set of three unwashed fabrics underwent the TCLP test (The EPA standard Method 1311; Toxicity Characteristic Leaching Procedure) to determine the leaching behavior from this procedure alone. Triplicate samples of fabric swatches washed once or ten times (in either color or oxi detergent) were also submitted to the TCLP test. Extraction fluid was prepared by adding 5.7 mL glacial acetic acid to 500 mL of deionized water. Then 64.3 mL of 1N NaOH was added and diluted to a volume of 1 L. The pH was 4.93 ± 0.05. As called for by the standard TCLP leaching test, the solid to liquid ratio was fixed at approximately 1:20 by mass; which equated to 1 g of fabric in 20 mL extraction fluid. The sample was rotated end-over-end at 40 rpm at 23 ± 2 °C for a period of 18 ± 2 h. The speed of rotation was adapted to equal the washing test. Fabrics were removed from the extraction fluid, dried and saved for aqua regia digestion to determine total

metal remaining on fabric. An aliquot of the extraction fluid was processed through a 10 kDa cutoff ultracentrifugal filter and another aliquot was saved for total metals analysis. Both were acidified to 2% HNO_3 for further analysis by ICP-MS.

In addition to determining the total amount of metal leached from the fabrics during the TCLP test, we determined the stability of these particles in the leachate solution both in terms of the leachate matrix and the test conditions (*i.e.* end over end rotation). Both Ag and Au NPs (60 nm) were used to investigate possible aggregation and settling of particles under several test conditions. Solutions of 500 µg L^{-1} 60 nm Au particles and (separately) 200 µg L^{-1} 60 nm Ag particles in DI H_2O or TCLP extraction fluid were suspended in plastic containers to monitor total metal concentration in solution for 18 hours while solutions were either resting on the bench top, moderately stirred, or rotated (*i.e.* end over end rotation as in the TCLP test). The matrix of experiments was further expanded to include each of these variants with the addition of 2% surfactant (sodium dodecyl sulfate, SDS) to further promote stability in test conditions, which could be used as a "best case scenario" for further particle stability. Finally, a dissolved indium (In) internal standard of 300 µg L^{-1} was used throughout to monitor general metal stability in the solutions over the experimental regime. Sampling time points consisted of 0, 4, 8 and 18 hours where solution were sampled from the top of the experimental container and acidified to 2% HNO_3 for total metals analysis by ICP-MS

After 18 hours, samples were disposed of and sample containers were washed with a high concentration of acid for metal recovery. For silver solutions, a 20 mL mixture of 10% HNO_3 and 1% H_2O_2 was added to the empty experimental containers and shaken for 24 hours, with subsequent ICP-MS analysis to determine sorbed metal to the vessel walls. For Au containing experiments, 10% HCl was used.

The section below describing the characterization methods includes methods used for both studies.

A.3.1.2 Characterization methods

Fabric and Washing Solution Analyses

Total Au or Ag concentrations in the textiles were determined by acid digestion followed by ICP-MS analysis (7700, Agilent Technologies). In a test series of Au and Ag fabric digest procedures using microwave digestion with HNO_3, aqua regia, and HF, it was discovered that HNO_3 microwave digestion did not provide complete recovery of either the Au or Ag metal content. Therefore, all digestions were performed by aqua regia under the following scheme: 0.2 g fabric was digested in 6mL HCL (30%), 2 mL HNO_3 (65%), 1 mL H_2O_2 (30%) and 5 mL Milli-Q H_2O. Small white flocs persisted after the procedure (likely Ti residues from the fabric) and so the supernatant was transferred to a fresh bottle with final concentration of HCL at a minimum of 3% to stabilize metals until ICP-MS analysis.

In each washing solution, ultrafiltration (VIVASPIN centrifugal filters, 10 kDa cutoff) with subsequent acidification of the filtered solution to 2% HNO_3 was performed and Ag was quantified by ICP-MS. Additionally, aliquots were taken for spICP-MS after the wash cycle (without acidification). To prevent further particle dissolution or aggregation until analysis, samples

intended for spICP-MS analysis were diluted directly in DI water for spICP-MS measurements and stored frozen until analysis. Without dilution, it was found particle size distributions were not preserved well upon freezing, especially for powder detergent samples where it is hypothesized the detergent material acted as a seed for NPs to gather on as the solution froze. The typical initial dilution was 1:1000 for freezing, with additional dilutions as necessary to account for correct particle number concentration in each sample set as required by spICP-MS analysis.

Scanning Electron Microscopy (SEM)

AgNP loaded fibers were imaged using a SEM (NanoSEM 230, FEI). The SEM was operated at an acceleration voltage of 3 kV in immersion mode using the vCD (low voltage – high contrast) detector for image formation. For elemental analysis, the SEM was operated in low vacuum mode (0.7 mbar H_2O) at an acceleration voltage of 15 kV and images were acquired using a gaseous analytical detector. Elemental analysis was conducted with an EDX system (Inca suite, v. 4.15, with an XMAX80 detector, Oxford Instruments) attached to the microscope.

Scanning Transmission Electron Microscopy (STEM) and EDX

As in our previously published studies (Mitrano et al., 2014; Mitrano et al. 2015), washing solution(s) that contained nanomaterials were centrifuged under gentle conditions (500 rpm for 4 min) to settle large solids. The supernatant was transferred to new vials where particles were deposited directly onto TEM grids by centrifugation using a swinging bucket rotor, with rotation speed of 45000 rpm for 2 h; conditions which completely deposited all particles (density 10.1 g cm^{-3}) > 10 nm in size onto the carbon-coated Cu TEM grid.

Particle images were obtained *via* scanning transmission electron microscopy (STEM) combined with EDX for element detection using a JEOL 2200FS TEM/STEM operated at 200 kV. The nominal spot size of the STEM probe was 0.7 nm using a beam convergence angle of 10.8 mrad. High-angle annular dark field STEM micrographs were recorded using an inner detector angle of 100 mrad, while the bright-field STEM images were recorded with a detector angle of 15 mrad. EDX spectra of individual particles were recorded either by positioning the electron probe on a selected particle.

spICP-MS

For fabrics incorporating 100 nm particles, the size and qualitative concentration of particles in the wash solution after laundering was measured using single particle spICP-MS (7700, Agilent Technologies), as described according to published methods (Laborda et al., 2011; Mitrano et al., 2012; Mitrano et al., 2012(b); Mitrano et al., 2014(b)). Previous efforts showed the feasibility of high quality particle size analysis in washing detergents using this method (Mitrano et al., 2015), yet here we added an extension of sample preparation by diluting the solution to an appropriate concentration for spICP-MS, immediately freezing to prevent further particle transformation and thawing directly before sample analysis (Furtado et al., 2014). An Agilent 8800 ICP-MS was used with 5 ms dwell time was collected for 120 s. Instrument calibration utilized a blank and four dissolved Ag solutions made in 2% HNO_3 (0-1 µg/L), collected in spICP-MS mode. 100 nm Au ENPs (and associated dissolved Au calibration curve) was used for determination of transport efficiency on a daily basis. To monitor instrumental drift over time, a single 100 ng L^{-1} Ag or Au dissolved calibration check standard was analyzed in spICP-MS mode after approximately every ten ENP samples. If drift in the standard signal was detected, the particle sizing equation was adjusted accordingly for the change in sensitivity.

XANES

Silver speciation in the textiles was assessed by XANES. This technique was chosen as it provides many advantages including 1) accessing the overall Ag speciation; it is not just limited to the analysis of the textile surface, 2) it does not depend on species crystallinity, and 3) it is not limited to detection or presence of particles/NPs but can also measure non-particulate species. Silver K-edge XANES of the textiles were collected at the XAS beamline of the Australian Synchrotron. Analysis was performed on all the Ag NP treated textile samples pre-washing and the majority of samples post-washing in a similar manner to Lombi et al. (2014). The textile samples were tightly rolled and mounted, using polyimide tape, on a sample holder for analysis. Principal component analysis (PCA) of the normalized sample spectra was used to estimate the likely number of species contained in the samples and linear combination fitting (LCF) of the relevant standards was used to identify Ag species in the sample spectra. Data normalization and LCF were performed using Athena (Ravel and Newville, 2005), where the fitting range was -30 to +100 keV relative to the Ag K-edge. For each sample, the combination of standards with the lowest residual parameter was chosen as the most likely set of components. Species with values less than 10% of the total were not reported as such low representation is at the limit of the techniques' resolution capabilities.

Zeta Potential Analysis

Zeta potential of 60 nm Au NPs (3 mg L^{-1}) in DI water and TCLP solutions (standing and shaking) were measured on a Malvern Zeta Sizer instrument at time points of 0, 1, 2, 4 and 8 hours. At each time point, triplicate measurements were obtained, each consisting of 100 sub-runs to evaluate the zeta potential. An average of the three main measurements with standard deviation representing triplicate measurements is reported.

A.3.1.3 Results

Ag NPs in Washing Detergent Only

Analysis of Au Particles in Various washing solutions

60 nm Au nanoparticles were suspended in each detergent and analyzed before and after the simulated washing procedure (Figure A.3.1-1). This was done to ensure the matrices of the various solutions themselves or the washing process did not affect the analysis either in terms of recovered particle number or altering the pulse intensity for each nanoparticle event. Since Au particles are stable, we expected to size the particles similarly in each iteration of the experiment with similar particle number and size distributions regardless of the matrix. Apparent changes to particle size would indicate signal suppression due to the matrix (which was not expected because of the high dilution factor necessary for spICP-MS) while changes to particle number after the washing procedure would indicate a physical loss of the particles during the process (e.g. adhering to the side of the experiment container, aggregation and settling, and/or complexing to washing detergent components and settling).

No changes were observed either to particle size or number; indicating that the Au particles are suitable to be used as a conservative tracer in the experiments and that the various washing solution chemistries themselves did not affect spICP-MS analysis. This is true regardless of the washing detergent form (i.e. liquid or powder) or chemistry (i.e. variety of oxidizing agents, pH,

etc.). Therefore, we expect spICP-MS analysis to be representative of the particle size and number distribution in each experiment with no analysis complications due to the nature of the matrix.

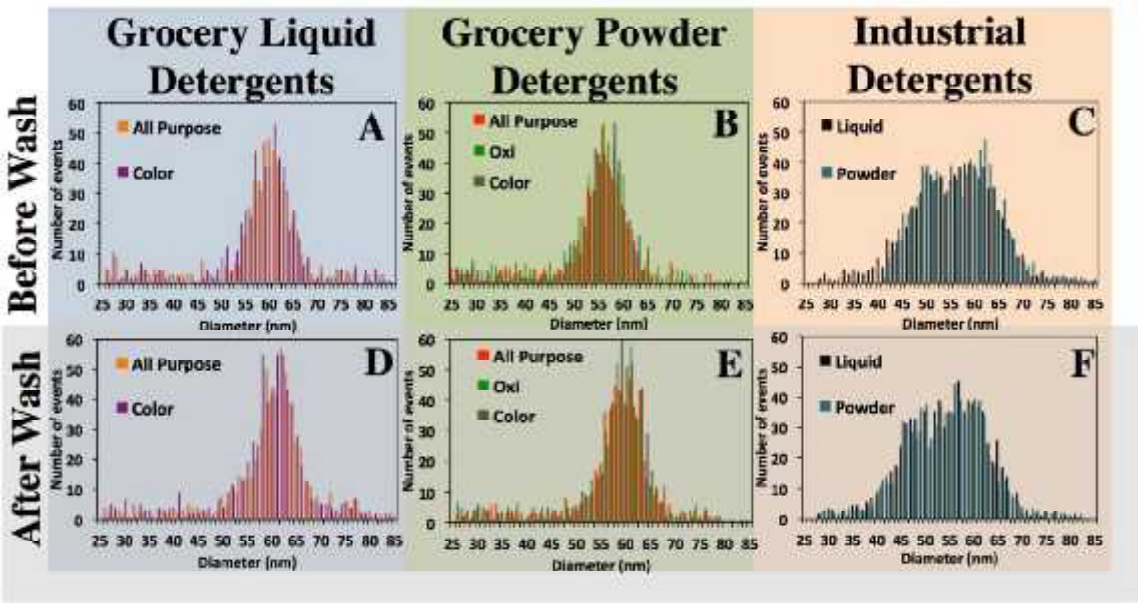

Figure A.3.1-1: 60 nm Au particle size distribution analyzed by spICP-MS in various washing solution chemistries, before and after simulated washing (average of triplicate samples). A) grocery liquid detergents before wash; B) grocery powder detergents before wash; C) industrial detergents before wash; D) grocery liquid detergents after wash; E) grocery powder detergents after wash; and F) industrial detergents after wash.

Analysis dissolved silver

Soluble silver species, as measured by ultracentrifugation, detected after washing 100 nm Ag particles in each of the detergents was a minimal fraction of the total silver added to solution, less than 2% of the total Ag in most cases. The exception to this was the industrial detergents, where the powder form dissolved 6% of the total Ag added as ENPs and the liquid form completely dissolved all Ag. This indicates that, aside from the industrial liquid detergent, outright dissolution of particles to remain as Ag^+ is not a prominent fate in the detergent solutions. Upon $AgNO_3$ addition to grocery powder detergents, a minimal fraction (less than 5%) remained in the dissolved form after the simulated washing procedure.

Behavior of $AgNO_3$ and Ag-ENP in Various Washing Solutions

Both Ag-ENPs and $AgNO_3$ were added into the washing solutions and analyzed for particle number and particle size by sp-ICP-MS. Average histograms of triplicate experiments for each of these experiments can be found in Figure A.3.1-2. Two representative example TEM images of Ag ENP suspended in each solution after the washing procedure and in solutions where $AgNO_3$ produced pulses by spICP-MS are depicted in Figure A.3.1-3.

Grocery Liquid Detergents

No particle formation (with sizes over 30 nm, the approximate detection limit of the spICP-MS technique under these conditions) was detected with the addition of $AgNO_3$ in the liquid detergents and no dissolution was observed to the ENP added in the liquid samples (Figure A.3.1-2, panels A-D). Along with the negligible size change in the TEM analysis (Figure A.3.1-3, shaded blue boxes), there were few visible surface changes to the particles with no appreciable speciation change from the pristine metallic Ag ENPs. Moreover, the particle number found before and after washing (and between the color and all-purpose detergents) is the same; indicating the particles are stable and neither settle from solution nor adhere to the sample container during the wash cycle.

Grocery Powder Detergents

Particle formation was visible with the addition of $AgNO_3$ in all powder detergents, both before and after the washing procedure. In Figure A.3.1-3, TEM shows that very small metallic ENPs form, but are often grouped in or around larger silicate or titanium-based materials originating from the washing solution.

ENP size in the grocery powder color detergent did not change appreciably during the washing process and the number of distinct particles detected remained constant before and after treatment. (Figure A.3.1-2, panel F) Conversely, a significant particle distribution shift to smaller sizes was noted in both the all-purpose and oxi detergents (Figure A.3.1-2, panels H and J, respectively), likely due to the increased concentration of peroxide in these solutions. The distribution of particle size became broader and additionally 40% more distinct particles were observed in the all-purpose solution after washing. In the oxi detergent, the individual particles measured by spICP-MS nearly doubled. Furthermore, the change in particle distribution is seemingly similar between both the all-purpose and oxi experimental sets, despite the all-purpose detergent having approximately only half the concentration of oxidizing agent contained in the formula; added as sodium carbonate peroxide at 6 wt% and 13 wt%, respectively.

Industrial Detergents

There were no particles observed by spICP-MS upon $AgNO_3$ addition to the liquid variant of the industrial strength washing solution (Figure A.3.1-2, panel K), and markedly less particle formation in the industrial powder formulation (Figure A.3.1-2, panel M) versus the grocery powder detergents. The excessive concentration of oxidizing agents, in partnership with the very low pH in the liquid formulation, is likely responsible to keep added $AgNO_3$ dissolved over time.

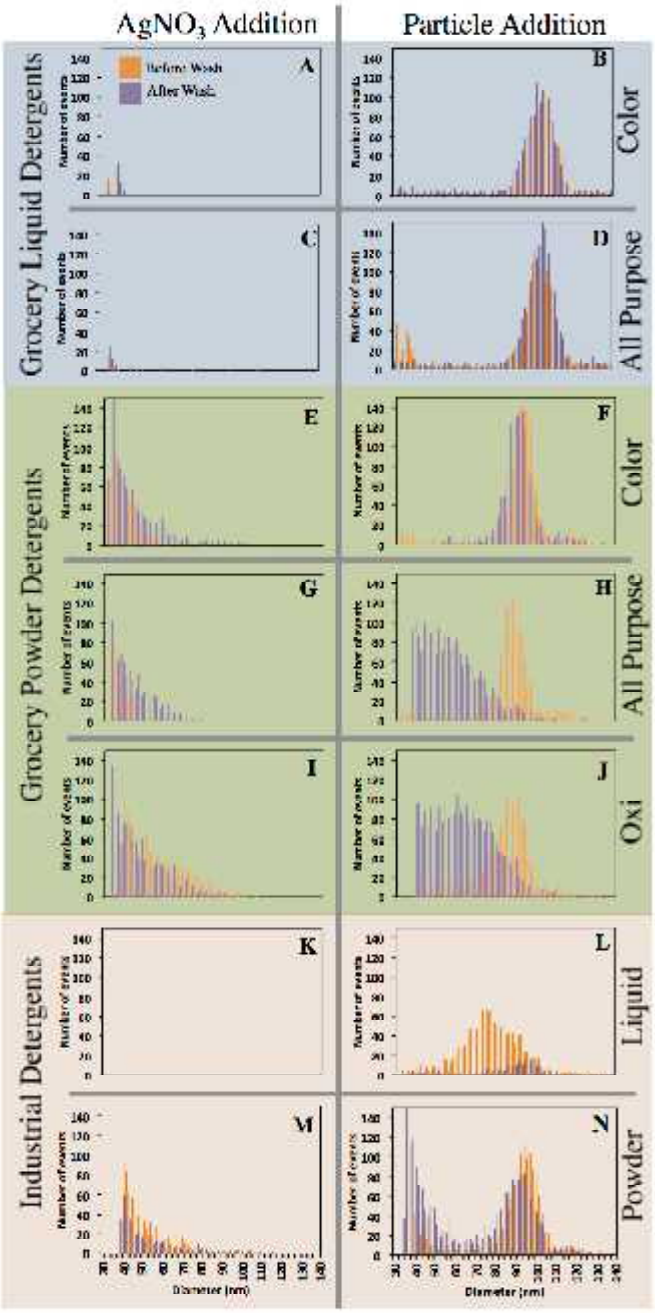

Figure A.3.1-2: Averaged histograms of triplicate sample analysis of the addition of $AgNO_3$ or 100 nm citrate-coated Ag nanomaterials to a variety of washing solutions; analyzed by spICP-MS before and after a simulated washing procedure. Two household liquid detergents are shaded in blue (color detergent panels A and B; all-purpose detergent panels C and D) with measured Ag particles found before and after wash indicated by orange and purple histograms, respectively. Powder variations of household detergents are shaded in green (color detergent panels E and F; all-purpose detergent panels G and H; oxi detergent panels I and J). Finally, two industrial strength detergents, highlighted in peach, were investigated both in liquid (panels K and L) and powder (panels M and N) forms.

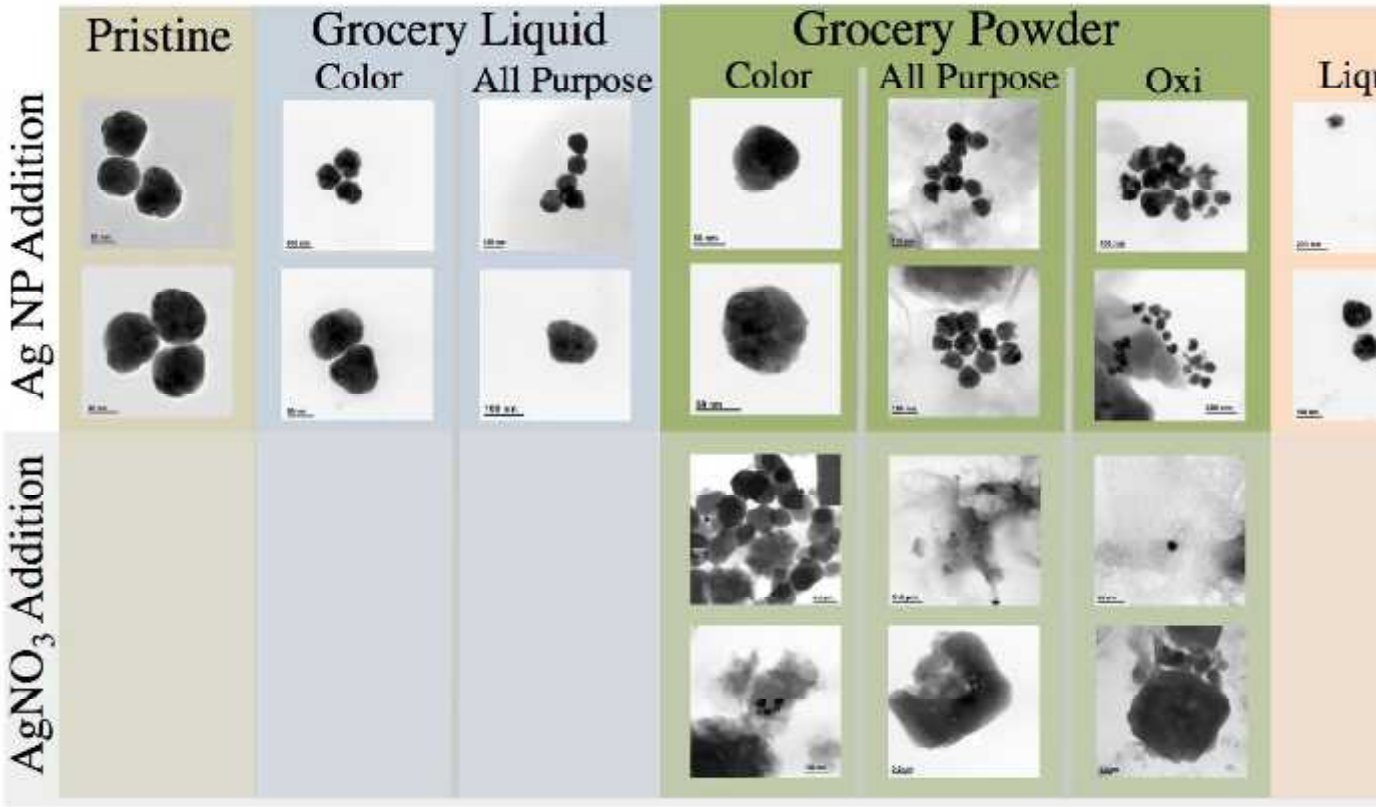

Figure A.3.1-3: Two representative STEM images each of pristine Ag nanomaterials (beige shading), suspended in gro shading), grocery powder detergents (green shading) and industrial detergents (peach shading); all after the washi particulate material formed through the addition of $AgNO_3$ to grocery powder detergents is depicted in the light gree

The ENPs added to the industrial liquid detergent had a very rapid and significant size and distribution change (Figure A.3.1-2, panel L). Even prior to washing, the particle size decreased in the short timeframe between sample preparation and analysis (maximum 15 min), relaying the strength of this solution. After the washing procedure, few particles remained in solution and the majority of Ag measured by spICP-MS analysis and ultracentrifugation and ICP-MS analysis was in dissolved form. In this regard, the industrial liquid detergent promoted the highest dissolution extent of any detergent studied here. ENP addition to the industrial powder detergent resulted in markedly less change than the liquid variant, with only slight particle size change to the primary particle histogram (Figure A.3.1-2, panel N). However, an increase in smaller sized Ag material was also observed after washing, as was seen previously upon addition of $AgNO_3$ to powder detergents. TEM analysis of the particles in both the liquid and powder variants of the industrial detergents depict a smooth, regular surface structure (Figure A.3.1-3, shaded peach) with EDX analysis confirming only metallic Ag.

Influence of water chemistry on washing profiles

Characteristic degradation profiles remained constant for grocery color detergents and oxi detergents regardless of if the solutions were made in DI or tap water. While previous studies suggested that the additional free residual chlorine in tap water promoted faster dissolution of particles than in DI water (Mitrano et al., 2014(b)), in this case the detergent chemistry appears to be the driving factor for either particle stability (e.g. in color detergent) or size changes (oxi containing detergents).

Continued degradation profiles of Ag ENPs after initial wash cycle

Initial, short contact/exposure time of Ag ENPs to an aging procedure (such as washing) can change the degradation profile over time, where particles may have different dissolution rates, surface chemistry reactions, agglomeration rates, etc. As described in section 3.5, there was little change both to the Ag ENP size (distribution) and surface characteristics when washed in color detergent on the first day. However, spICP-MS analysis indicates that over time (2 days and 5 days after washing) the particle size decreases and the size distribution becomes increasingly widespread (Figure A.3.1-4, panel A), yet the particle number stays approximately constant over five days. The particle surface continued to evolve over time: with more pitting on the surface noted, and small Ag “droplets” forming around the primary/parent particles (Figure A.3.1-4). Furthermore, by day 5, there is an increasingly complex speciation change noted, in some cases with Ag associated strongly with Si or O, suggesting binding with zeolites from the detergent or precipitation of new particle formations.

In sharp contrast, there is little change to particle size (and distribution) for solutions washed in oxi detergent over time. This indicates that changes which occur to particles in these solutions, at least in terms of particle size distribution occurs during the initial wash treatment and remains constant and unchangeable over time. Indeed, the particle surface chemistry in the all-purpose and oxi detergents is changed significantly, with evidence of Ag/O and Ag/S formation, which can inhibit further particle dissolution of the primary particles. A number of Ag complexes did not resemble the original particle in size or shape at all, suggesting that the ionic Ag released from the particles during the first wash re-precipitated alongside the other washing solution components over the course of time but were stable thereafter.

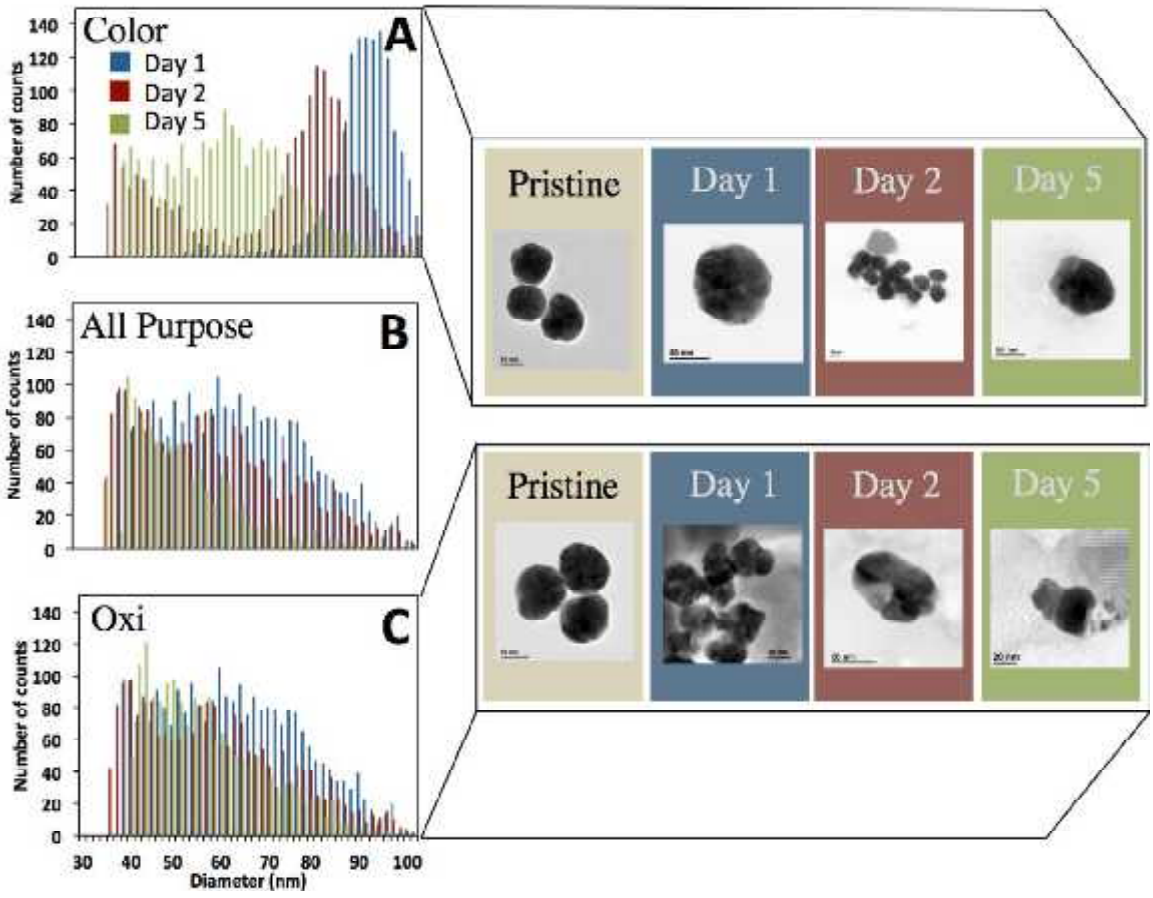

Figure A.3.1-4: Averaged histogram of triplicate samples of 100 nm Ag particles which underwent a simulated wash cycle in various grocery powder detergents (panel A, color; panel B, all purpose; panel C, oxi) over multiple time points (Days 1, 2 and 5 with blue, red, and green histograms, respectively). Representative TEM image examples of nanoparticulate Ag found in color and oxi grocery powder detergent varieties over time intervals of 1 day (blue shading), 2 days (red shading) and 5 days (green shading). Reference of the pristine 100 nm particles shaded in beige.

The dominating factor for particle change lies in the type of detergent that is used rather than the chemistry of the water used for washing; which did not have any discernable influence. The higher buffering capacity of the detergent solution likely compensates for the residual chlorine found in the tap water solution, where in un-buffered systems dissolution had previously been shown to be an important particle transformation in this matrix (Mitrano et al., 2014(b)). This suggests that differences in water treatment facilities in different locations or natural variations in the water chemistry used for washing may be inconsequential to particle (in)stability when compared to the detergent which is selected for laundering clothing. How different solution chemistries effect NP transformations can is outlined in the Venn diagram in Figure A.3.1-5.

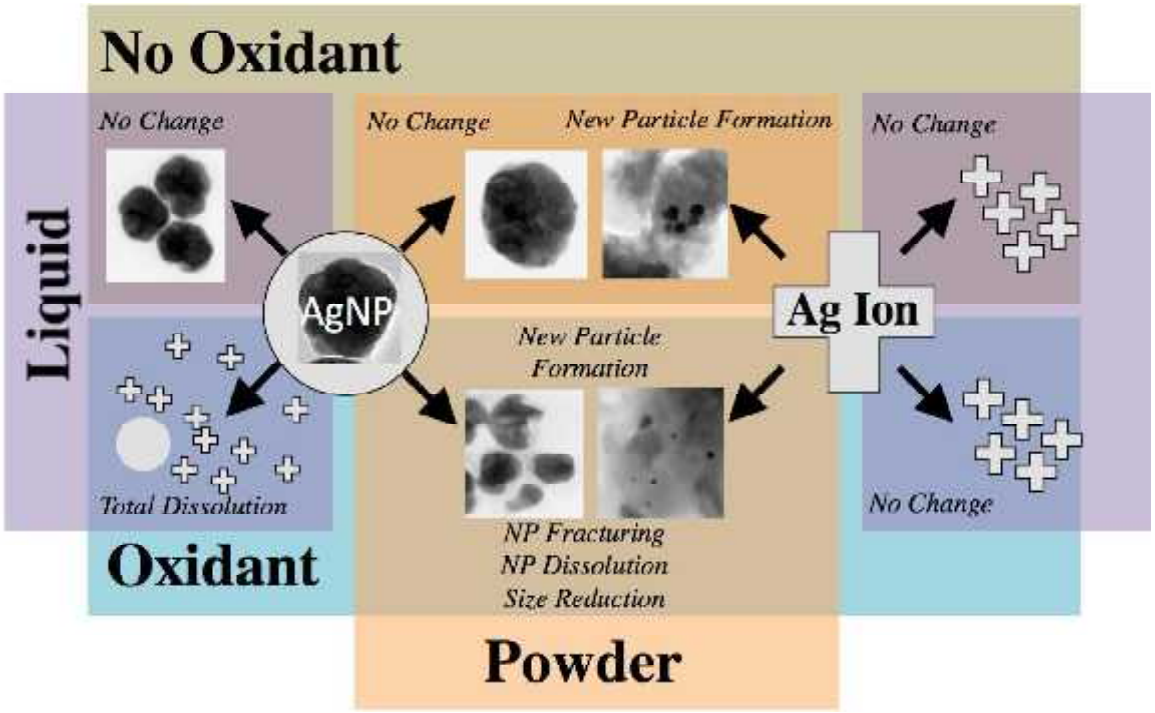

Figure A.3.1-5: Venn diagram of the most likely transformations of Ag ENPs or Ag^+ added to various washing detergent solutions. TEM images depict examples of particles found in each condition. Note that a characterization defined as "no change" means no changes detected by our experimental techniques: e.g. screening by spICP-MS with further characterization of particulates measured by TEM. Furthermore, the figure does not explicitly depict the possibility of silver adhering to washing particulate matter or binding with washing solution additives, which could occur in any of the solutions.

Nanoparticles released from nano-enhanced Fabrics

Many previous washing studies of nano-enhanced textiles are too limited in scope to suggest which properties of either the NP or aging truly influences the transformation and release of NPs during their use. The experimental procedures followed in this work combines a comprehensive selection of NP properties (size: 20 and 100 nm, capping agent: PEG and citrate, metal: Ag and Au), precise incorporation into laboratory prepared fabric, sequential aging parameters under many conditions (sunlight irradiation, washing with 7 different commercially available detergents: with/without oxidizing agents, powder/liquid form) and complete characterization of NPs which remain on the textiles and are released into the wash water (Figure A.3.1-6). Washing formulations included 5 purchased from a grocery store; two liquid detergents ("color" and "all purpose" (CL and APL)) and three powder detergents ("color", "all purpose", and "oxi" (CP, APP and OP)) as well as two industrial scale detergents (one liquid and one powder; IL and IP). For brevity in the text and figures, detergent formulations are mentioned only by their abbreviations, explanation of which can be found in the materials and methods section. By studying several different textiles with known additives prepared and aged in the same fashion, we can tease out which factors of NP choice, fabric composition, or use parameter is most responsible for NP transformation and/or release from nano-textiles.

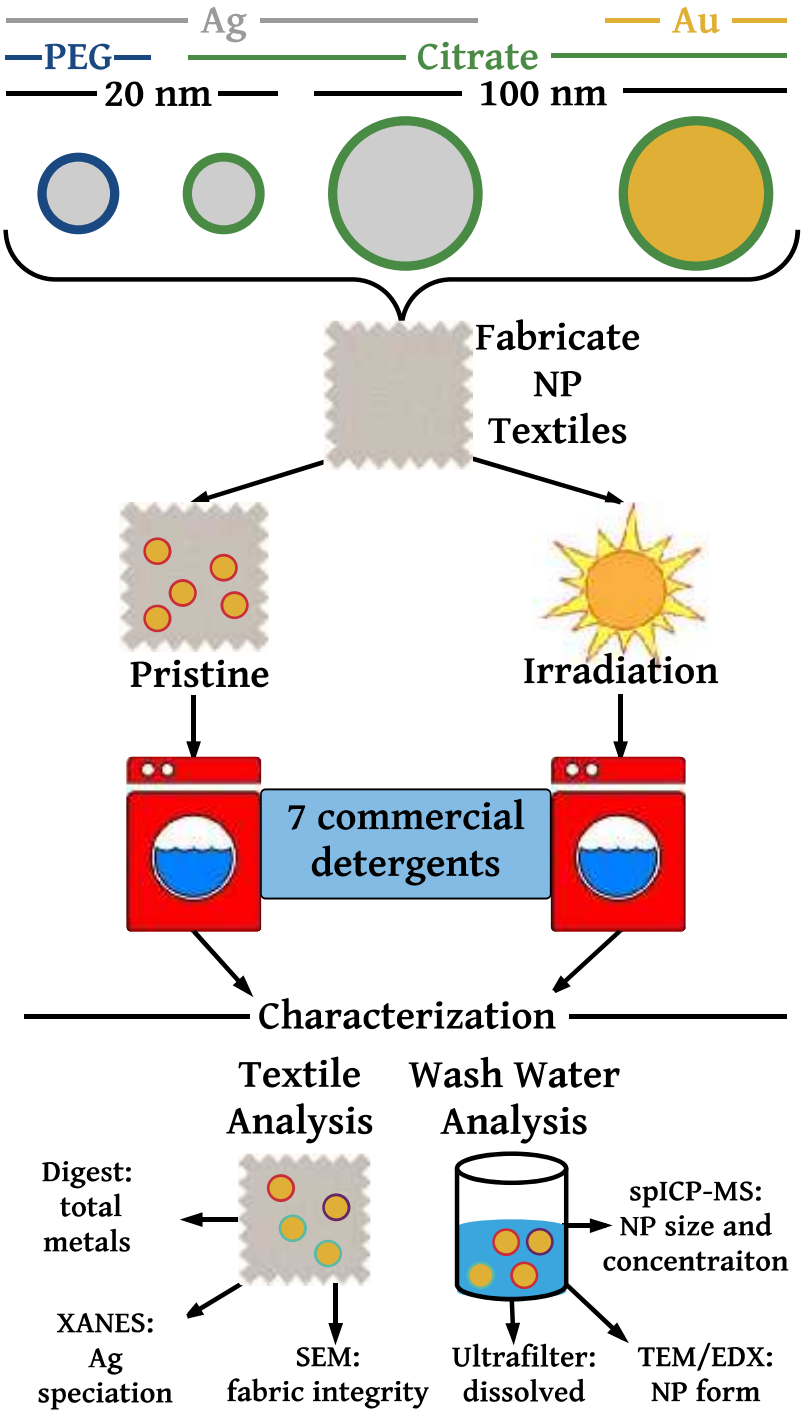

Figure A.3.1-6: Schematic of NP selection, textile fabrication, exposure and the analysis/characterization of both the fabric and wash water.

Physical integrity of fabrics through the aging processes

The amount of Ag release is not solely dependent on (changes to) the Ag NP chemical structure but also to the morphological and topological properties of the fibers, which influence the Ag mode of binding, adhesion ability, adsorption capacity and moisture content necessary for Ag release (Simončič

and Klemenčič, 2015). The physical integrity of the fabric remained intact throughout the different aging tests despite the physical stresses they underwent during simulated sunlight (QSUN) exposure and washing, as assessed by SEM analysis (Figure A.3.1-7). Small bright dots on the fabric surface are expected to be Ag NP, though no chemical identification was possible under these imaging conditions. Some smoothing appears on the surface of the fabrics in the post-washing images, which may be indicative of residual washing residue not removed in the rinse cycles. Nevertheless, since the textile fibers do not appear to be physically damaged we assume that the majority of silver and gold releases observed in the wash solutions originated from the release of metal from the surface treatment and not attached to fiber fragments.

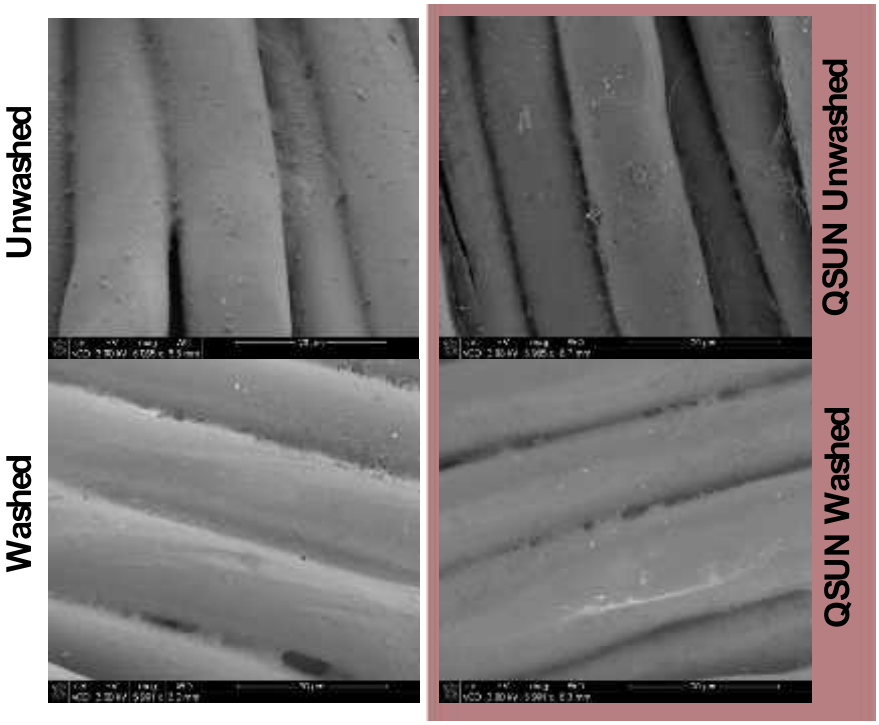

Figure A.3.1-7: SEM images of 100 nm Ag treated fabric; which have undergone various (and sequential) aging treatments including QSUN exposure and washing in oxi detergent. Ag particles can be seen simply by small bright dots. Fabric fibers are fully intact under all conditions, though some smoothing appears to have taken place post-washing, which may be indicative of residual washing residue not completely removed in the rinse cycles.

Washing induced releases of ENM from fabrics

Our previous studies concerning the washing of silver containing textiles (both conventional and nano varieties, fabricated with these same conditions) with a standard laboratory detergent (containing no oxidizing agent) approximated the release of silver between 10 and 35% (Mitrano et al., 2014). Furthermore, when investigating the behavior of Ag NP in a variety of washing detergents, we concluded that those which contained a higher concentration of oxidizing agent resulted in enhanced oxidative dissolution of the Ag particles over the course of the wash cycle, though no changes to Au particles were observed (Mitrano et al., 2015). Physical incorporation of the NPs with the fabric and the external washing environment (i.e. mechanical abrasion and chemical wear) are both contributing factors to the concentration and form of release. With this framework in mind, we systematically determined which factors are responsible for the metallic material released into the wash water.

As an example, for the 20 nm citrate and PEG Ag sample treatments, the transformation and/or release of Ag material can be noted visually due to the color change before and after washing. The Ag NP suspension stained the application liquor a pale yellow, which was visible on the treated fabric and has been a noted side effect before due to the reflectance intensity which corresponds to the plasmon resonance band of Ag NPs (Ilić et al., 2009). However, upon washing the fabric in the various detergents this coloring appeared faded; which was visually approximately inversely correlated with the strength of the oxidizing agent contained in the corresponding detergent used. However, this visual observation cannot distinguish between detachment of the particle from the textile (release) and dissolution of the Ag, where the paler color after washing could be due to partial dissolution. Therefore these visual observations can simply be indicative of Ag transformations during the wash cycle.

Because Au is an inert metal, the incorporation of Au NPs onto the textiles served as a measurement for the physical release of NP associated only with mechanical stress on the fabrics during the washing process or of material which was only weakly bound to the textile surface. Despite the drastically different washing detergent chemistries, a constant amount of Au was retained on the fabrics, with approximately 85-90% of the Au recovered after fabric acid digestion (Figure A.3.1-8). This suggests a baseline of particulate release from the first wash due to purely mechanical stress, either because the particles were not fully imbedded into the binder during the textile fabrication process and/or because the mechanical abrasion in the washing containers released particles from the textile surface. While it is possible that some chemical factors may have broken down the matrix of the binder and/or textile threads to release Au particles, this is less likely given the very different chemical properties of the various detergents and the evenness with which Au was released across the experimental set.

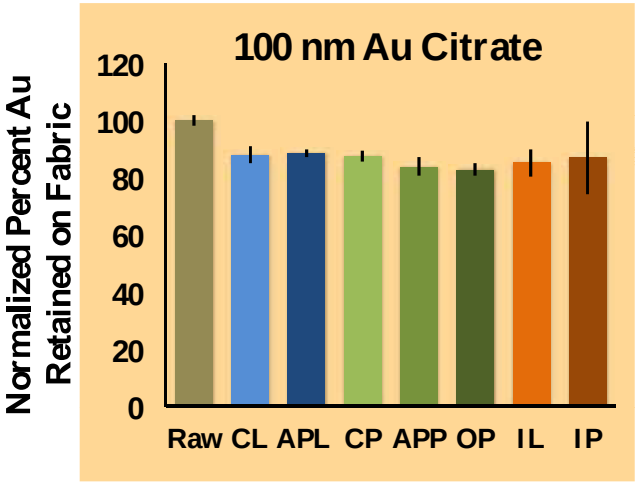

Figure A.3.1-8: Concentration of Au remaining on fabric after one wash cycle as determined by aqua regia microwave digestion of fabric and ICP-MS analysis, normalized to unwashed (raw) fabric. Blue bars indicate grocery liquid detergent varieties, green grocery powder and orange industrial detergent. Error bars indicate standard deviation of duplicate fabric washes and digests. The amount released in this case represents the mechanical stress of washing and/or mechanical removal or particles by the detergents; i.e. a lower threshold of possible release of NPs from the fabric under these washing conditions. For details on washing detergent composition, see methods section.

In contrast to equal release of Au across all washing conditions, variable Ag release was noted with different detergents, ranging from approximately 10 to 25 percent for most detergents to over 75% for the IL detergent. The dominating factor affecting release across all textile treatments was the detergent chemistry where those containing oxidizing agents released more silver (*e.g.* APP, OP, IL and IP). Mild detergents, i.e. those containing no oxidizing properties, released similar concentrations of Ag as Au, suggesting predominantly mechanical release was at play in those systems. Severity of oxidant often directly correlated with Ag release, where, for example, in the strongest detergent, IL, only 20% of the Ag remained on the fabric after one wash.

The preferential chemical release of Ag compared to the mechanical release of Au is depicted in Figure A3.1_10, where the ratio of the relative gold release to the silver release is shown. A ratio larger than 1 refers to a preferential release of Ag over Au. The amount of Ag released from the textiles is shown by grey dots. Detergent chemistry plays a large role in concentrations of Ag released, where those containing oxidizing agents clearly assist in release of Ag particles from Ag NP functionalized textiles (but less so of Au NPs), inferring an additional chemical release reactions specific to Ag. Nevertheless, taken as a whole, the detergent chemistry and (additional) chemical release of Ag compared to Au is of relatively minor influence, expect in a few cases, such as the stronger industrial detergents or Ag capped with PEG.

An additional factor that influenced the concentration of metal that was retained on the fabric after washing was the Ag NP coating composition. 20 nm and 100 nm citrate capped Ag NP treatments released similar concentrations of metal for the majority of treatments, yet the 20 nm PEG capped Ag NPs released significantly more metal in the wash solutions containing oxidizing agents (Figure A.3.1-9C). We hypothesize this is due to the interactions of the capping agent and the binder. In this instance, the binder used was a blocked polyisocyanate with cationic ion character; so the citrate capped particles (negative ionic charge) may more strongly bind to the matrix than the PEG capped particles (neutral) in the matrix. This disparity is also noted when compared to the release of Au particles, which were also citrate coated (Figure A.3.1-10, panel B).

However, when fabrics were first irradiated by the QSUN and then washed (Figure A.3.1-9 panels B, D and F), less Ag was released than when washing alone (Figure A.3.1-9 panels A, C and E) for all detergent types and all across all Ag NP treatments. While the strongest bleaching detergent still leached the most amount of Ag from the fabrics, the overall chemical influences were reduced as compared to the amount of Au released from the fabrics (Figure A.3.1-10, red dots). The continuous release of Ag^+ and Ag^0 is only possible if Ag is bound to the fibers through physical sorption (Montazer et al., 2012); chemical binding of Ag to the fibers may significantly reduce the release of Ag^+ into solution (Klemenčič et al., 2013). Therefore, the influence of the QSUN irradiation to inhibit Ag release may be caused by changing the linkages of Ag to the fiber/binder. For example, UV irradiation has been shown to form silver polyacrylate complexes and these species are very stable against re-oxidation (Ershov and Henglein, 1998; Ershov and Henglein, 1998(b); Falletta et al., 2008), which would be a limiting step in the further oxidative release of Ag NPs in subsequent washing procedures. Additionally, photoreduction of Ag^+ on the particle surface decreases the amount of oxidized silver available for dissolution and may thus result in a better-crystallized metallic Ag that is less prone to dissolution. Therefore the main mechanism to inhibit Ag NP release from the textile is either a stronger particle bonding to the fabric or the formation of more binding sites for the Ag that is not dissolved during the washing process, or some combination of both possibilities.

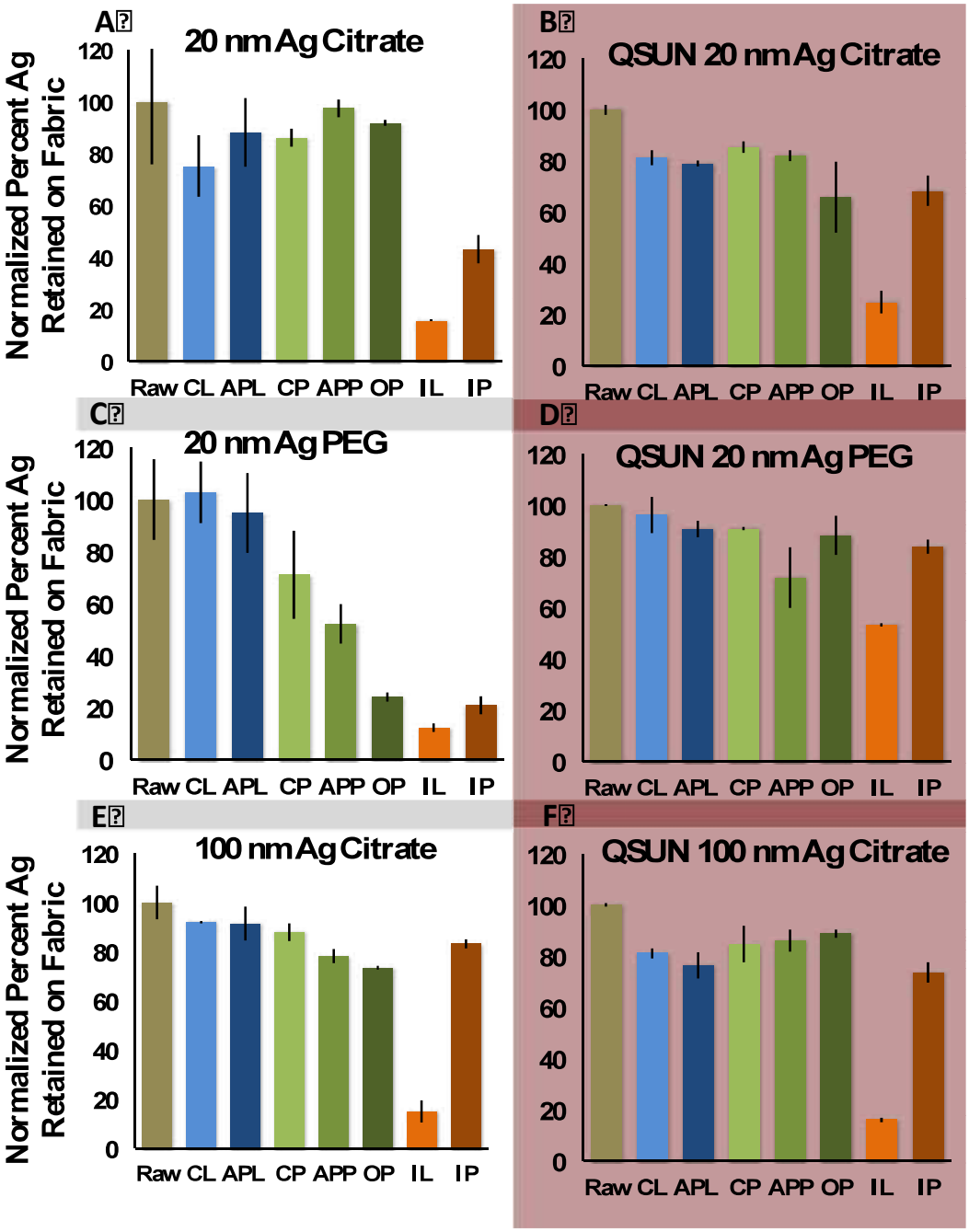

Figure A.3.1-9: Concentration of Ag remaining on fabric after one wash cycle as determined by aqua regia microwave digestion of fabric and ICP-MS analysis, normalized to unwashed (raw) fabric. Blue bars indicate grocery liquid detergent varieties, green are grocery powder and orange are industrial detergent. Error bars indicate standard deviation of duplicate fabric digests. Three Ag NP variants are depicted with 20 nm citrate, 20 nm PEG and 100 nm citrate in plots A, C, and E, respectively. Corresponding sequential aging procedures (sunlight exposure and subsequent washing) are shown in plots B, D, and F. For details on washing detergent composition, see methods section.

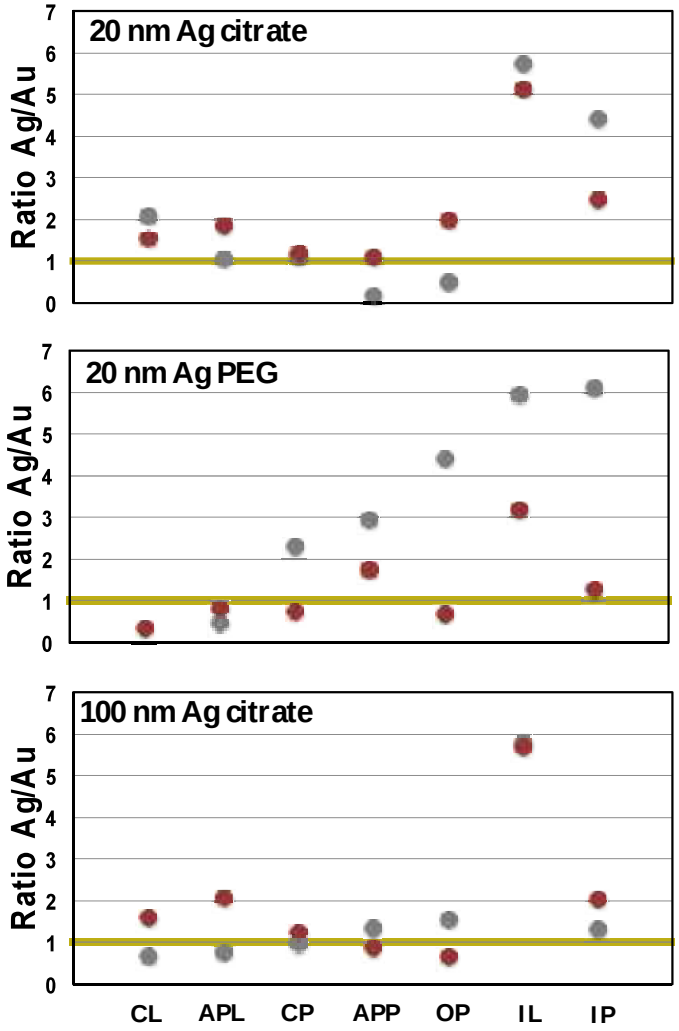

Figure A.3.1-10: Ratio analysis of preferential chemical release of Ag compared to mechanical release of Au with 20 nm Ag citrate capped NPs; 20 nm Ag PEG capped NPs and 100 nm Ag citrate capped NPs. Yellow line at one represents the release of Au from fabrics under each washing condition. Grey dots are fabrics only washed, red dots are fabrics with sunlight exposure and subsequently washed.

Metal in the wash water: total metal and particulate analysis

Analyzed by spICP-MS, Au recovery from all washing detergent varieties showed no change in particle size distribution compared to the pristine particles (Figure A.3.1-11). This confirmed that 1) NPs were released directly from the fabrics into the wash water, 2) given the sample preparation scheme (*e.g.* dilution in DI water, freezing, thawing and analysis by spICP-MS) we achieved reproducible results of particle distributions (i.e. no agglomeration, *etc.*) and 3) primary Au particle size was not altered in any detergent solution. With the spICP-MS technique, total concentration of metal released can also be estimated and directly compared to releases determined by fabric digestion and total metals analysis. Although the spICP-MS concentration sometimes over estimated metal concentrations as compared to fabric digest results (especially in liquid detergents) and other times underestimated the concentration, values were in the same order of magnitude, which, given the differences between measurement analyses, we consider this good agreement.

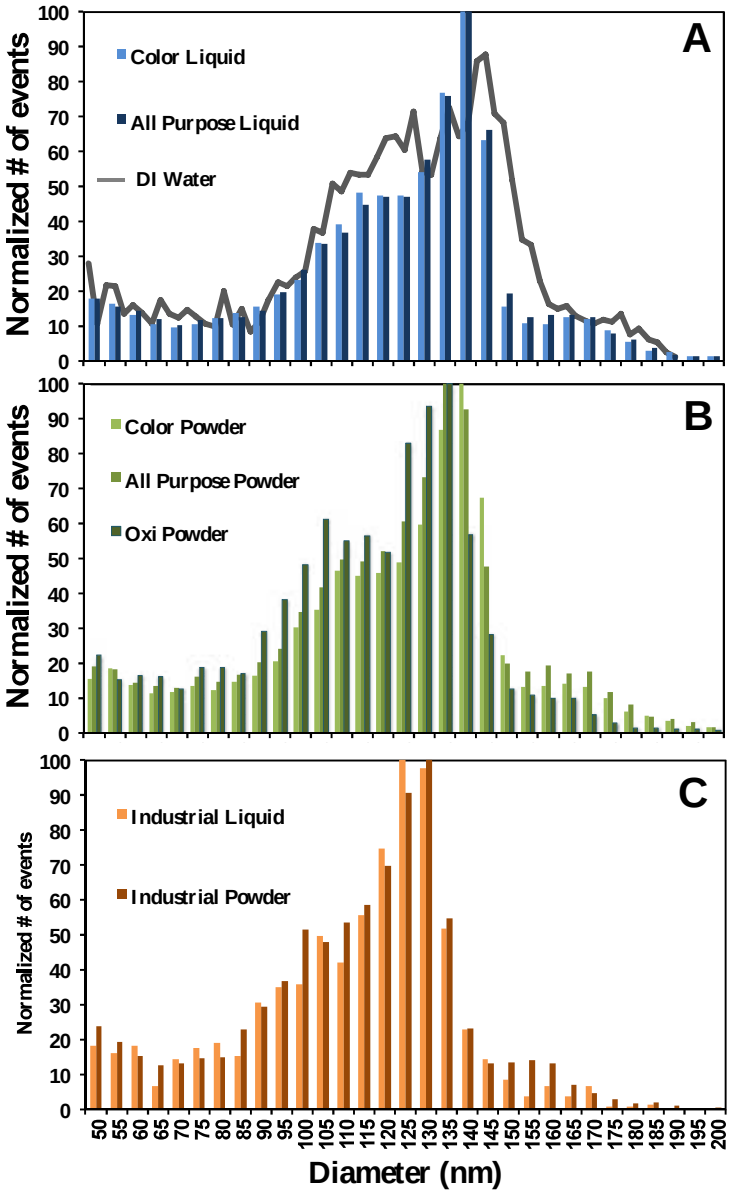

Figure A.3.1-11: Au NPs released into wash water from fabrics washed in various detergents as determined by spICP-MS. Grocery liquid detergents (panel A, liquid and all-purpose variants represented by light and dark blue bars), grocery powder detergents (panel B, color, all purpose and oxi detergents represented by increasingly darker green bars) and industrial detergents (panel C, liquid and powder variants represented by light and dark orange bars) had similar particle release profiles. Each histogram is the average of triplicate measurements, normalized for total particle release after background subtraction. Dark trance in panel A is the 100 nm Au NP size distribution analyzed by spICP-MS in DI water.

Particulate Ag in the washing solution was measured by spICP-MS for grocery store liquid and powder variants for 100 nm Ag standard textiles and those exposed to simulated sunlight (Figure A.3.1-12), but particle recovery was not high enough to definitively determine a size distribution for fabrics washed in industrial detergents by this method. The wash water from fabrics containing 20 nm particles were not analyzed because the size (distribution) was too close to the detection limit of spICP-MS. Ag particles washed in grocery liquid detergents did not have a significant change in particle size (Figure A.3.1-12A) compared to the pristine particles nor did size or surface structure appear

different with TEM analysis (Figure A.3.1-13A). All particles imaged by TEM were found to be metallic Ag as assessed by EDX measurements. While there was a slight downward shift in particle size in the grocery detergent which had the highest amount of oxidizing agent (Figure A.3.1-12C, oxi powder), the minimal change in particle size is a large contrast to the notable size changes to particles suspended in oxidant containing washing detergent alone in our previous work (Mitrano et al., 2015). At least two factors may contribute to this difference: 1) when fabrics are washed in the detergent, the oxidizing agent also reacts with the textile and so less is available to interact with the particles on the textile or when particles are released into solution and 2) the particles are, to some extent, physically encapsulated by the binder and so are less permeable to oxidative dissolution than pristine particles which remain free in suspension. While no coating was distinctly visible on the NP surface (Figure A.3.1-13C), the particles appear visually more intact when released from the fabric than when simply suspended in oxi detergent (Mitrano et al., 2015). As with the Au analysis, total released Ag concentration as assessed by spICP-MS was in the same range as the concentrations measured by fabric digest, and only a very small fraction (< 1%) was dissolved except in the case of the IL detergent, where approximately 20% was dissolved. Likewise, with the 20 nm particles of both capping agents, a minimal concentration of Ag was noted in the ultrafilter analysis except in the stronger industrial detergents.

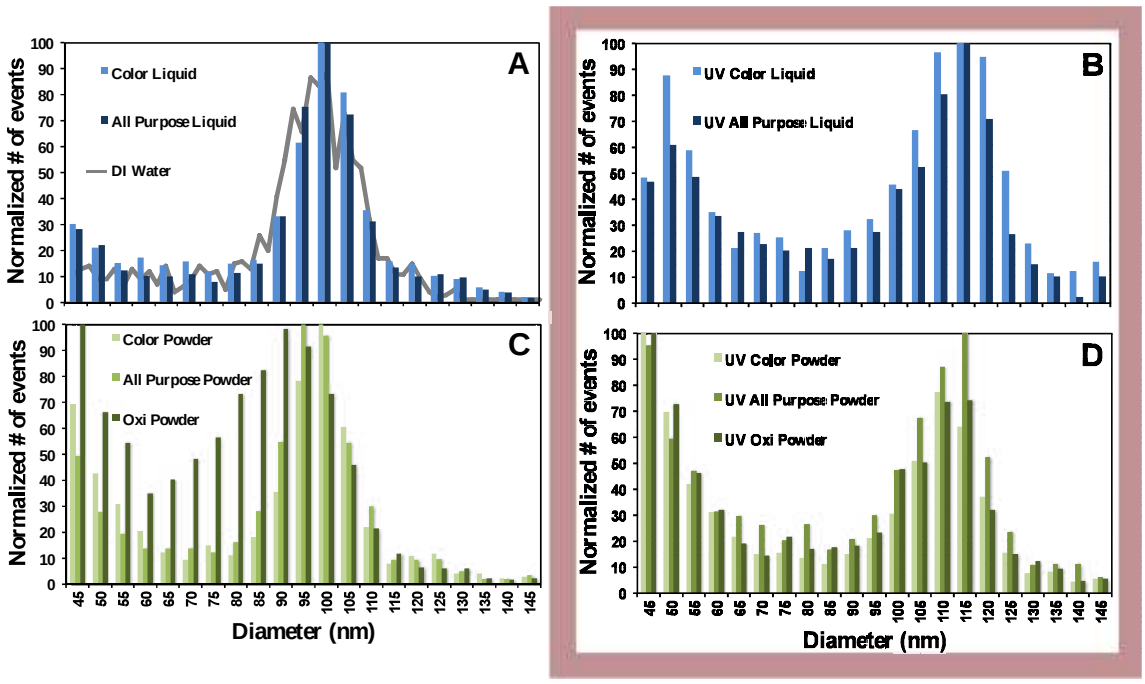

Figure A.3.1-12: Ag NPs released into wash water from fabrics washed in various detergents as determined by spICP-MS. Grocery liquid detergents (panel A, liquid and all purpose variants represented by light and dark blue bars) and grocery powder detergents (panel C, color, all purpose and oxi detergents represented by increasingly darker green bars) and sequential aging of fabrics from QSUN solar spectrum then washing in grocery liquid detergents (panel B) and grocery powder detergents (panel D). Each histogram is the average of triplicate measurements, normalized for total particle release after background subtraction. Dark trance in panel A is the 100 nm Ag NP size distribution analyzed by spICP-MS in DI water.

For fabrics which underwent simulated sunlight (QSUN) exposure prior to washing, two discrete particle size distributions are apparent in the wash solution: the unaltered, primary particle size and smaller particles, i.e. < 50 nm; presumably also including particles smaller than the size detection limit of spICP-MS of 30 nm (Figure A.3.1-12, panels B and D). There does not appear to be differences in the distributions due to the washing detergent, but rather the physical structure of the particles has been altered, as seen by TEM analysis of the particles released into the wash water (Figure A.3.1-13, panels B and D). As with the non-irradiated samples, all particles imaged in the detergent solution were metallic Ag, as evidenced by EDX analysis of particles. The concentration of Ag released after washing is less for the textiles that were exposed to sequential aging as determined by fabric digestion, yet as before the fraction of NPs released when calculated by spICP-MS is overestimated.

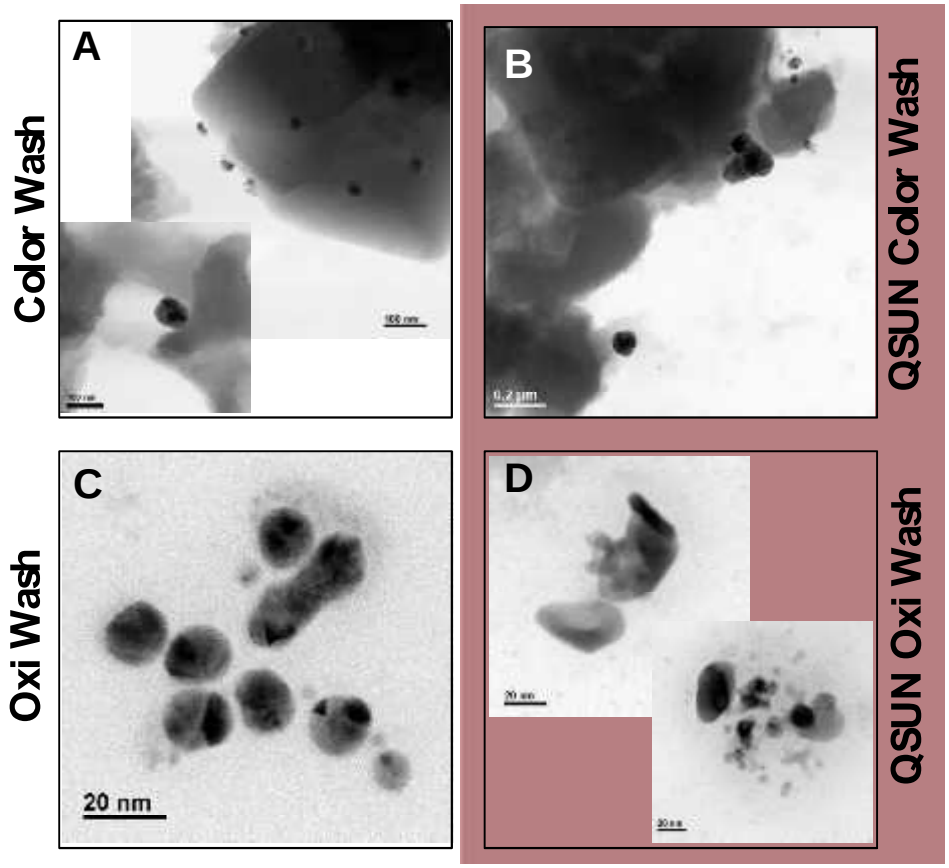

Figure A.3.1-13: Representative TEM images of Ag particles released from fabrics in wash water in grocery color powder detergent (panel A), UV aging with grocery color powder detergent (panel B), grocery oxi detergent (panel C) and UV aging with grocery oxi detergent (panel D). Particles found were either metallic Ag or Ag with associated Si. Particle size and form varied by detergent, with particles similar to primary particles in the color wash solution, fused particles in the UV and color detergent (but with similar size to primary particles), or particles of varying size which appeared fractured along clearly defined lines in oxi detergents (either with or without the additional UV treatment).

Silver on the textiles: speciation changes across subsequent treatments

Washing textiles with different detergents resulted in marked changes in Ag-speciation in the textile after washing as assessed by XANES (Table A.3.1-1, Ag K-edge spectra of standards used in LCF of sample spectra). In 100 nm Ag fabrics, the initial Ag speciation was 100% metallic Ag, though for the 20 nm fabrics (both citrate and PEG coated), the composition was closer to 80% metallic Ag and 20% AgCl. While metallic silver was still the largest contributor to the speciation profile for all NP inclusion variants and under all washing conditions, AgCl and Ag_2S species were found to coexist alongside metallic Ag in many instances. No apparent trends in the change of speciation were found based on correlations of either detergent chemistry or NP inclusion. Particle release and transformation from the washing of textiles is naturally diversified due to the complex chemistry of Ag in various detergents. The washing procedure appeared to promote the formation of more stable Ag species (for example, Ag_2S, AgCl) on the textile surface (a phenomena also observed by Lombi et. Al (2014)) but only metallic Ag was observed in the wash water by TEM/EDX. This may indicate only the more mobile fraction is released from the fabric surface (found in the wash water) and the more stable fraction remains on the textile through the washing process. In many instances TEM observations suggested particles found in the wash water were of similar size and physical form as the pristine particles, yet we cannot exclude the possibility that some of these formed in solution from ionic Ag released from the fabric (Mitrano et al., 2014). A variety of different Ag species coexist after washing which has important implications for the risk assessment of Ag textiles because metallic Ag is only one of the many silver species that need to be considered. Additionally, Ag_2S is unlikely to provide the same efficacy as Ag^0 in terms of antimicrobial properties (Reinsch et al., 2012), which may have ramifications for how effective the textile treatment is after normal washing circumstances (Lorenz et al., 2012). Conversely, AgCl is now the most commonly available form of silver antimicrobial used for commercial textiles treatments and AgCl has similar efficacy to Ag^0 (as Ag NP). The efficacy of all Ag antimicrobials is ultimately driven by availability of Ag^+.

The pre-washing speciation of the fabrics after sunlight irradiation was entirely (100%) metallic Ag. For the 100 nm Ag textiles, this was no change, but this was a transformation step for the 20 nm Ag treated fabric, where the AgCl was reduced to metallic Ag. This seems to corroborate with the fact that less dissolution is seen in the irradiated material and that photoreduction of the Ag is likely occurring. The post-washing speciation of textiles that were first exposed to the QSUN had a surprisingly different speciation profile than unexposed nano-textiles; with the vast majority of Ag measured as only metallic Ag (Table A.3.1-1.). In the case of the 20 nm particles, which were initially comprised of both metallic Ag and AgCl, the QSUN irradiation initiated photo-reduction of the particles resulting in a transformation of the nano-composite even without washing. How the irradiation inhibited further chemical changes to the NPs through the washing procedure is not entirely defined, but photoreduction of the Ag likely made the particles more stable, or rather, at least less soluble as noted by the decrease in dissolution after irradiation. However, as to why the particles do not release in their entirety (opposed to oxidative dissolution) is another matter; and this may not necessarily be because of a direct transformation of the particles themselves. For example, prolonged exposure to the simulated sunlight may have also altered the physical and/or chemical properties of the binder, which further physically protected the Ag from detergent solutions and thus inhibited particulate release.

Table A.3.1-1: Best-fit Ag speciation as identified by Linear Combination Fitting (LCF) of K-edge XANES. Bottom set of tables (written in red text) represent the analysis of fabrics with sunlight irradiation prior to washing. Species proportions are presented as percentages with standard deviation of three replicates in brackets. Species with less than 10% of the total were omitted. Goodness of fit is indicated by the R-factor. Cells with dashes (----) indicate measurements were below detection limit. Cells with starts (****) indicate no measurement was taken for that variant.

100 nm Ag Citrate
Treatment: Washing only

Component	*Unwashed*	*CL*	*APL*	*CP*	*APP*	*OP*	*IL*	*IP*
Ag^0	100 (0)	88 (1.6)	97 (2.5)	99 (0)	73 (2.1)	52 (3.4)	----	77 (9.1)
AgCl		13 (1.5)			13 (2.1)	13 (3.2)	----	
Ag_2S					15 (2.1)	34 (5.9)	----	13 (9.1)
R-Factor	0.00222	0.00388	0.0028259	0.00382	0.0016441	0.00403		0.0067661

20 nm Ag Citrate
Treatment: Washing only

Component	*Unwashed*	*CL*	*APL*	*CP*	*APP*	*OP*	*IL*	*IP*
Ag-NP	81 (0.9)	91 (0.9)	57 (2.4)	78 (2.5)	75 (2.5)	79 (1.3)	***	66 (2.1)
AgCl NP	19 (0.8)	9 (0.8)	41 (2.5)				***	34 (2.2)
Ag_2S NP				19 (2.5)	16 (4.3)	22 (1.2)	***	
R-Factor	0.001053	0.0023	0.001	0.0028	0.0034	0.0012999		0.003213

20 nm Ag PEG
Treatment: Washing only

Component	*Unwashed*	*CL*	*APL*	*CP*	*APP*	*OP*	*IL*	*IP*
Ag-NP	73 (0.8)	56 (0.9)	78 (0.9)	89 (0.9)	56 (2.8)	75 (2)	***	58 (1.8)
AgCl NP	26 (0.8)	44 (0.9)	22 (0.9)	10 (0.9)	11 (3.1)	26 (1.9)	***	41 (1.7)
Ag_2S NP					26 (9.3)		***	
R-Factor	0.00099	0.0011139	0.001	0.001132	0.0022792	0.0058065		0.004413

100 nm Ag Citrate
Treatment: QSUN then washing

Component	*Unwashed*	*CL*	*APL*	*CP*	*APP*	*OP*	*IL*	*IP*
Ag^0	100 (2.5)	99 (1.6)	81 (2.6)	100 (0)	82.5 (2.6)	95 (2)	----	99 (2)
AgCl							----	
Ag_2S							----	
R-Factor	0.00309	0.003279	0.0179	0.003957	0.0016441	0.002839		0.0056525

20 nm Ag Citrate
Treatment: QSUN then washing

Component	*Unwashed*	*CL*	*APL*	*CP*	*APP*	*OP*	*IL*	*IP*
Ag-NP	95 (0.7)	93 (0.8)	***	98 (0.7)	***	95 (1.3)	***	***
AgCl NP		8 (0.8)	***		***		***	***
Ag_2S NP			***		***		***	***
R-Factor	0.000152	0.0009627		0.0007		0.0021744		

20 nm Ag PEG
Treatment: QSUN then washing

Component	*Unwashed*	*CL*	*APL*	*CP*	*APP*	*OP*	*IL*	*IP*
Ag-NP	96 (0.6)	84 (0.8)	***	98 (0.8)	***	98 (1)	***	***
AgCl NP			***		***		***	***
Ag_2S NP		13 (0.8)	***		***		***	***
R-Factor	0.0005444	0.0034797		0.0008956		0.0015419		

Washed fabrics under landfill conditions

Metal release from textiles during laundering and TCLP test

Total Ag and Au content in impregnated PES fabrics before and after wash were assessed by aqua regia digestion and subsequent ICP-MS analysis (Figure A3.1-14). The Ag and Au concentrations were obtained from washing and TCLP exposure samples in triplicate. Because the initial NP loading varied between textile treatments, a more direct way to observe trends across particle types is to assess the relative percent of metal remaining on the fabric compared to the unwashed samples (Figure A3.1-15; A – C). Oxi washing detergents (blue bars) released a higher amount of metal than color detergents (orange bars) across all NP inclusions. Likewise, fabric swatches subjected to 10 wash cycles (darker shaded bars of each color) released more metal than a single wash, especially Ag-embedded fabrics washed in oxi detergent. Nevertheless, some differences between the washed fabrics can be found depending on the NP inclusion. The 60 nm Ag NP fabric released more metal into the wash solution under every experimental condition compared to the 100 nm Ag fabric. This suggests some slight size preference for the release of smaller particles. In many cases, the 60 nm Au fabric released the least amount of metal under a given set of washing conditions. Because Au is an inert metal, the loss of these particles from the fabrics represents 1) the portion of particles which were not strongly physically attached to the textile surface during manufacturing and/or 2) the fraction of metal which was released due to the mechanical/physical stress of washing the fabrics. Since Ag has additional chemical reactions which can significantly enhance possible release, namely the oxidative dissolution of the particles, it is reasonable to find these textile treatments release more metal, especially under oxidative conditions, compared to the inert tracer material. The preferential chemical release of Ag compared to the physical release of Au during washing is depicted in Figure A3.1-16 A, where the ratio Ag/Au release of Ag textiles washed in a given detergent/cycle number and the related to the amount of Au released from the textiles is indicated by the green and orange dots, for 60 nm Ag and 100 nm Ag NP inclusions, respectively. A ratio higher than one indicates a preferential release of Ag over Au. Here it becomes more evident that smaller Ag particles are always released from the fabric in higher concentrations than the larger Ag particles and additional washes in the oxi detergent release more Ag than Au.

Additional Ag and Au was released from many textile variants during the simulated landfill leachate test (Figure A3.1-15, panels D-F). Depending on particle inclusion, the TCLP test removed between 10 and 30% of metal from the unwashed textiles (green bars). The percentages of metal remaining on the fabrics after the TCLP test for all variants that also included a washing step were directly compared to corresponding washed only samples. For example, the 100 nm Ag fabric washed once in oxi detergent released 15% of Ag from the textile after the wash procedure (Figure A3.1-15A, light blue bar). When calculating the additional release of Ag after the TCLP test (Figure A2.1-15D, light blue bar), the mass of Ag corresponding to the 85% of Ag remaining on the fabric corresponds to 100% remaining of the fabric at the start of TCLP test (i.e. if no additional Ag was lost). However, in this example, an additional 15% Ag was released from the fabric but this refers to the total mass in the already washed textile, not the unwashed (original) textile. Again, we find that Ag is released in higher concentrations from 60 nm doped fabrics than the 100 nm counterparts. In these experimental sets, slightly more metal was released for fabrics first washed in the color detergents opposed to the oxi variants, where the most metal was released in those sets that underwent only one wash. This suggests that the fraction of material which remains on the textiles that were exposed to more harsh washing conditions (*i.e.* increased washing replicates and/or oxi washing detergent) is less likely to be released during the TCLP test and, therefore, the washing conditions promote a higher likelihood of metallic release from the textiles than when the textile reaches the end of life phase in the landfill. In short: under these conditions the use phase of the life cycle appears to be responsible for higher metal release than the

disposal phase. Comparing the relative Ag release to the Au release upon TCLP test exposure (Figure A3.1-16 B), we find that Ag fabrics that were first washed in oxi detergent subsequently release more Ag into the TCLP solution than corresponding Au fabric variants.

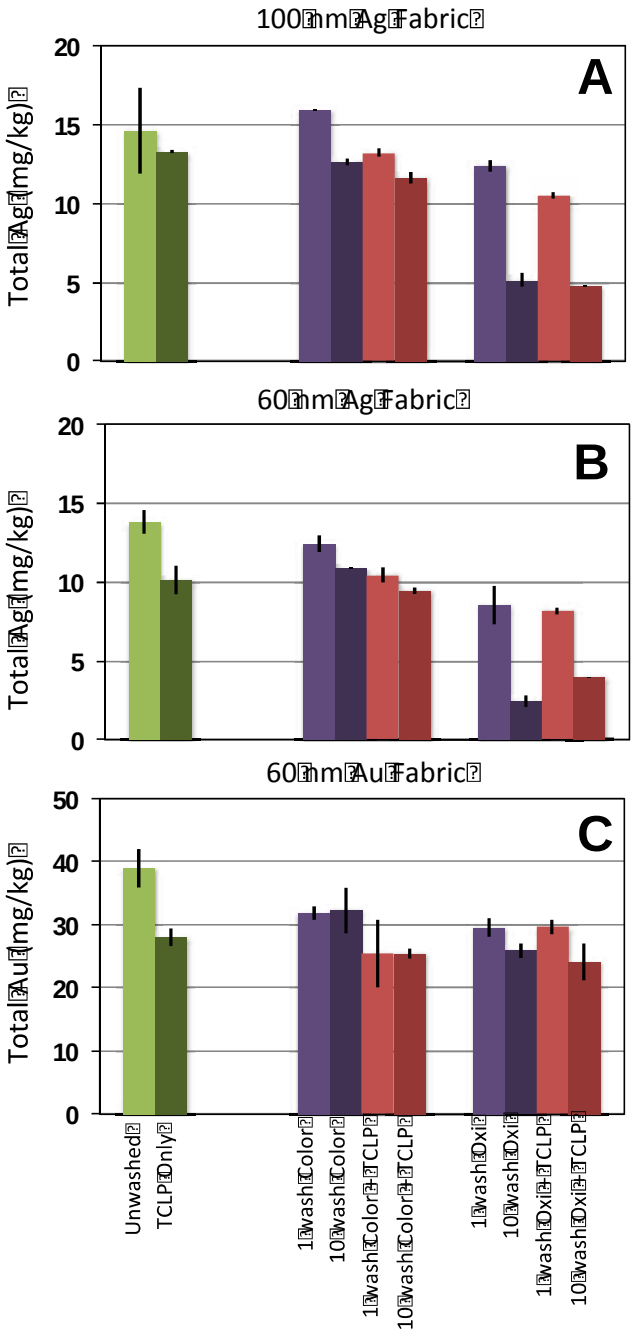

Figure A3.1-14: Total metal analysis from fabric digests for 100 nm Ag treated fabric (panel A), 60 nm Ag treated fabric (panel B) and 60 nm Au treated fabric (panel C). Green bars are indicative of fabrics that did not undergo a washing procedure, with the unwashed (raw) fabric sample and the TCLP test only in the light and dark green bars, respectively. Purple bars indicate the total metal in fabrics that were only washed 1 time (light purple) or 10 times (dark purple). Red bars depict fabric samples which were first washed then exposed to the TCLP test, with one wash being indicated by the light red bars and 10 washes by the dark red bars. Samples washed in color detergent are in the center group while fabrics washed with oxi detergents are in the right grouping.

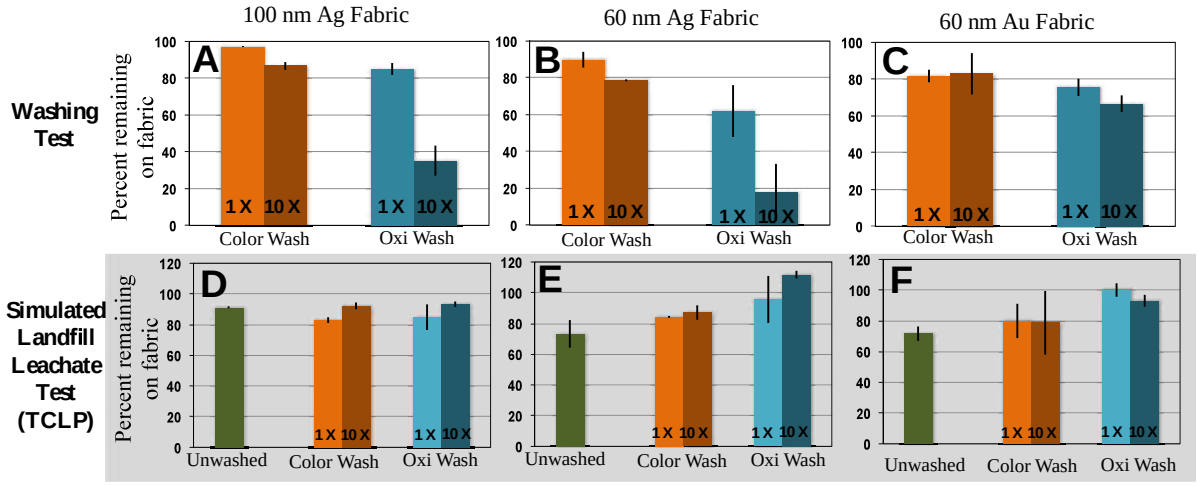

Figure A3.1-15: Relative percent of metal remaining on each fabric after washing as compared to the unwashed fabrics are displayed in panels A-C, with 100 nm Ag fabric, 60 nm Ag fabric and 60 nm Au fabric. Fabric swatches washed in color detergent are orange with oxi variants in blue. In both cases, the lighter shade indicates one washing cycle and the darker shade indicates 10 washing cycles. Results of the percent of metal remaining on the fabric after the simulated landfill leachate test (TCLP) is shown in panels D-F as compared to the corresponding treatment before the TCLP test. Note the scale on the lower graphs exceeds 100.

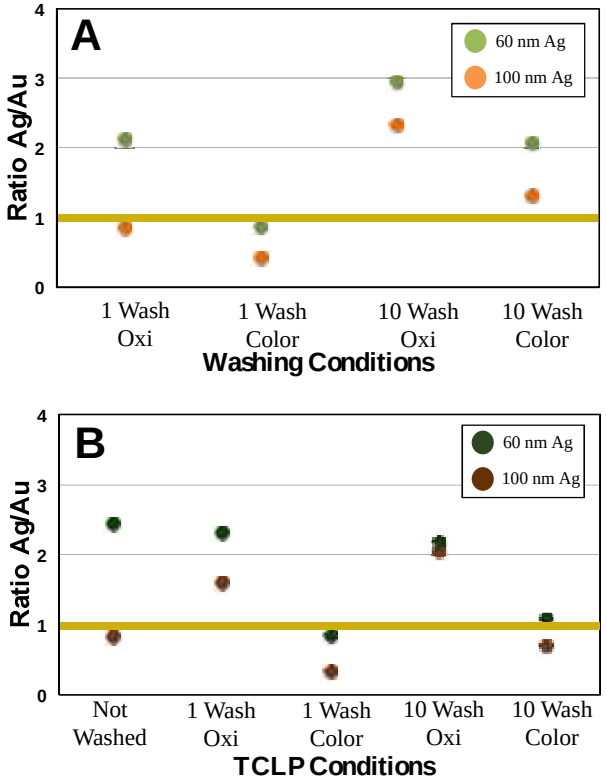

Figure A3.1-16: Ratio analysis of preferential chemical release of Ag compared to mechanical release of Au with A) washing only conditions and B) washing with subsequent TCLP exposure. The yellow line at one represents the release of Au from fabrics under each corresponding experimental condition. Green dots represent fabrics containing 60 nm Ag NPs and orange dots are 100 nm AgNP fabrics (light and dark colors indicating washing only conditions and sequential exposures, respectively, in panels A and B).

Characteristics of metal released to TCLP solution

Total metal concentrations and the dissolved fraction of metal after ultrafiltration in the TCLP leaching solution were analyzed for all samples. When translated into amount of metal leached from the fabric under each experimental variant, the most metal leached from the unwashed fabrics and significantly less leached from the pre-washed fabrics (Figure A3.1-17). When unwashed textiles were directly exposed to TCLP extraction fluid, nearly all of the metal detected in solution from either 100 nm Ag or 60 nm Au doped fabrics was particulate (Figure A3.1-17A) but the 60 nm Ag textiles was of mixed characteristics (i.e. dissolved and particulate metal was detected in solution). Additionally, Ag fabrics which were first washed had a much higher variability in released material measured in the TCLP solution, where between 20 – 50% of Ag passed through the centrifugal ultrafilter (Figure A3.1-17, panels B and C). In all cases, fabrics released less than 2 mg kg^{-1} metal into the TCLP solution and in most cases the amount released was less than 0.5 mg kg^{-1}. The amount of metal measured in the TCLP solution can be further linked to the total metal remaining on the fabric after the initial washing step (Figure A3.1-18). In this context, a significant fraction of metal was released from fabrics were not washed first (green bars), but a much less material was extracted from the TCLP solution from fabrics which had first underwent any type of washing procedure. Therefore, in both absolute and relative terms, the amount of metal recovered during the simulated landfill test is small, especially when compared to the release of metal from the unwashed textiles. This further indicates the necessity of life-cycle aging sequences to properly assess the likelihood and characteristics of material released from nano-enhanced textiles.

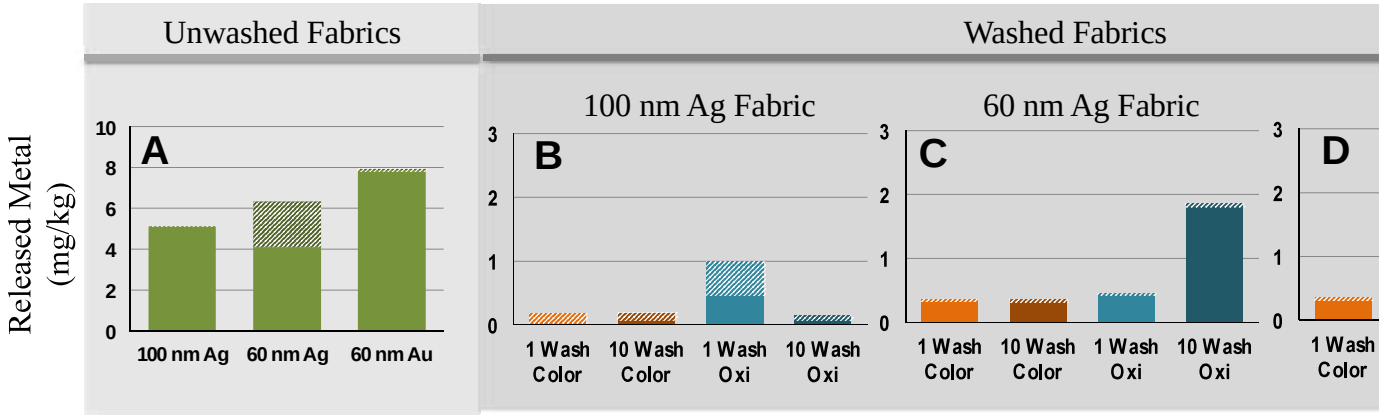

Figure A3.1-17: Concentration of metal released into TCLP extraction fluid based on fabric weight. A) unwashed fabric fabric type), and washed fabrics: B) 100 nm Ag fabrics, C) 60 nm Ag fabrics and D) 60 nm Au fabrics, where the x-axis Solid portions of bars represent particulate matter with hashed sections indicating dissolved metal. Unwashed fabrics color detergents in orange and oxi detergents in blue, with ten washes in darker variants.

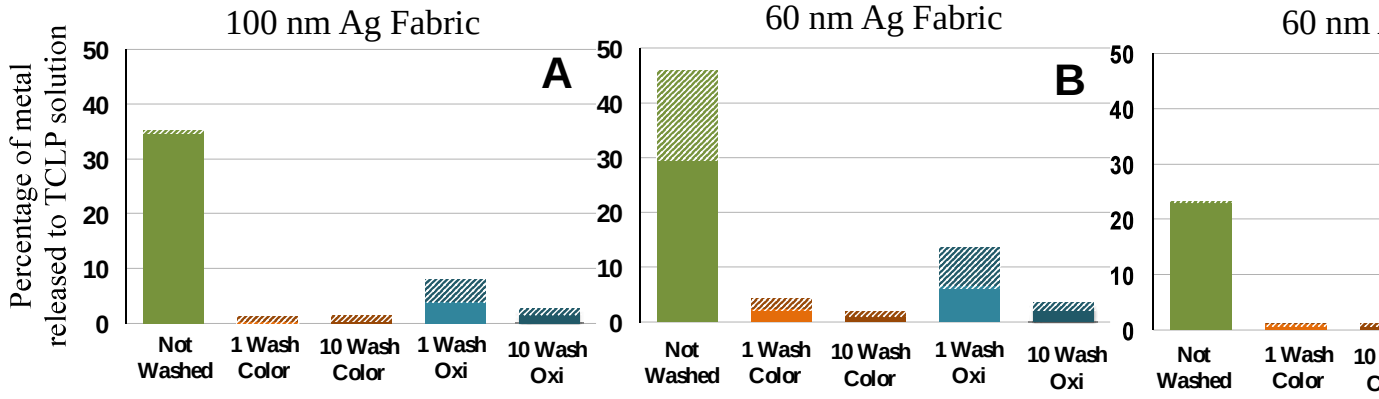

Figure A3.1-18: Percentage of metal released to TCLP solutions after initial washing steps for A) 100 nm Ag treated fa 60 nm Au treated fabric. Solid portion of bars represent particulate matter with hashed sections indicating dissolved m in green, washed with color detergents in orange and oxi detergents in blue, with ten washes in darker variants.

Stability of NPs in DI H_2O and TCLP extraction fluid

The inconsistency between the percentage of metal released from the fabrics during the leaching test (Figure A3.1-15, panels D-F) and the amount recovered from the TCLP solution (Figure A3.1-17), speaks to the (in)stability of the particles themselves in the TCLP solution. We therefore further investigated this aspect of particle stability in the TCLP solution (Figure A3.1-19). Total recoverable Ag is higher in the DI H_2O variants under all conditions except shaking without SDS surfactant (panel A) than in the experiments in TCLP extraction fluid without additional surfactant (panel B). Here, while the addition of SDS appears to stabilize the particles in terms of total recovery from the solution, when no SDS is added the particles have an enhanced probability of sticking to the experimental container wall, especially with additional agitation (*e.g.* panel B, stirring or shaking, medium orange or dark orange traces, respectively). Notably, the same overall trends can be observed when studying the AuNPs despite the different particle chemistry. Again, in these experimental sets more than 90% of the total Au is recoverable from the DI H_2O experiments under all conditions (panel C), whereas a drastic decrease in Au recovery is found with AuNPs suspended in TCLP extraction liquid when additional agitation is applied without the presence of surfactant (panel D). In short, for both Ag and AuNPs spiked into the TCLP solutions containing no surfactant, the particle stability was severely decreased in a short amount of time upon any agitation to the system.

Furthermore, the form of agitation promoted various amounts of instability, where bottles which where were allowed to stand on the bench top appeared to have the best stability, followed by stirring and finally shaking (the conditions under which the tests with the fabrics were performed). Because the ionic In internal standard concentrations remained stable between the measurements at time 0 and 18 h, a particle aggregation and/or sticking effect is seemingly at play. When experimental containers were rinsed with acid to recover metal that adhered to the container wall, a significant fraction was recovered from systems where particle recovery from the solution was lowest.

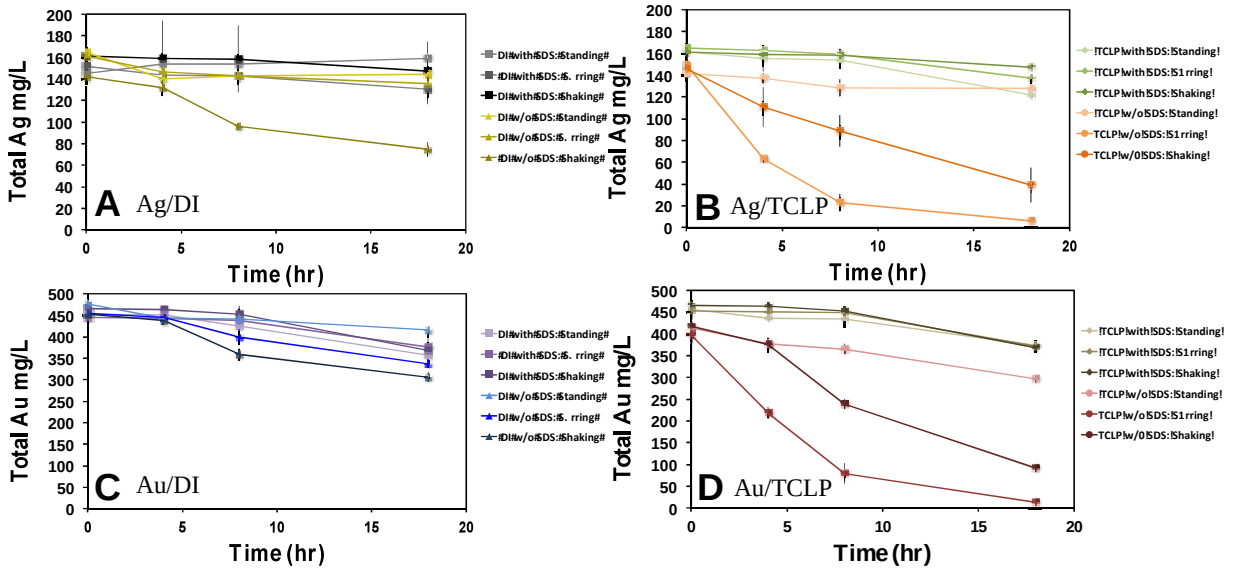

Figure A3.1-19: Stability of 60 nm Ag (panels A and B; initial concentration 200 mg/L) and 60 nm Au (panels C and D; initial concentration 500 mg L^{-1}) NPs in DI H_2O or TCLP extraction fluid under different physical aging conditions (standing, stirring, shaking); with or without the addition of surfactant (SDS) as a stabilizing agent. Error bars indicate standard deviation of triplicate experiments.

A.3.2 Aging of Ag NPs with UV/Temperature (CEA)

A.3.2.1 Summary of the aging experiments

Stock suspensions (20 mg L^{-1} for citrate-stabilized Ag AL NPs, and 40-50 mg L^{-1} for citrate- or PEG-coated Ag UoB NPs) were aged as received in the QSUN under soft conditions: irradiance of 1.44 W m^{-2} at 420 nm, $T_{black\ panel}$ = 70 °C, T_{air} = 40 °C, relative humidity N.A.). For kinetics study purposes, 20 mL of each suspension were poured in a glass vial sealed with PTFE liner-screw caps. 2 mL aliquots were withdrawn at different times of aging.

A.3.2.2 Characterization methods

Size and zeta potential, TEM, and XRD were acquired using the same devices as those described in § A.1.2. For DLS measurements, homogenization of the suspensions was achieved by vortex stirring (ca. 15 s) instead of ultra-sonication, unless otherwise stated. For TEM observations, the 3µL sample droplets were deposited on a Cu grid covered with a SiO membrane.

A4F

Asymmetric field flow fractionation (FFF) was performed using a device composed of a metal-free HPLC system (1260 Infinity, Agilent Technologies), a flow controller (Eclipse AF4, Wyatt Technology) and a separation channel (Wyatt Technology). The FFF system was coupled to a series of on-line detectors: a UV spectrophotometer (Agilent Technologies), a MALLS detector (Dawn Heleos II, Wyatt Technology), and an ICP-MS (7700x, Agilent Technologies). The separation channel was 275 mm long, 50 mm wide and its height was defined by a 350 µm-thick spacer. Sodium hydroxide (pH adjusted to 10, filtered to 0.1 µm) was used as the eluent. The samples were diluted in water to reach an injected Ag NP concentration of ca. 1 mg L^{-1}.

SEM

Observations were performed using a ultra-high resolution SEM (LEO 1530, LEO Electron Microscopy Ltd) set at an accelerating voltage of 10 kV. The liquid samples were deposited on a polystyrene substrate and left overnight for drying in a closed box before sputter coating with a 10-nm platinum layer to prevent sample charging and damage from electron beam.

UV/Vis

Spectra were acquired with a double beam UV/Vis/NIR spectrophotometer (UV 3100, Shimadzu Corporation) equipped with a deuterium lamp and a tungsten lamp. The slit was set to 2 nm. The suspensions were diluted in UP water to ensure that maximum absorbance is below 1 A.U.

A.3.2.3 Results

UV/Vis

One of the most striking evolutions of the suspensions of nano silver is their color change (Figure A.3.2-1). These changes are due to particle alteration in size/morphology and aggregation/agglomeration state. Ag AL 20nm resist do not show visible alteration of their appearance till 92 hours of aging: the suspension

turns brownish and then greyish with partial sedimentation. The color change takes place faster with Ag AL 60nm, beginning after only a few hours. However, the orange/brownish color obtained remains stable even after one week of exposure. Larger particles (Ag AL 100nm) readily form a light brown precipitate.

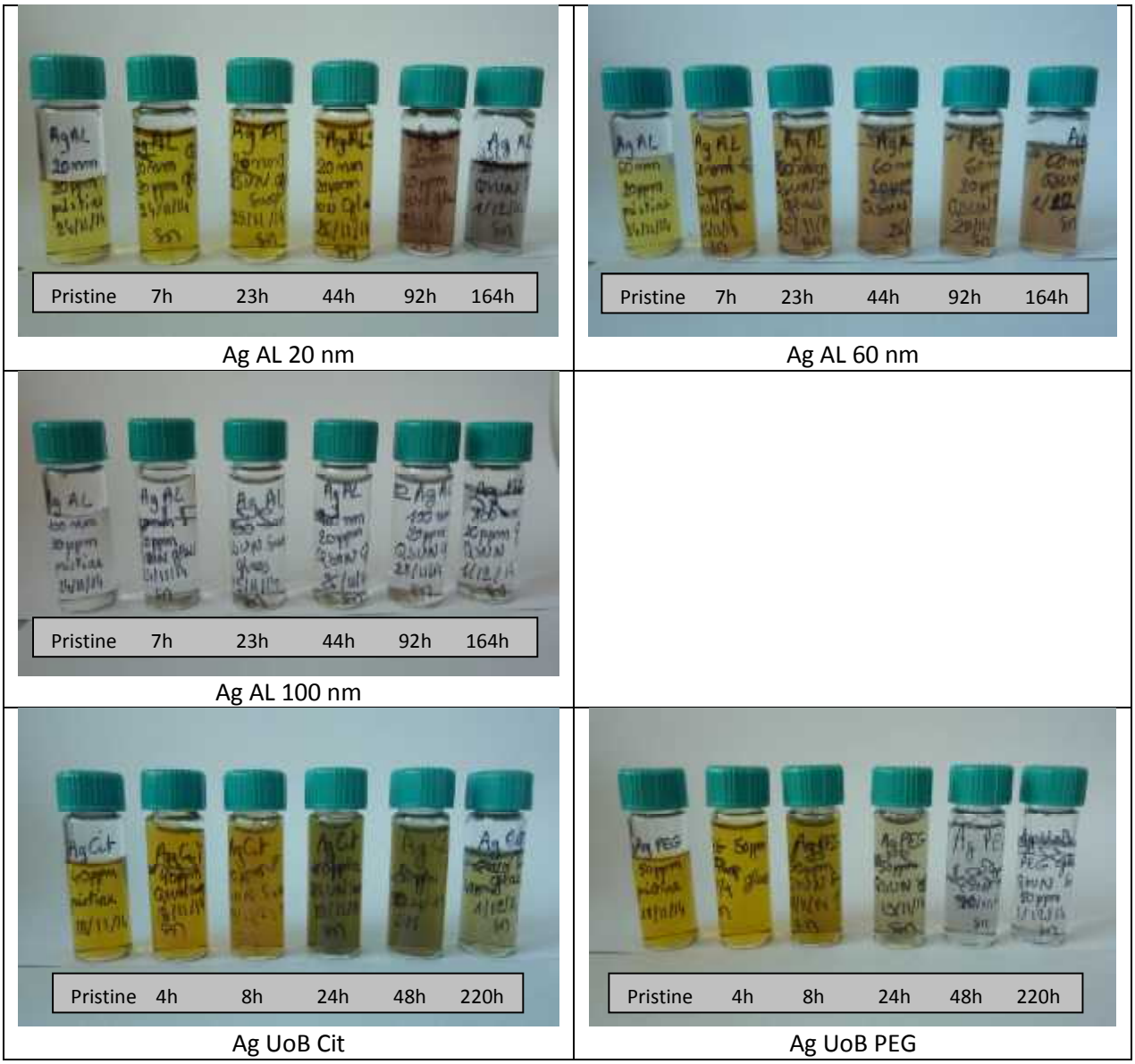

Figure A.3.2-1: alteration of the suspensions of Ag NPs according to exposure time.

The behavior of Ag UoB NPs is somewhat different from that of Ag AL NPs. Indeed, citrate-coated Ag UoB NPs do evolve in color with aging time but to a greenish shade of grey (24h-48h) before sedimentation (220h). The evolution is faster with PEG-coated Ag UoB NPs with a black precipitate occurring within 2 days and leaving a clear supernatant.

This difference between Ag AL and Ag UoB Cit might originate from the matrix in which the NPs are suspended, presumably the concentration of the stabilizing agent (citrate), although this hypothesis needs to be confirmed.

Color changes can be monitored by UV/visible spectrophotometry. The alteration of the absorbance spectrum with time is observed in Figure A.3.2-2. The characteristic plasmon resonance absorption band is centered at 405 nm for Ag AL 20nm and 435 nm for Ag AL 60nm while Ag AL 100nm NPs do not display any specific absorption band.

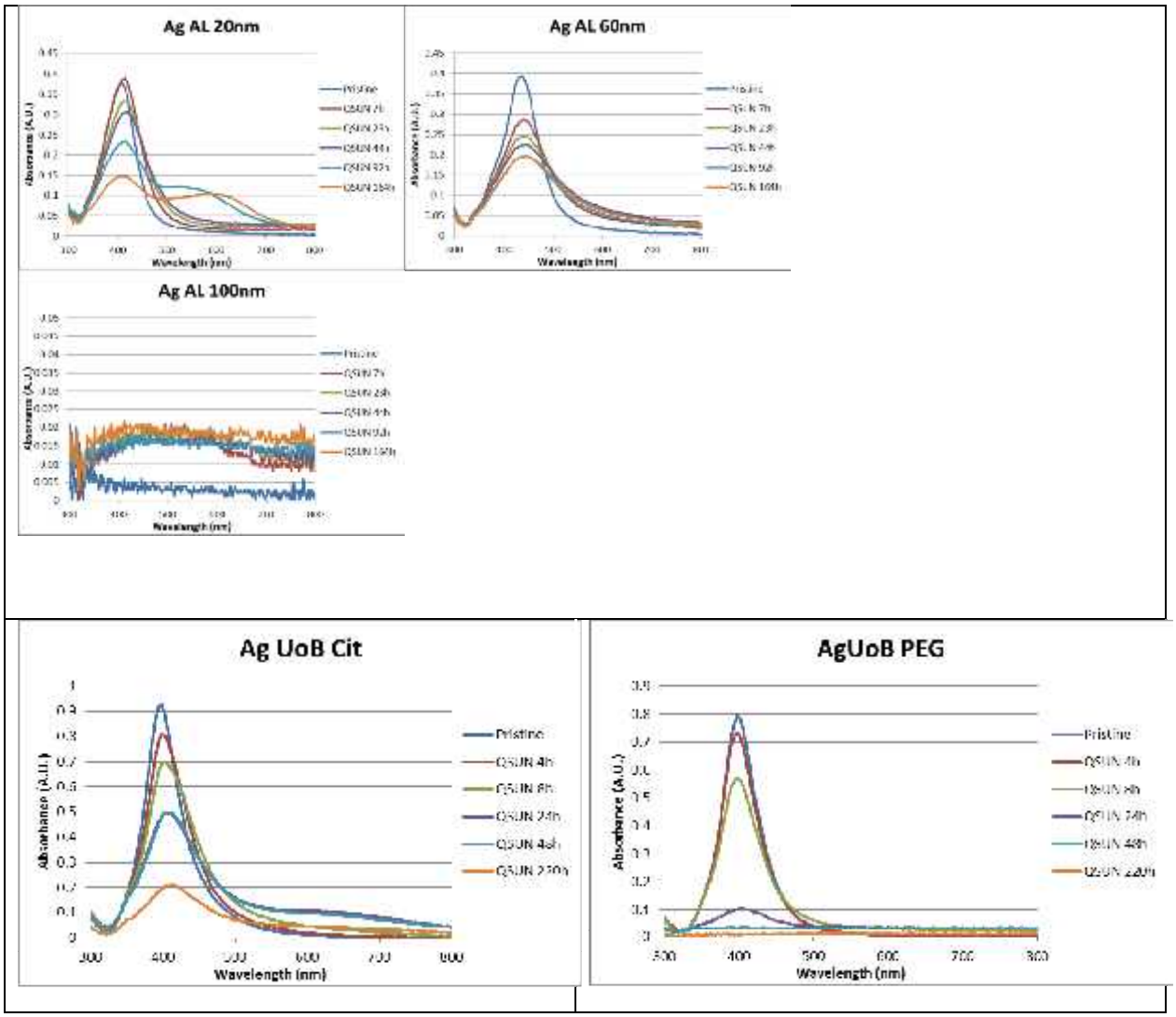

Figure A.3.2-2: Evolution of the absorbance spectra of Ag NP suspensions with exposure time. Dilution factor: 5 for al Ag AL samples, 6 for Ag UoB Cit, and 10 for Ag UoB PEG.

Aging of the NPs results in a decrease in the intensity of the main absorption band together with a slight red shift and a broadening of the band. Besides, a second absorption band emerges between 500 nm and 700 nm for the citrate-coated Ag AL 20nm after 92 hours of exposure. A similar tendency arises with Ag UoB Cit: a decrease in the intensity of the major plasmon resonance band (396 nm) concomitantly with an increase in absorption in the same wavelength range occur but to a lesser extent, though. These NPs are quite comparable in size, even though dispersity is higher for the UoB Ag NPs, which confirms the same trend for the aging behaviour of this type of particles in a citrate-stabilizing medium. This red shift and secondary band reflect transformations of the particles, either a growth in the primary particle size and/or formation of agglomerates/ aggregates and/or formation of a new species and/or existence of an oxidized layer on the surface (Henglein et al., 1991, Kapoor, 1998, Li et al., 2010)

PEG-coated NPs behave quite differently: only the overall decrease in the main band (397 nm) is observed (no shift and no secondary band) with aging time, which may be significant of a simple dissolution of the primary particles. However, the global increase of the baseline level of absorbance in the whole visible region, a phenomenon that is observed for all Ag suspensions at longer times of exposure, confirms the occurrence of black particles in the suspensions. These particles settle quickly in the case of Ag AL 100nm, as can be seen in Figure A.3.2-1.

Size and ZP by DLS

a) Preliminary experiments

Ionic strength and scan direction for titration were identical as those optimized with TiO_2. The NP concentration optimization was carried out in preliminary experiments with some requirements concerning the maximum concentration. Indeed, Ag NP stock suspensions are already diluted (20 to 50 mg L^{-1}) and, for some of them, come in small amounts (a few mL). The aging experiments could thus only be achieved with limited volumes of initial suspensions and, given the minimum volume for titrations, the aged suspensions had to be somewhat diluted. Plus, the tendency of Ag (NPs or diluted) to adsorb to a certain number of surface materials has imposed use of a glass vial and short PTFE tubing between the titrator and the measurement cell.

Basically, changing the NP concentration by a factor of 10 does not change much the agglomeration state of the Ag UoB NPs: the suspensions are stable at the concentrations investigated here (Figure A.3.2-3). These concentrations lie below the agglomeration threshold observed for TiO_2 and CeO_2, if ever such threshold exists for Ag NPs given the negative profile of the zeta potential throughout the pH range. Data dispersion is increased when the concentration is minimum (4 or 5 mg L^{-1}) while the general trend is preserved. Hence, despite the lower quality of the results, the highest dilution was finally chosen for Ag NPs titrations.

It may be noted that the investigated range was extended to more acidic pHs (pH = 2) in some instances in order to check the propensity of Ag NPs to agglomerate at small absolute ZP values. This trend is clearly observed in the case of citrate-coated Ag NPs for which the hydrodynamic diameter increases sharply (from 40 nm to 160 nm) below pH = 2, i.e. when the ZP absolute value falls below 15 mV. PEG-coated Ag NP suspensions are more stable as for dispersion properties: even for ZPs close to zero ($|ZP| < 5$), the hydrodynamic diameter is not changed in a tremendous way (from 55 nm to 80 nm), showing the major role of the polymeric coating to resist agglomeration.

Because such acidic pHs are unrealistic in natural conditions, and damage the ZP cells used for titrations, only the usual pH range (4-9) was further investigated.

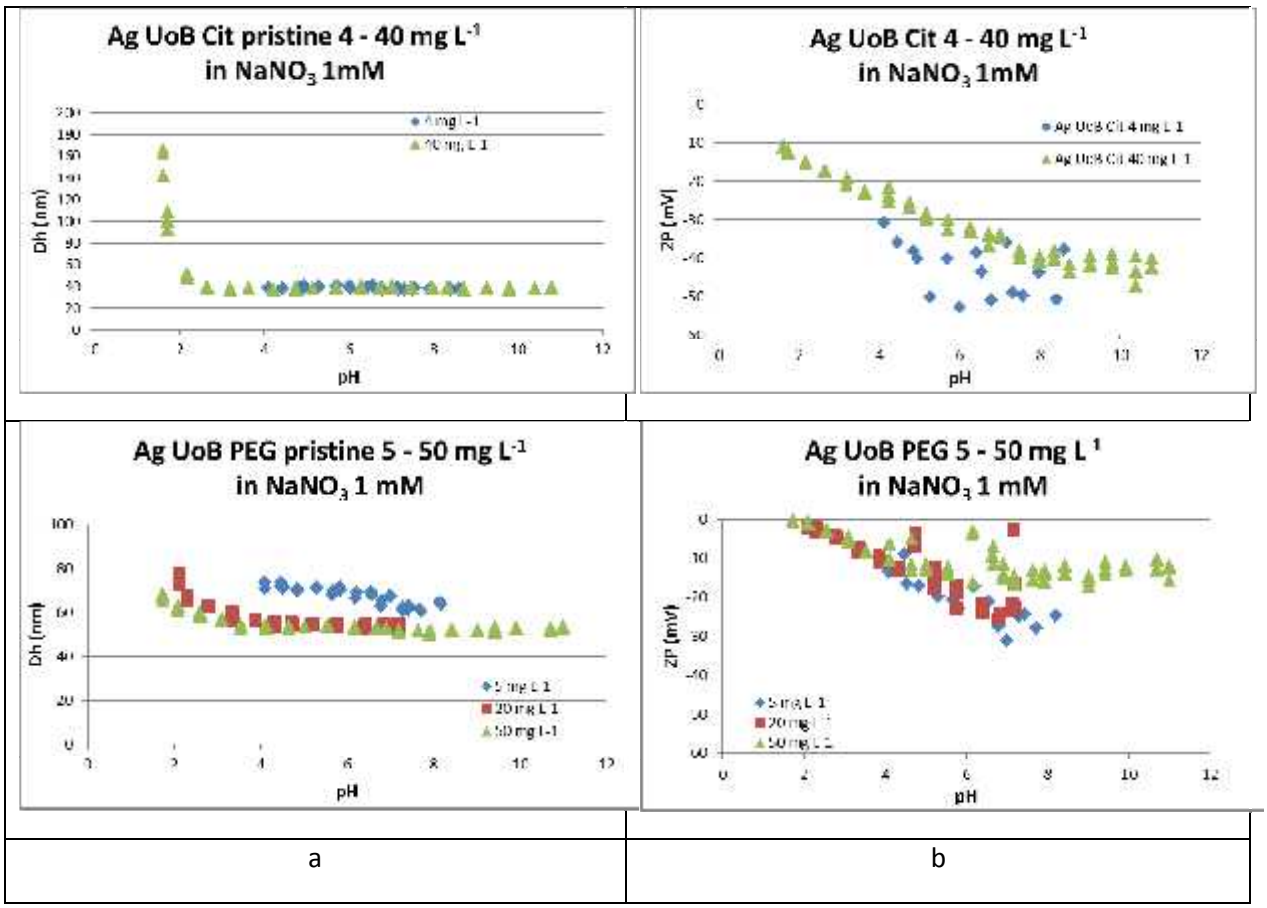

a b

Figure A.3.2-3: Influence of the NP concentration in suspension on the pH titration profile of Dh (a) and ZP (b). Experimental conditions: suspensions in $NaNO_3$ 1 mM, pH scan from 9 to 4 or 11 to 2.

b) Characterization of pristine and aged NPs using DLS

pH titrations of the hydrodynamic diameter and the zeta potential are presented in Figure A.3.2-4 at different aging times for all the Ag NPs investigated.

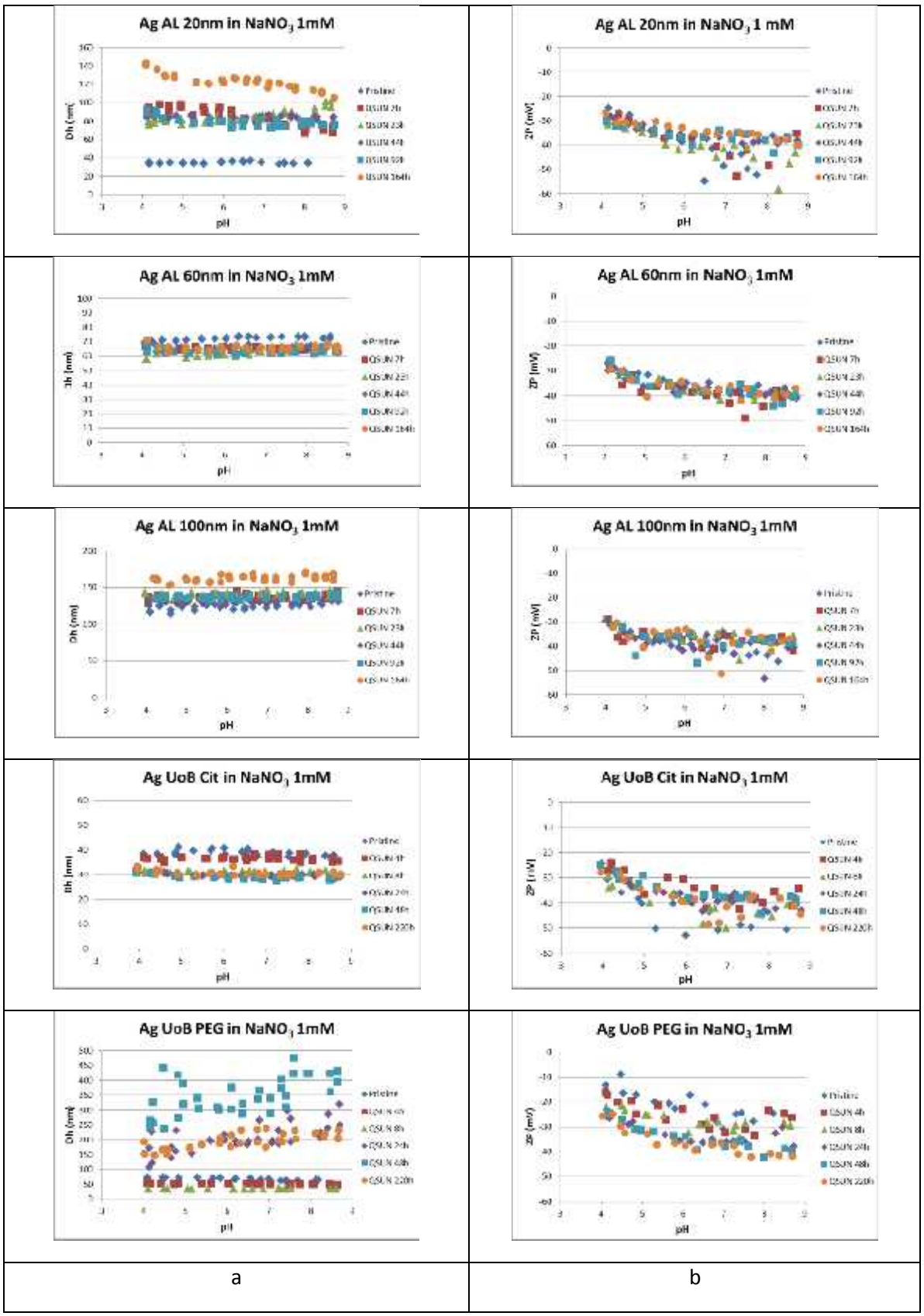

Figure A.3.2-4: Evolution of Dh (a) and ZP (b) as a function of pH for Ag NPs at different aging times. Experimental conditions: [Ag AL NPs] = 4 mg L^{-1}, [Ag UoB Cit NPs] = 4 mg L^{-1}, [Ag UoB PEG NPs] = 5 mg L^{-1} in $NaNO_3$ 1 mM, pH scan from 9 to 4. The aged Ag AL 100nm NPs were sonicated for 1 min to re-disperse the brown precipitate.

First, let's notice that Dh and ZP values are in good agreement with those provided by UoB (Dh = 40 nm, Zp = -44 mV for Ag UoB Cit and Dh = 59 nm, ZP = -16 mV for Ag UoB PEG) for the pristine NPs.

The Ag AL NPs in the citrate form show different evolutions depending on their size. For the smallest Ag AL 20nm, Dh is roughly doubled after the first hours of exposure, and remains at this value until 92h, then increases again as the suspension turns grey. It is supposed that the first increase be due to the early formation of agglomerates. Indeed, the Rayleigh approximation of the intensity of light scattered ($I \alpha (Dh)^6$) promotes the contribution of larger particles and hinders that of the small particles to the total light scattered. These agglomerates are likely to occur at a sufficiently low concentration not to modify the absorbance spectrum (major band broadening solely). Degradation would start with little alteration of the surface chemistry, promoting little agglomeration, followed by more severe agglomeration/aggregation processes.

Dh evolution is less visible for 60nm NPs, with only a slight decrease in size, even though the absorbance spectrum shows there is some suspension evolution. This could suggest that agglomeration may not be the primary aging transformation, although it is likely to occur to some extent, but particle transformation itself may well be the major phenomenon in this case.

100 nm NPs do not show much evolution of size and ZP. It seems that, although they flocculate immediately after the first hours of exposure (see Figure A.3.2-1), with a possible change in surface chemistry, they do not change in size.

A slight decrease of Dh can be observed with Ag UoB Cit (from 38 nm to 28 nm), which is comparable in proportion to what was observed for Ag AL 60nm. Since these particles are stabilized by the same molecules and their sizes are set between 10 nm and >40 nm, one would have expected a behaviour closer to that of Ag AL 20nm. However, the larger polydispersity and the difference in concentration of the NPs and of the stabilizing agent may explain the observed discrepancy.

The decrease in Dh is more significant with PEG-coated particles (from 67 nm to 34 nm after 8 hours of exposure). This initial trend is followed by an important increase reflecting major agglomeration/aggregation processes, in agreement with the formation of a black deposit in the vial.

Concerning zeta potential measurements, and given the poor quality of data due to dispersion, no specific influence of the aging process can be observed for citrate-coated Ag NPs: ZPs all lie between -40 mV and -50 mV at alkaline pHs. They rise to ca. -25 mV at pH = 4, whatever the exposure time. PEG-coated Ag NPs display less negative ZPs over the entire pH range. Plus, a clear trend of ZP decrease with aging time can be observed in Figure A.3.2-4b (bottom). It is noteworthy that the final titration curve of Ag UoB PEG at 220h of exposure is superimposed with those of the citrate-stabilized Ag NPs (ZP = -40 mV at pH = 9 to ZP = -25 mV at pH = 4). From this, we can infer that, even if the way it is obtained depends on the stabilization agent, the final "product" of the aging in our experimental conditions is likely to possess the same surface characteristics whatever the original particles. In other words, the PEG coating is most probably seriously damaged or even destroyed during this process.

In order to limit the contribution of larger particles and/or clusters in the mean hydrodynamic diameter as measured by DLS, measurement of the sole supernatant was proposed by simple dilution of the supernatant in $NaNO_3$ 1 mM to the target NP concentration. The data obtained for UoB Ag NPs are presented in Figure A.3.2-5.

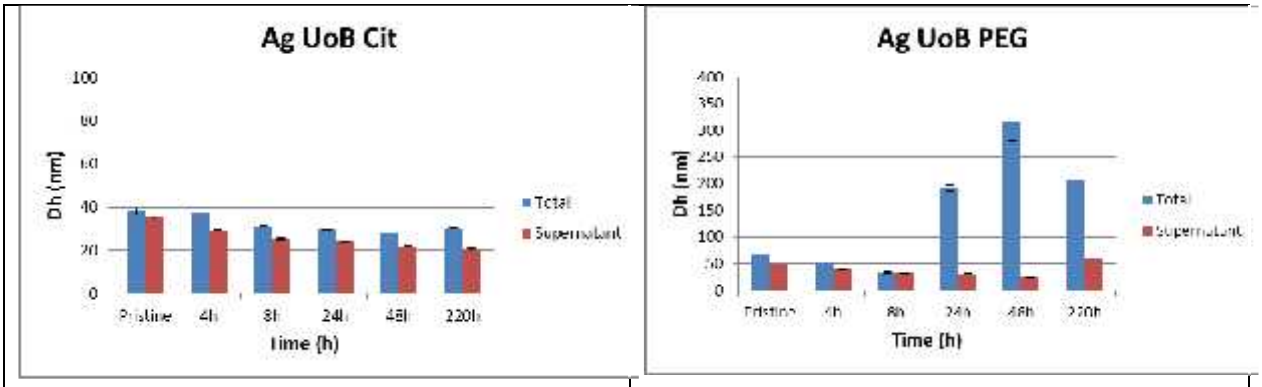

a b

Figure A.3.2-5: Comparison of the hydrodynamic diameters of the silver suspensions after homogenization of the suspension (Total) or not (Supernatant) for (a) Ag UoB Cit or (b) Ag UoB PEG NPs.

It is observed that in both cases, the dispersed portion tends to decrease in size, with a higher rate in the case of PEG-coated NPs. Interestingly, Dh values follow the same trend for homogenized suspensions and supernatants up to a point (24h for Ag UoB PEG and > 220h for Ag UoB Cit) where the particles seem to be significantly altered to promote higher agglomeration/aggregation.

A4F

Given the polydispersity of the suspensions, highlighted by the above batch DLS analyses, further investigation with A4F makes perfect sense here. This technique is based on a true separation of the particles based on their diffusion, which offers better resolution and accuracy in analysis of size distributions. Fractograms of the studied silver suspensions at different exposure times of the aging kinetics are presented in Figure A.3.2-6, showing two on-line detector signals (ICP-MS and MALLS).

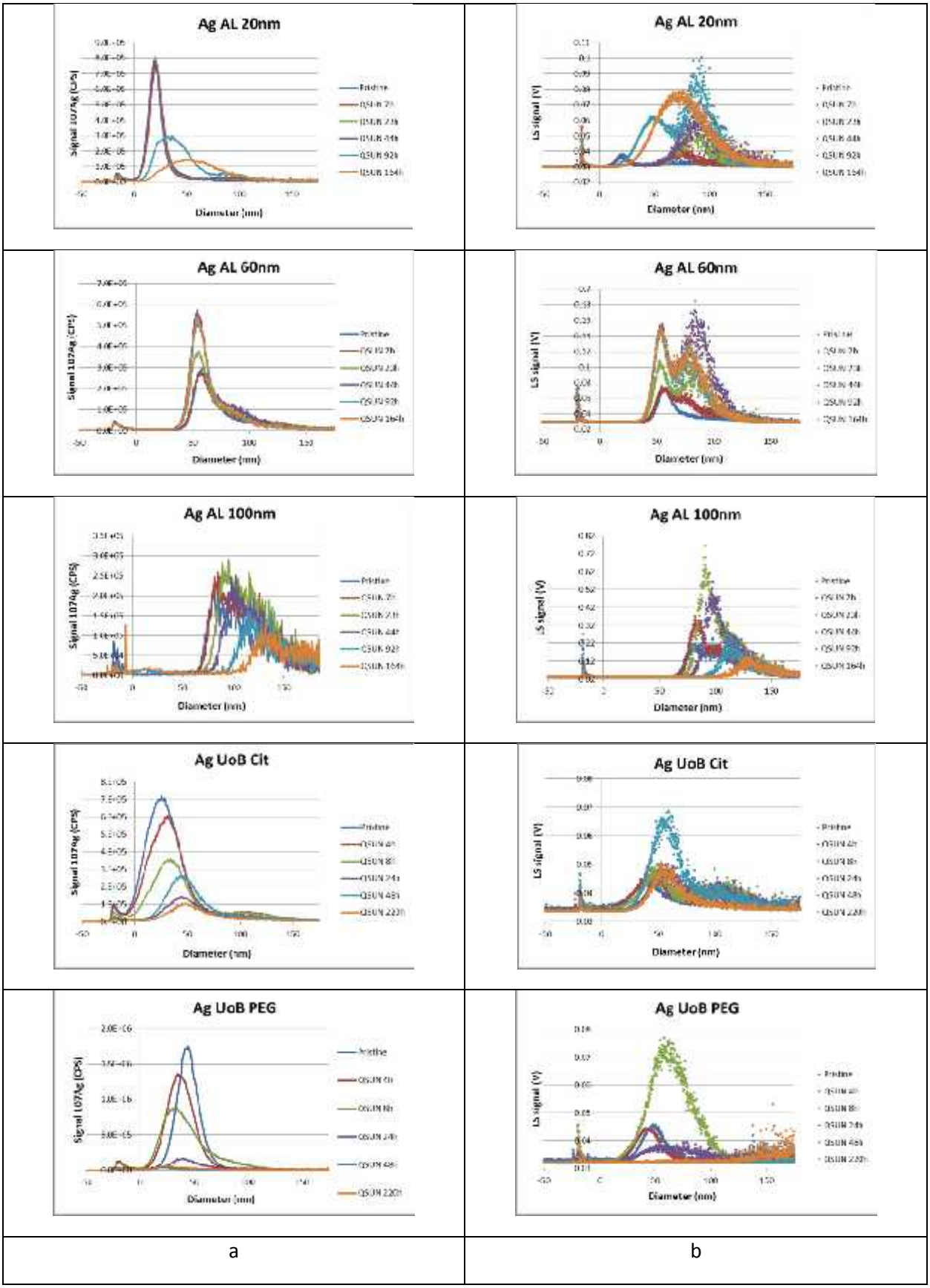

Figure A.3.2-6: Fractograms of the silver suspensions: evolution of their distribution in size with exposure time. (a): on-line ICP-MS signal for ^{107}Ag and (b): on-line MALLS signal (90° detector).

Let's first notice that the populations of pristine particles are well centered on their expected size as determined by DLS. In the case of Ag AL 20nm, the ICP-MS fractograms look quite superimposed in the early times of exposure, with no visible shift of the peak standing for the main population. However, the MALLS signal, which emphasizes larger particles, clearly shows the occurrence of a second newly-formed population with a mean diameter around 80 nm, a value that corresponds to that obtained by DLS on the same suspensions. This new population increases in size and concentration with time; it becomes visible with the ICP-MS. As with absorbance spectra, the great change in shape occurs at 92h: a significant shift towards larger diameters simultaneously to broadening of the main population is observed with both detectors, showing major particle alteration.

60nm and 100nm basically behave similarly, i.e. increase in size and dispersity with the occurrence of a new higher-average-size population. This phenomenon seems to proceed at a higher rate in the case of Ag AL 100nm compared with smaller Ag AL 60nm.

The fractogram profiles of Ag UoB Cit look pretty much like those of Ag AL 60nm and 100nm suggesting they follow the same type of degradation process. The new population is centered on a diameter of 110 nm. Conversely, Ag UoB PEG fractograms show a singular evolution, with a substantial decrease of the mean diameter of the main population. One cannot observe secondary population as in previous cases but rather a progressive tailing of the peak towards larger diameters, particularly after 8h of exposure. The scattered data points at diameters above 150 nm calls for the occurrence of large clusters that are not completely eluted in the analytical conditions and "stick" to the separation membrane. This result is in agreement with the DLS data that also detected such large particles at 24h of exposure and more.

SEM

The behavior of Ag UoB Cit and Ag UoB PEG was further investigated by microscopy techniques such as SEM and TEM. Particularly, the appearance of the different coatings was of special interest since it is supposed to be the parameter that favors or prevents particle dissolution and/or aggregation. Figure A.3.2-7 shows some SEM images of the citrate-coated and the PEG-coated NPs before and after 7 days (168h) of aging in the QSUN.

The Ag UoB Cit pristine sample show isolated particles, though most of the particles occur as clusters with rounded edges, as if the NPs were embedded in a gangue. The overall appearance does not change much after one week of aging in the QSUN: the same rounded-shaped clusters occur as before exposure.

How PEG-coated NPs are organized is very different from the citrate-coated ones: they form a spider web-like network of rather well dispersed primary particles. After aging, this aspect is changed and the particles gather in clusters of a few hundreds of nanometers in diameter.

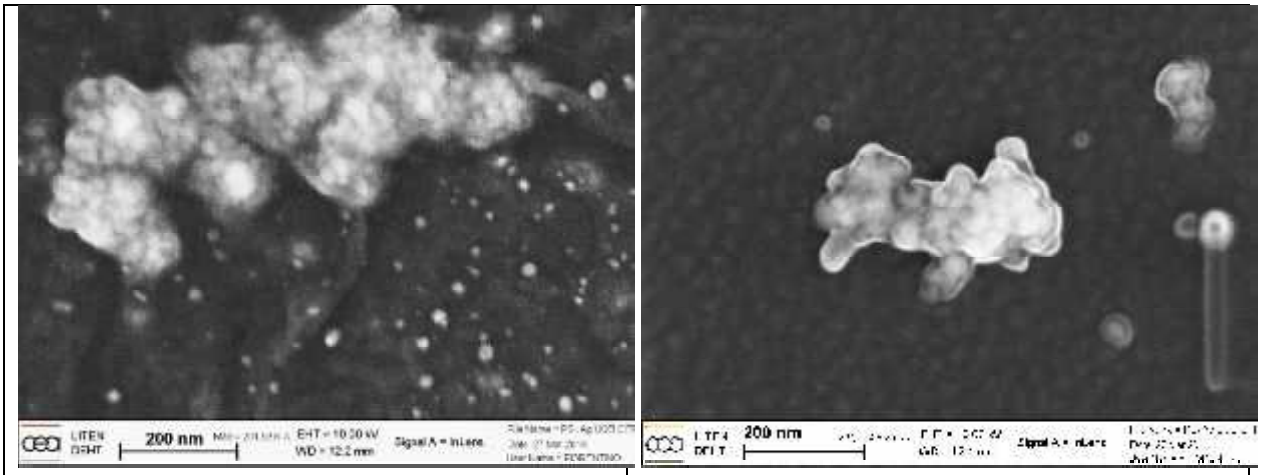

Ag UoB Cit pristine | Ag UoB Cit QSUN 168h

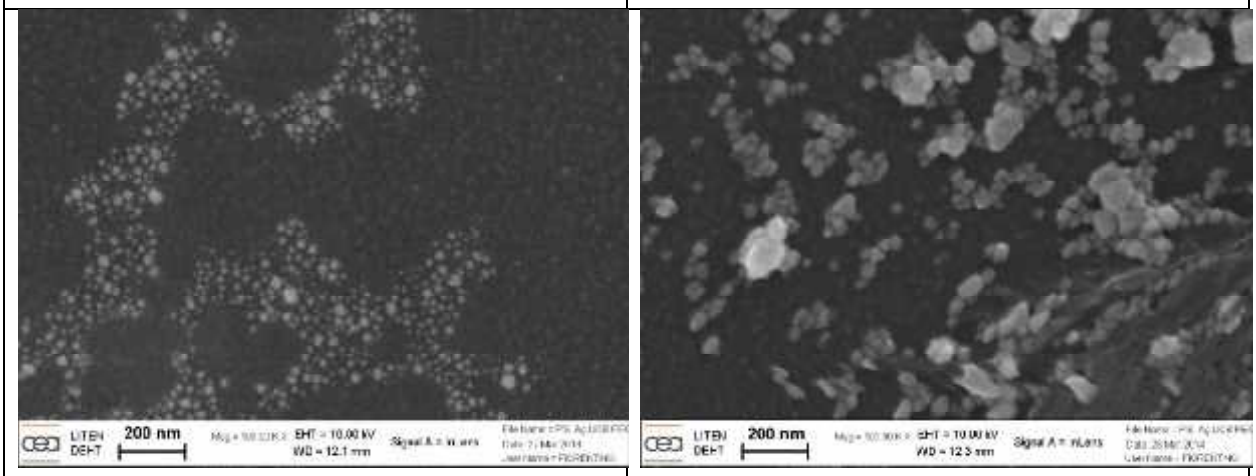

Ag UoB PEG pristine | Ag UoB PEG QSUN 168h

a | b

Figure A.3.2-7: SEM images of pristine (a) and QSUN 168h aged (b) Ag UoB suspensions.

These observations are consistent with the results from DLS and A4F analyses. In the case of citrate-coated NPs, it is very likely that the inter-particle binding within these clusters is rather weak and corresponds to agglomeration via the organic shell made of citrate and counter-ions such as Na. This assumption is confirmed by DLS (mean Dh = 38 nm) and A4F experiments (a major peak around 20 nm in size, after vortex stirring). The little evolution in Dh and the increase in size of the major peak of the fractogram are in favor of a possible evolution of the primary particles but with only minor change in agglomeration state (witness the increase in MALLS signal between 100 nm and 150 nm) for Ag UoB Cit sample. PEG-coated samples, as already discussed, seem to suffer more marked changes. The increase in Dh together with the increase of MALLS signal above 150 nm are probably related to the phenomenon of particle gathering observed in Figure A.3.2-7b (bottom).

EDX analyses were performed in STEM acquisition mode (Figure A.3.2-8). The spectra profiles look very much alike, with the same X-rays peaks characteristic of C, O, Ag, Na (which was assigned to a likely pollution), and Pt (from sample preparation coating). Sulfur was not detected in this series of observations. The decrease in intensity of the O-characteristic peak for Ag UoB Cit may be assigned to a decrease or modification of the citrate capping agent, although this hypothesis would need further investigation.

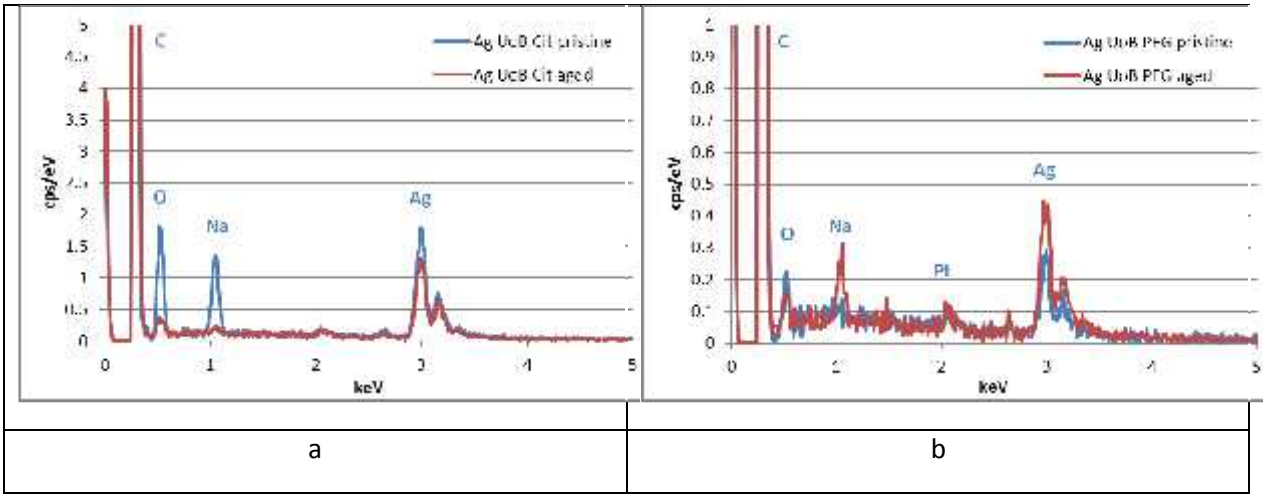

a b

Figure A.3.2-8: comparison of EDX spectra of pristine and QSUN 168h aged Ag UoB suspensions. (a): Ag UoB Cit and (b): Ag UoB PEG.

TEM

In order to better characterize the primary particles for morphology and chemical composition, TEM observations were proposed on the same NPs (Ag UoB Cit and Ag UoB PEG). Some relevant images and EDX spectra are given in Figure A.3.2-9.

The TEM images of the pristine Ag UoB Cit display the same pattern as the SEM images, i.e. clusters of mostly spherical, 5 nm to 50 nm particles along with the same scattered single particles. After 48h of QSUN exposure, the density of particles within the agglomerates looks higher and, most obviously, the shape of some of the particles has transformed into edge-cut polygons and triangular nanoplates of ca. 100-120 nm in size. These newly-formed particles can be attributed to the concomitant effect of light irradiance and temperature (40 °C), as already observed by Jin et al. (2001) and Jin et al. (2003). These authors observed the photo-induced conversion of spherical Ag NPs by irradiation with fluorescent light. The suspension color changed from yellow (spherical NPs) to green and finally blue within a 70h time frame, with UV/Vis absorption spectra showing similar evolution as that observed for Ag AL 20nm here, and calculations allowed to assign this phenomenon to the existence of those truncated triangular nanoplatelets.

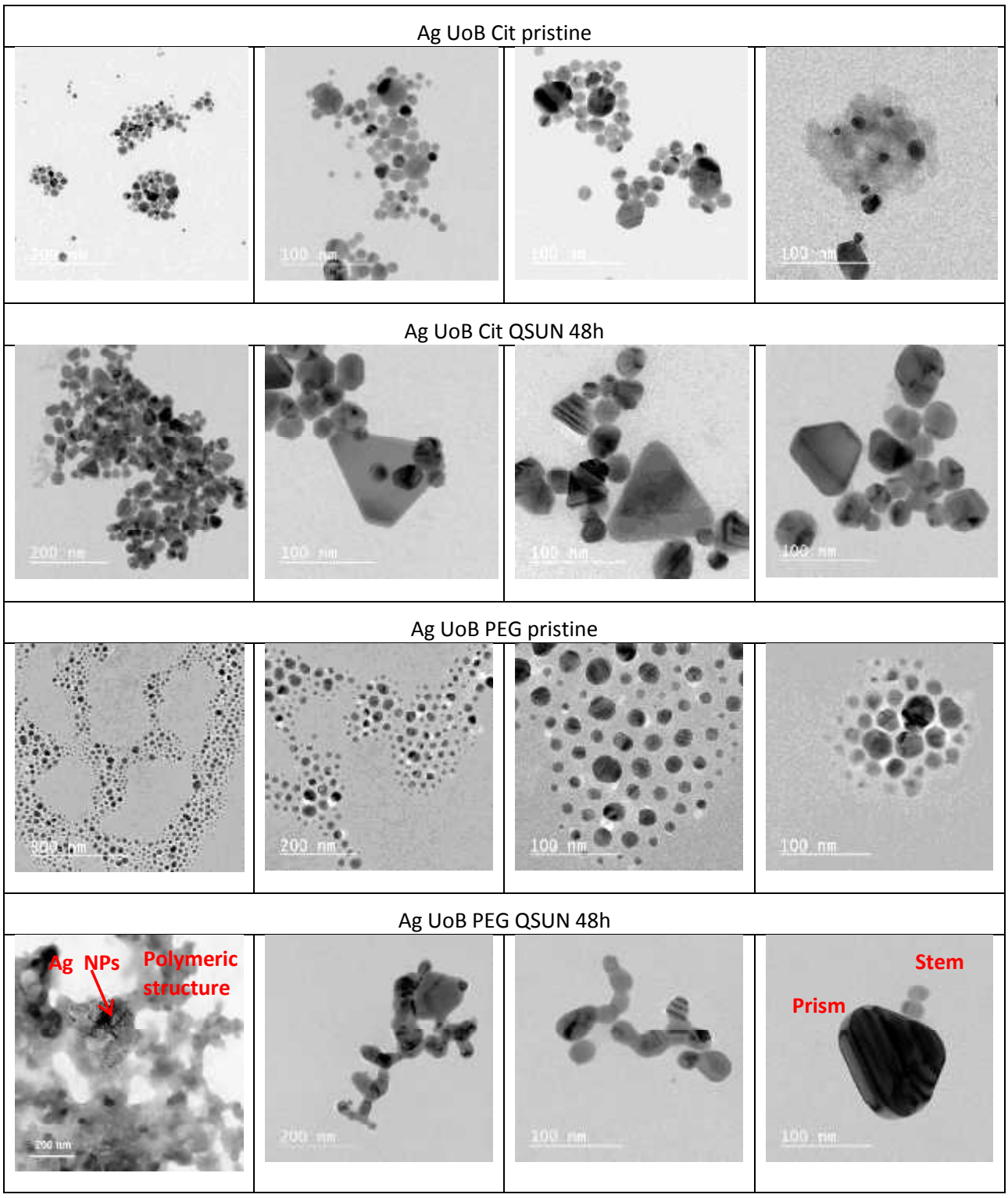

Figure A.3.2-9: TEM images of pristine and 48h QSUN-aged Ag UoB NPs.

Such typical morphology was also found in aged Ag UoB PEG samples but in smaller quantities. From the spider web-like network of pristine NPs that resembles that obtained by SEM, one mainly obtained particles that looked like they were bridged together, as well as large (several µm) units of polymer-like structures with very small (a few nm) Ag NPs attached to them.

A possible explanation is that the formation of the observed Ag structures (either nanoprisms or bridged particles) originates from these small "seeds" which, themselves, come from the dissolution of the pristine NPs followed by re-precipitation/reduction processes favored by the organic stabilizers (either citrate or PEG). Jiang et al. (2010), for instance, reported the influence of citrate ion concentration on the reaction rate, particle shape and size in the synthesis of silver nanoplates. They found that the higher the [Cit]/[Ag^+] ratio, the larger the edge length of the nanoplates. It is most probable that in our case, the ratio is small enough to keep the size of the nanoprisms no larger than ca. 100 nm.

An evaluation of the average size from the TEM images of pristine NPs gave:

$D_{Ag\ UoB\ Cit}$ = 15.9 (std dev = 7.2, n = 203) and $D_{Ag\ UoB\ PEG}$ = 15.4 (Std dev = 7.9, n = 202).

These values are lower than those provided by the producer:

$D_{Ag\ UoB\ Cit}$ = 21.2 (std dev = 7.0, n = 100) and $D_{Ag\ UoB\ PEG}$ = 21.3 (Std dev = 5.7, n = 124).

but, based on the uncertainty on the data due to the dispersity of the population, one can conclude that they are coherent.

EDX spectra (Figure A.3.2-10) show the same pattern as those established with SEM. Only in the case of Ag UoB PEG aged for 48h did we find a peak for sulfur when focusing on the very small NPs attached to the polymeric structures. However, sulfur was also present on the PEG itself (in particle-free zones). The nanoprisms do not contain significant amounts of S to be detected by EDX, which means that, if transformation of the Ag(0) core occurs in our experimental conditions, the expected Ag_2S phase is only present in a limited thin shell.

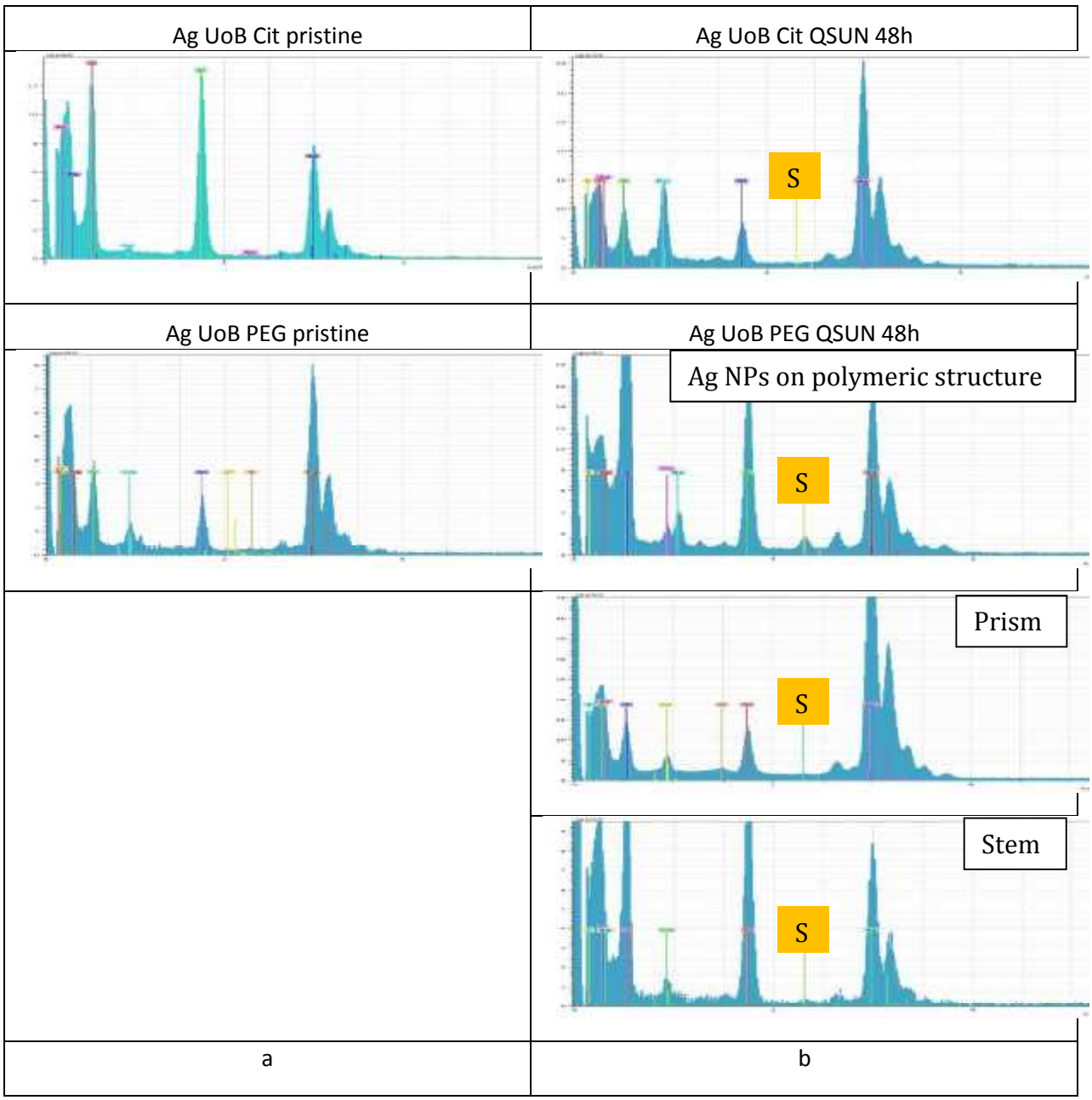

Figure A.3.2-10: EDX spectra of pristine (a) and 48h QSUN-aged (b) Ag UoB NPs. The 3 last spectra in (b) correspond to the images bottom left and bottom right in Figure A.3.2-9.

HRTEM on Ag UoB citrate QSUN 48h

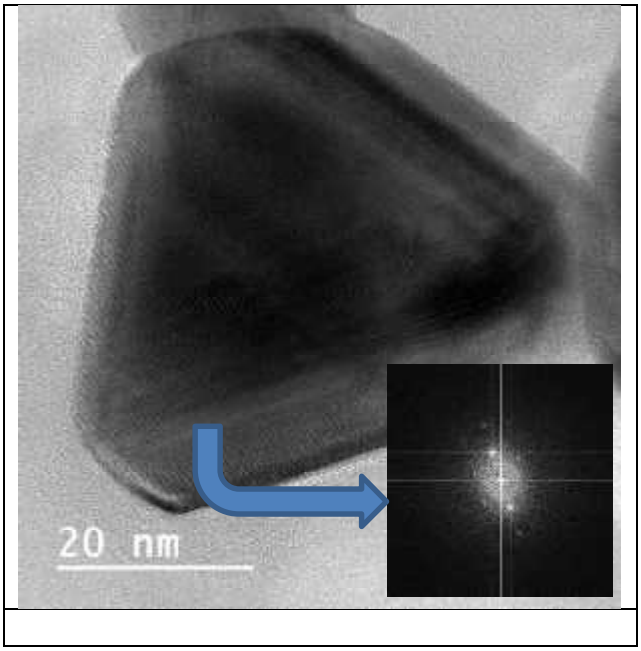

Figure A.3.2-11: HRTEM image and diffraction analysis (inset) of newly-formed nanoprism in Ag UoB QSUN 48h suspension.

The diffraction images obtained in Figure A.3.2-11 are characteristic of the particle crystallinity, and the interplanar distance is obtained from the Fourier transform of the spot array diffraction pattern. The measured distance between two adjacent plans is d = 0.237 nm. This estimate returns a lattice parameter value of a = 4.099 Å, that is very close to tabulated values ($a_{Ag(fcc)}$ = 4.086 Å). It may then be concluded that the newly-formed particles are of the same face-centered cubic system as the pristine particles. This result was somewhat expected since it is the most favoured crystalline phase for silver and the physico-chemical conditions are very similar to those during synthesis.

XRD

Figure A.3.2-12 shows the XRD patterns of the pristine Ag UoB NPs. Crystallite sizes deduced from the line widths are gathered in Table A.3.2-1.

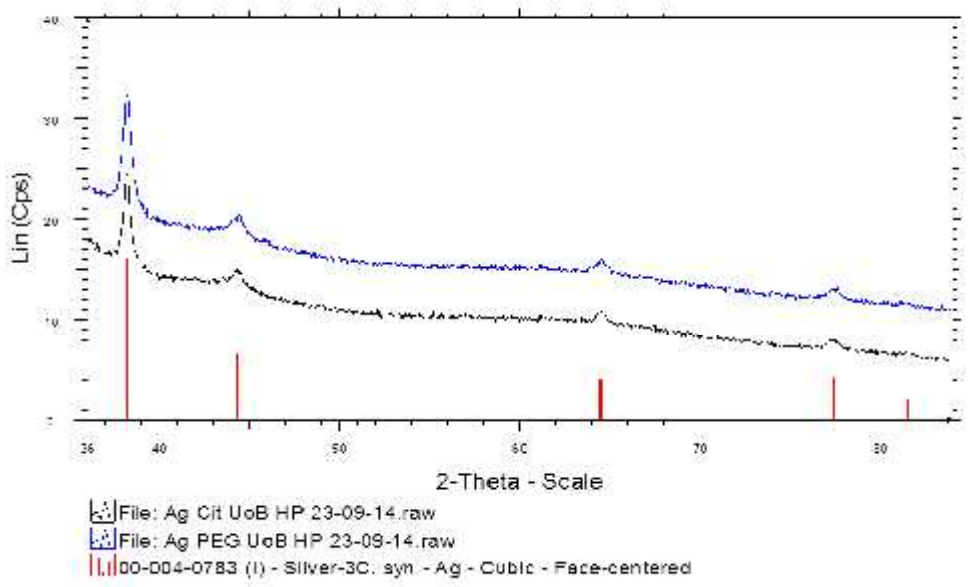

Figure A.3.2-12: XRD diffraction patterns of pristine Ag UoB NPs.

Table A.3.2-1: XRD characteristic parameters

Ag NP	Crystallite size (nm)	ε	a (Å)
Ag UoB Cit	31	$3\ 10^{-3}$	4.0863
Ag UoB PEG	22	$4\ 10^{-3}$	4.0836

The scans show a face-centered cubic profile, confirming the HRTEM observations. The line widths are thinner for Ag UoB Cit (crystallite size of 31 nm) than for Ag UoB PEG (crystallite size of 22 nm). These values are higher than expected, given the mean diameter of the particles, and may be attributed to the polydispersity of the populations (see TEM estimates).

Part B: Characterization of the MNMs from Milestone 6 (delivered to WP 4-8)

B.1 TiO_2 - Aging with UV/Temperature (CEA)

B.1.1 Summary of the aging experiments

The commercial stock suspension (TiO_2 PVP MILE005d) was used as received (1.05% w/w TiO_2, PVP stabilized from Promethean Particles Ltd., see D3.2). It was dried in a thermal chamber prior to the aging procedure in the QUV for 42 days.

B.1.2 Characterization methods

The methods and protocols used for the investigated NPs are identical to those presented in § A.1. BET characterization (carried out by UoB) was performed with a SA3100 Surface area analyzer. The degassing temperature was set at 120 °C for 180 min.

B.1.3 Results

Remark: In the results given below, all concentrations refer to the metal content of the considered suspension (i.e. Ti for TiO_2 NPs).

Size and ZP by DLS

The dependence of the hydrodynamic diameter and the zeta potential of the suspension is given in Figure B.1-1. The profiles look quite similar as those obtained in § A.1. Maximum agglomeration occurs at the PZC. The same decrease in PZC with aging (by ca. 0.8 pH unit) concomitantly to difficult de-agglomeration

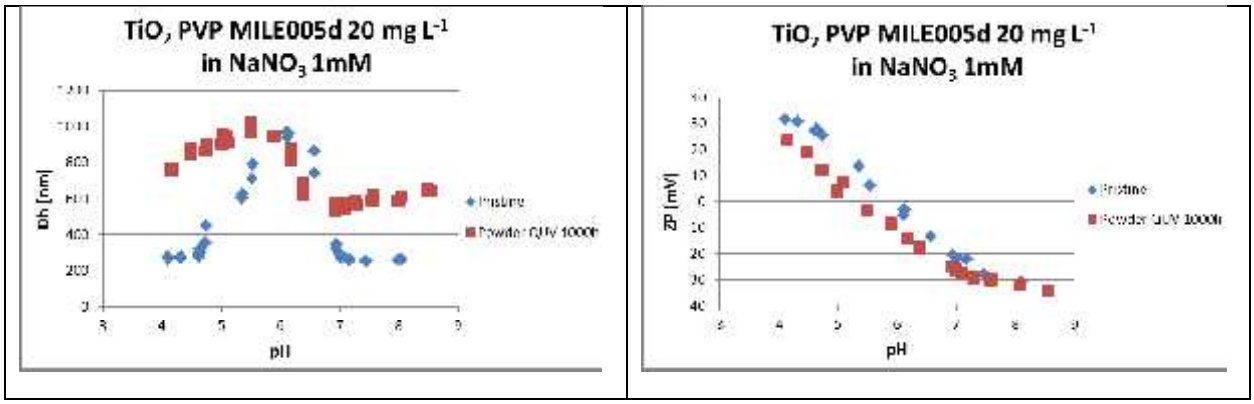

Figure B.1-1: Evolution of Dh (a) and ZP (b) as a function of pH for pristine and aged TiO_2 NPs.

The size of TiO_2 MILE005d pristine (Dh) **at pH 7** is 291 nm (σ = 35 nm) with a PDI of 0.322 (σ = 0.048); the corresponding ZP at the same pH is -21.1 mV (σ = 0.8 mV)

The size of TiO_2 MILE005d aged 1000h (Dh) **at pH 7** is 555 nm (σ = 19 nm) with a PDI = 0.412 (σ = 0.041); the corresponding ZP at the same pH is -26.1 mV (σ = 0.9 mV)

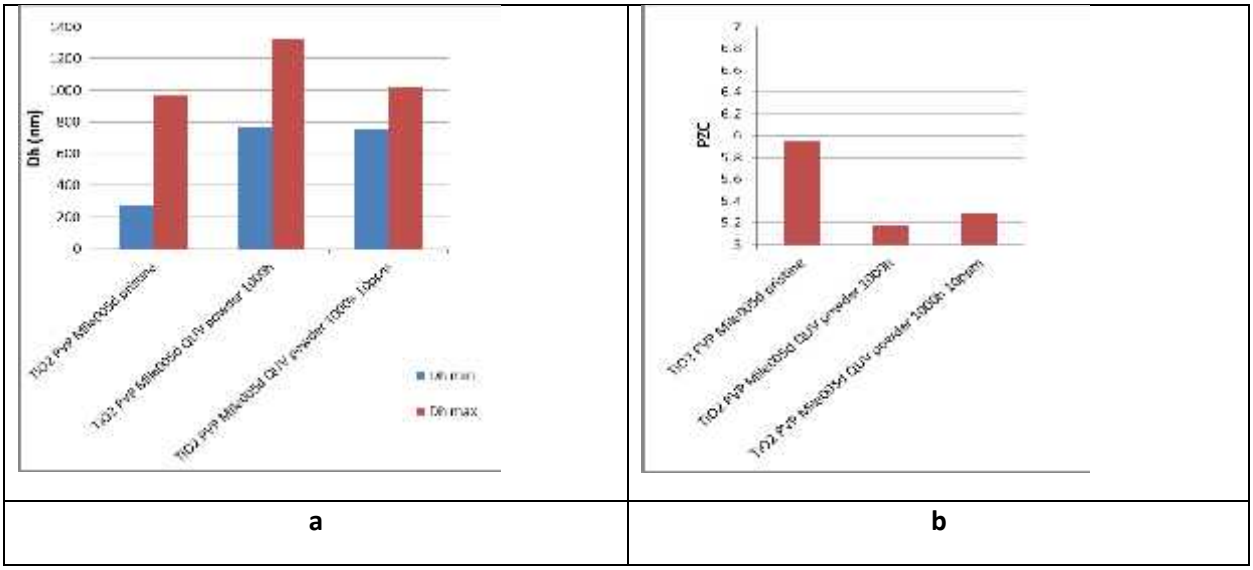

a b

Figure B.1-2: Influence of the aging protocol on the size of the agglomerates (a) and on the value of PZC (b) for TiO_2 MILE005d NPs. Dh min: minimum size for optimum dispersion conditions, and Dh max: maximum size for optimum agglomeration conditions.

TEM

TEM images and EDX spectra are presented in Figure B.1-3.

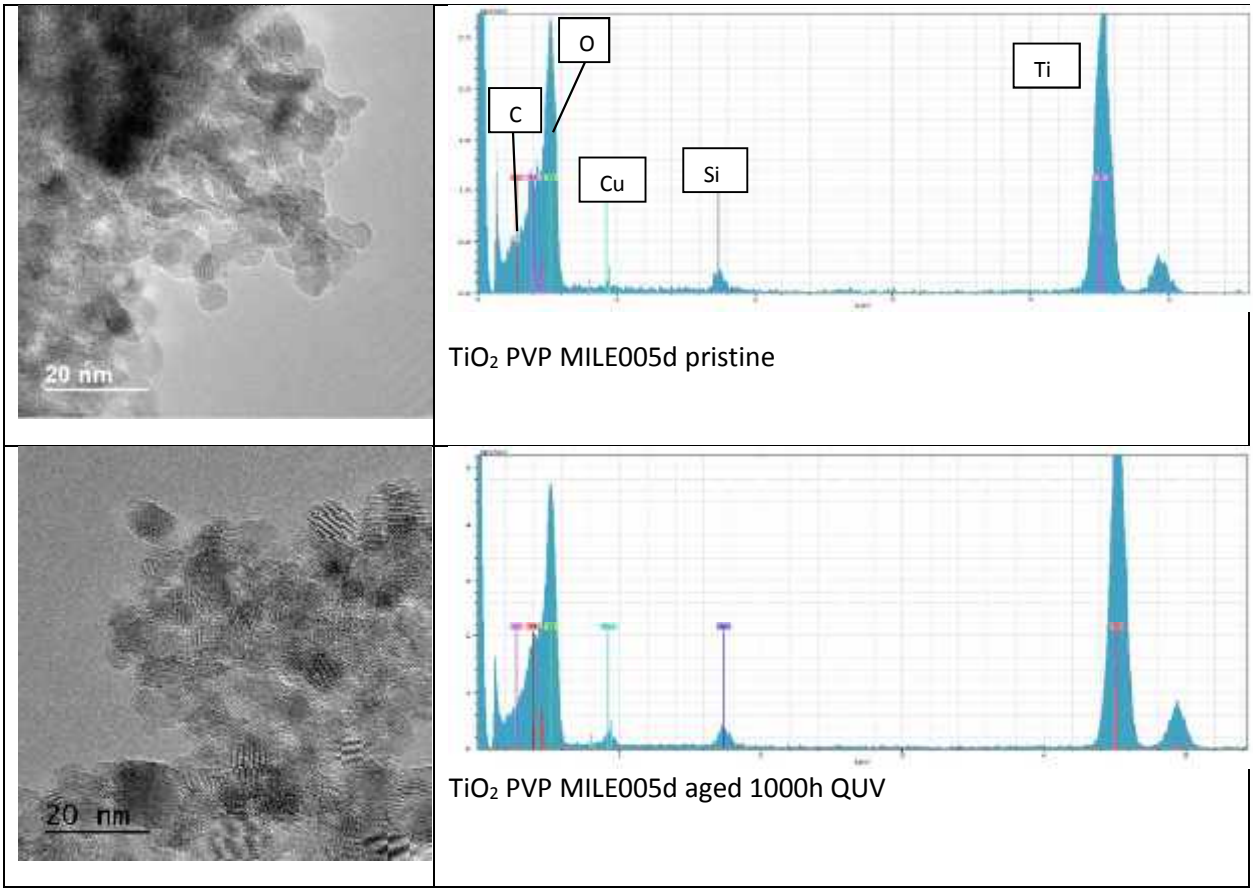

TiO_2 PVP MILE005d pristine

TiO_2 PVP MILE005d aged 1000h QUV

Figure B.1-3: TEM images and EDX spectra of pristine and 1000h QUV-aged TiO2 PVP MILE005d NPs.

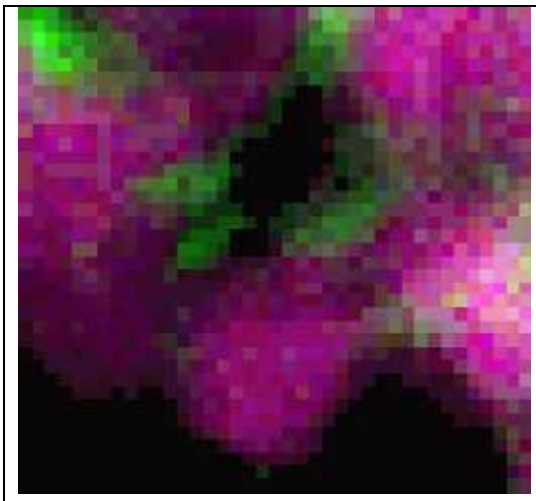

(a) TiO_2 PVP MILE005d pristine

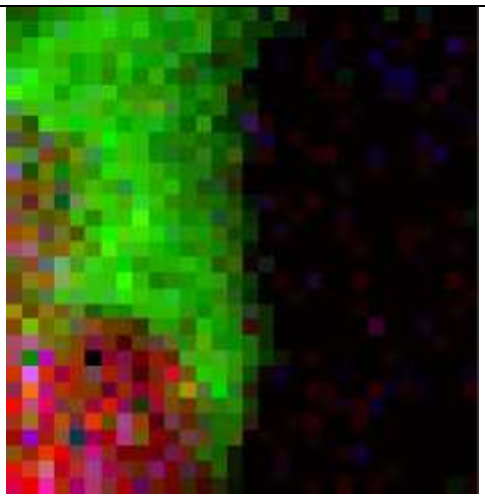

(b) TiO_2 PVP MILE005d aged 1000h QUV

Figure B.1-4: EELS maps of TiO_2 PVP MILE005d pristine (a) and aged 1000h in the QUV (b). Ti in red, C in green, and O in blue.

The same conclusions as those in § A.1 can be given here: no visible alteration of the morphology of the grains neither significant modification of the EDX spectrum is observed. EELS analyses were undertaken to try to bring out any possible change in the polymeric coating of these NPs. An example is given in Figure B.1.3-4. Again, it was not possible to conclude as to the possible degradation of the PVP since some carbon phase is still visible around the TiO_2 core of the particles even after 1000h of QUV aging.

BET (UoB)

The results of BET analyses are given in Table B.1-1.

Table B.1-1: BET characterization of aged TiO_2 NPs

Number of times analysed (n>2)		
	S_{BET} (m^2/g)	V_P (cm^3/g)
TiO2 MILE005d		
Measurement 1	208.86	47.9878
Measurement 2	204.98	47.0948
Mean ± Std. Dev.	(206 ± 2)	(47.5 ± 0.6)

B.2 CeO_2 - Aging with phosphate (UoB)

B.2.1 Summary of the aging experiments

The particles (in solution, 3.1% in concentration) were added to a solution of 5mM of KH_2PO_4, citric acid and ascorbic acid, 5 times the concentration as the one used by Zhang et al. (2012), and the pH was adjusted to 5.5. The final concentration of CeO_2 NPs in the suspensions was 6200 mg L^{-1}. After 21 days of static incubation, the 6200 mg L^{-1} suspensions were dried out in a 50 ^oC oven for three days and used to measure XRD. CeO_2 NPs suspensions of 496 mg L^{-1} in concentration were used for UV-vis and zeta potential, at 7 and 21 days, and for TEM observation, after 21 days.

B.2.2 Characterization methods

Size (Dh) and zeta potential (ZP) were acquired using DLS with a Zetasizer 5000 (Malvern). Size measurements were done at an angle of 173° (backscatter) with reference to the 633nm-laser beam. The pH of the suspension was 7 for the pristine suspension and 5.5 for the aged one.

TEM observations were performed with a JEOL JEM2100F apparatus. Samples were prepared by partially drying a drop of the particle solution on a cumesh400 holey carbon film (Agar scientific) at room temperature. The grid was washed thoroughly with UHP water and re-dried.

UV/Vis spectra were acquired using a 6800 Jenway double beam UV-Vis spectrophotometer.

B.2.3 Results

DLS

The results obtained for Dh and ZP of the pristine and phosphate-aged CeO_2 PROM NPs are presented in Table B.2-1.

Table B.2-1: DLS characteristics of pristine and aged CeO_2 PROM MNMs.(Std dev).

	Dh (nm)	**PDI**	**ZP (mV)**
CeO_2 PROM - pristine	172 (2)	0.272 (0.009)	50.3 (0.7)
CeO_2 PROM - aged	Too polydisperse	Close to 1	55.7 (0.6)

TEM

Figure B.2-1 illustrates the change in morphology of CeO_2 NPs with phosphate.

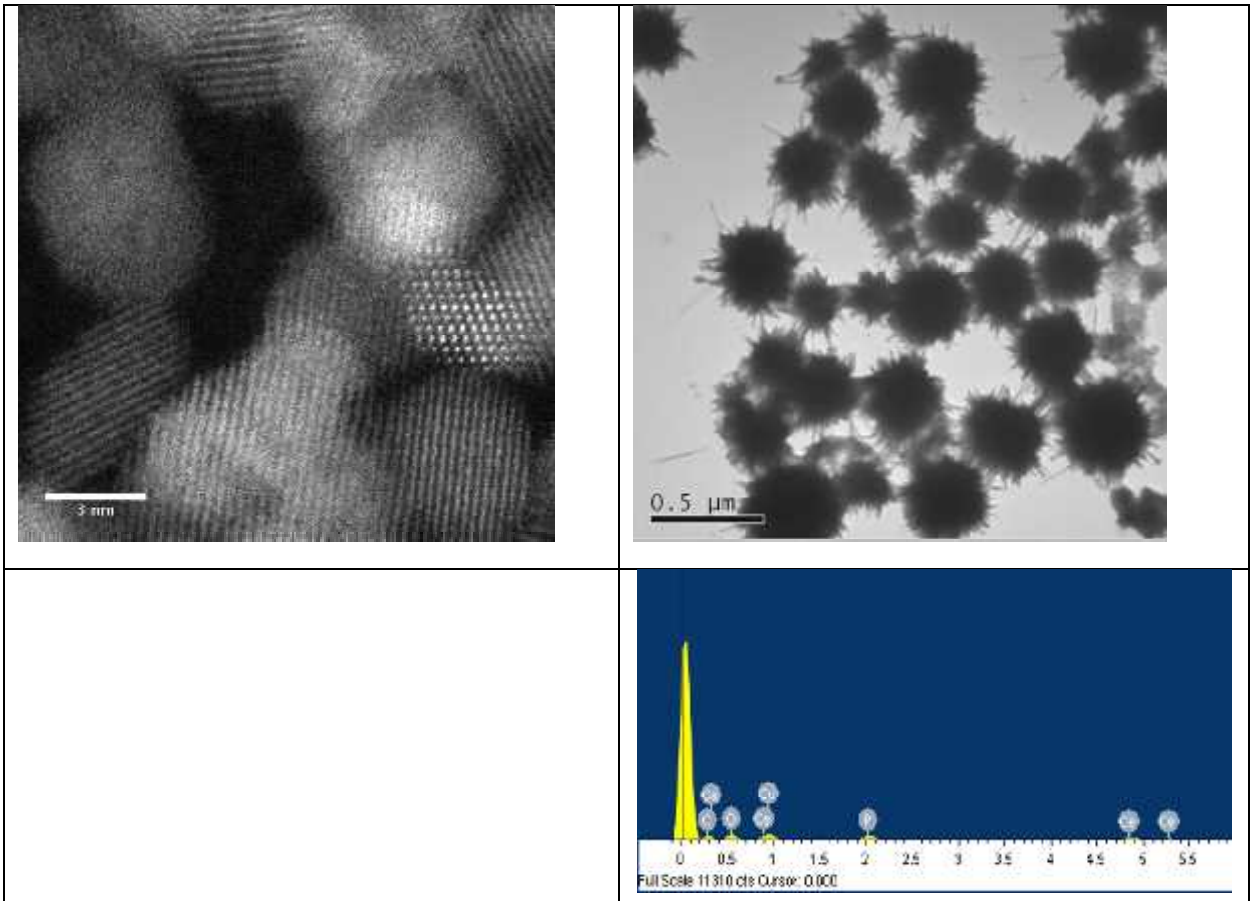

a b

Figure B.2-1: TEM imaging of (a): pristine CeO_2 PROM and (b): phosphate-aged CeO_2 PROM

The average diameter derived from TEM analyses was D = 4.7 nm (n = 140, σ = 1.4 nm) for the pristine population. Upon phosphatization, the "sea urchin"structures are observed, showing the formation of $CePO_4$.

UV/Vis

The UV/Vis spectra of the pristine and aged CeO_2 PROM NPs are displayed in Figure B.2-2.

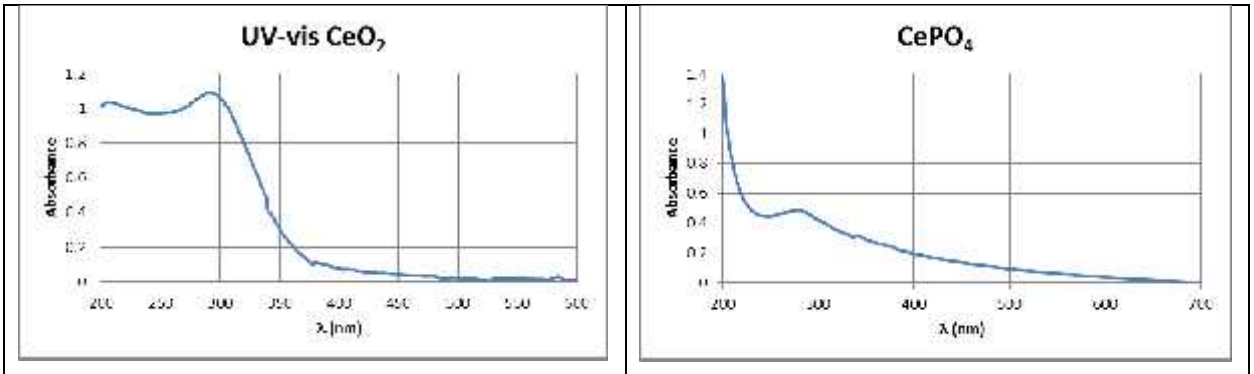

a b

Figure B.2-2: UV/Vis spectra of (a): pristine CeO_2 PROM and (b): phosphate-aged CeO_2 PROM.

An obvious change can be observed in the UV-vis signal, in the case of $CePO_4$, the peak observed at around 270nm corresponds to Ce^{3+} absorption. The UV-vis spectrum for CeO_2 shows to peaks that correspond to Ce^{3+} and Ce^{4+}.

B.3 ZnO - Aging with UV/Temperature (CEA)

B.3.1 Summary of the aging experiments

The commercial NPs were received as powder and dispersed either in UP water (ZnO NM110) or in ethanol (ZnO NM111, hydrophobic) and dried in a thermal chamber prior to the aging procedure in the QUV for 42 days. (see D3.2).

B.3.2 Characterization methods

Size (Dh) and zeta potential (ZP) were acquired using the same instrument and protocol as those presented in § A.1.

TEM observations (carried out by UoB) were performed with a JEOL JEM2100F apparatus. Samples were prepared by partially drying a drop of the particle solution on a cumesh400 holey carbon film (Agar scientific) at room temperature. The grid was washed thoroughly with UHP water and re-dried.

BET characterization (carried out by UoB) was performed with a SA3100 Surface area analyzer. The degassing temperature was set at 120 °C for 180 min.

B.3.3 Results

Remark: In the results given below, all concentrations refer to the metal content of the considered suspension (i.e. Zn for ZnO NPs).

Size and ZP by DLS

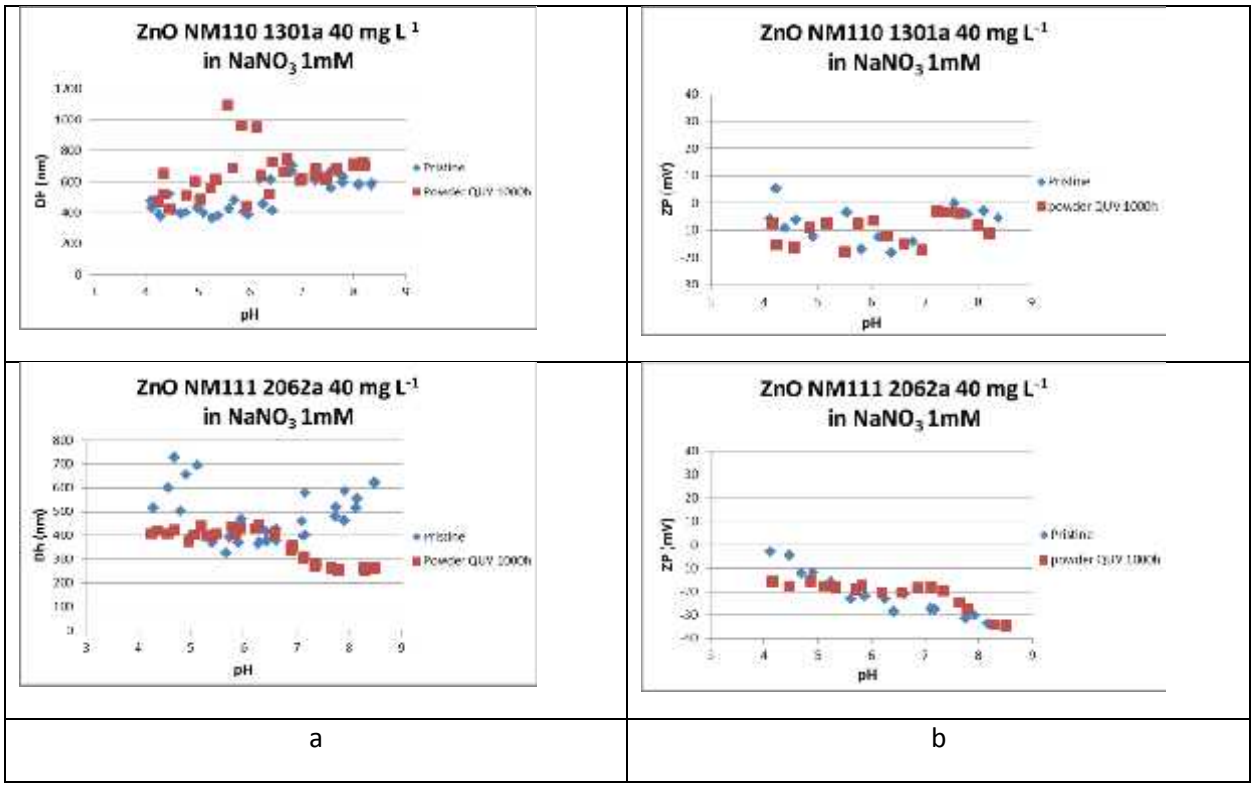

Figure B.3-1: Evolution of Dh (a) and ZP (b) as a function of pH for pristine and aged ZnO NPs.

It can be inferred from the titration curves in Figure B.3-1 that the ZnO suspensions are most aggregated in the whole pH range (4 to 9) even if the zeta potential remains negative whatever the pH in the investigated range. It can be noted that the values below pH 5 may not have much meaning since dissolution is likely to occur in a significant manner for these NPs in acidic media.

Some relevant parameters deduced from the experiments conducted above are given in Table B.3-1.

Table B.3-1: Mean ZP, Dh and PDI of ZnO NPs. All values are measured at pH 7 or higher. (Std dev).

ZnO NPs	ZP (mV)	Dh, mean (nm)	PDI
ZnO NM110 pristine Batch 1301a	-3.2 (2.0)	606 (37)	0.41
ZnO NM110 aged QUV 1000h Batch 1301a	-5.8 (3.6)	675 (43)	0.53
ZnO NM111 pristine Batch 2062a	-27.6 (0.2)	459 (84)	0.377
ZnO NM111 aged QUV 1000h Batch 2062a	-18.8 (0.8)	355 (24)	0.320

The values of the hydrodynamic diameter are larger than those obtained previously (Charanjeet et al., 2014): Dh = 275 nm (PDI = 0.145) for ZnO NM110 and Dh = 253 nm (PDI = 0.401) for ZnO NM111. TEM observations showed that particles sizes are between 10 and 450 nm, which may explain the difference

of data, together with the sample preparation (concentration and US process). Given the uncertainty on the data, one cannot conclude to a significant alteration of the particles during the aging process by using DLS characterization.

TEM (UoB)

Images of the aged ZnO NPs are provided in Figure B.3-2

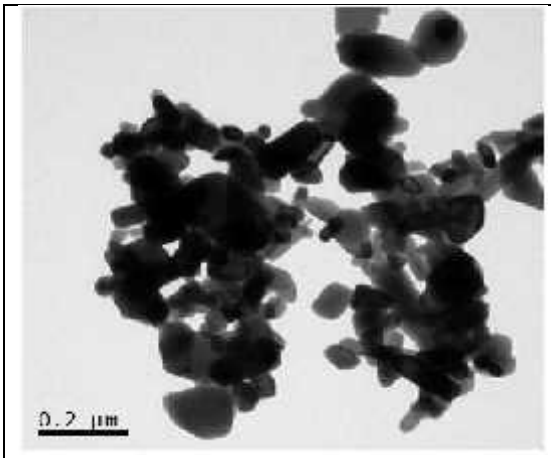

ZnO NM110 pristine

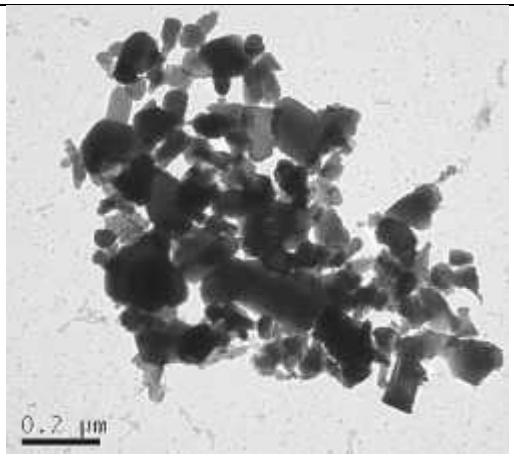

ZnO NM110 Aged

ZnO NM111 pristine

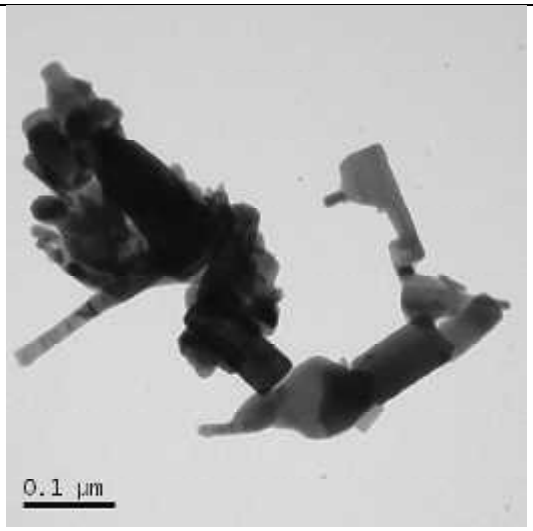

ZnO NM111 aged

a

b

Figure B.3-2: TEM images of ZnO NPs. a: pristine and b: 1000h-QUV-aged.

There is no evidence of morphology changes between the pristine and the aged NPs for both ZnO NM110 and ZnO NM111.

BET (UoB)

The results of BET analyses are given in Table B.3-2.

Table B.3-2: BET characterization of aged ZnO NPs

Number of times analysed (n>2)	Pristine particles		Aged particles	
	S_{BET} (m^2/g)	V_P (cm^3/g)	S_{BET} (m^2/g)	V_P (cm^3/g)
ZnO NM110				
Measurement 1	12.189	2.8004	12.423	2.8524
Measurement 2	12.708	2.9198	12.083	3.0034
Mean ± Std. Dev.	(12.44 ± 0.37)	(2.86 ± 0.08)	(12.3 ± 0.3)	(2.9 ± 0.1)
ZnO NM111				
Measurement 1	15.050	3.4578	14.543	4.2605
Measurement 2	14.970	3.4394	14.452	3.8204
Mean ± Std. Dev.	(15.01 ± 0.06)	(3.45 ± 0.01)	(14.50 ± 0.06)	(4.0 ± 0.3)

The specific surface area and the pore volume are quite similar in the case of ZnO NM110. In the case of hydrophobic triethoxycaprylysilane-capped ZnO NM111, the specific surface area tends to decrease while the pore volume increases slightly, showing that the coating may have been modified (degraded?) during the UV aging.

B.4 Ag NPs - Aging with sulfide (EMPA)

B.4.1 Summary of the aging experiments

Ag NPs (as a suspension in NM300) were combined with Na_2S at an approximate 2:1 molar ratio of S to Ag in light blocking polypropylene bottles without adjusting the pH. The bottle was placed in a fume hood, to capture hydrogen sulfide gas, throughout the length of the aging procedure. To provide sufficient dissolved oxygen (DO) air was bubbled through the solution at ambient temperatures using a plastic tube connected to the in-house air ducts commonly used for experimental work.

After a minimum of 48 hours reaction time, the particles were washed once with 18 mega-ohm DI water via centrifugation and re-suspended in nanopure water at a neutral pH until further analysis (TEM, EDX) were performed. After confirmation of particle transformation to Ag/S, the particles were shipped to the University of Birmingham for further distribution to the NanoMILE partners.

B.4.2 Characterization methods

The sulfidized Ag NPs were characterized by TEM/EDX. Nanomaterials were drop deposited onto carbon coated Cu TEM grids. All samples used for microscopic analysis were processed within one week of preparation. Particle images were obtained *via* scanning transmission electron microscopy (STEM) combined with EDX for element detection using a JEOL 2200FS TEM/STEM operated at 200 kV. The nominal spot size of the STEM probe was 0.7 nm using a beam convergence angle of 10.8 mrad. High-angle annular dark-field STEM micrographs were recorded using an inner detector angle of 100 mrad, while the bright-field STEM images were recorded with a detector angle of approximately 15 mrad. EDX

spectra of individual particles were recorded either by positioning the electron probe on a selected particle or by scanning the electron probe on a small frame centered on the particle.

B.4.3 Results

A series of 7 TEM images (light field and dark field) with accompanying EDX analysis was completed to get a representative characterization of Ag NP sulfidation. A selection of these images is provided in Figures B.4.1 – B.4.3.

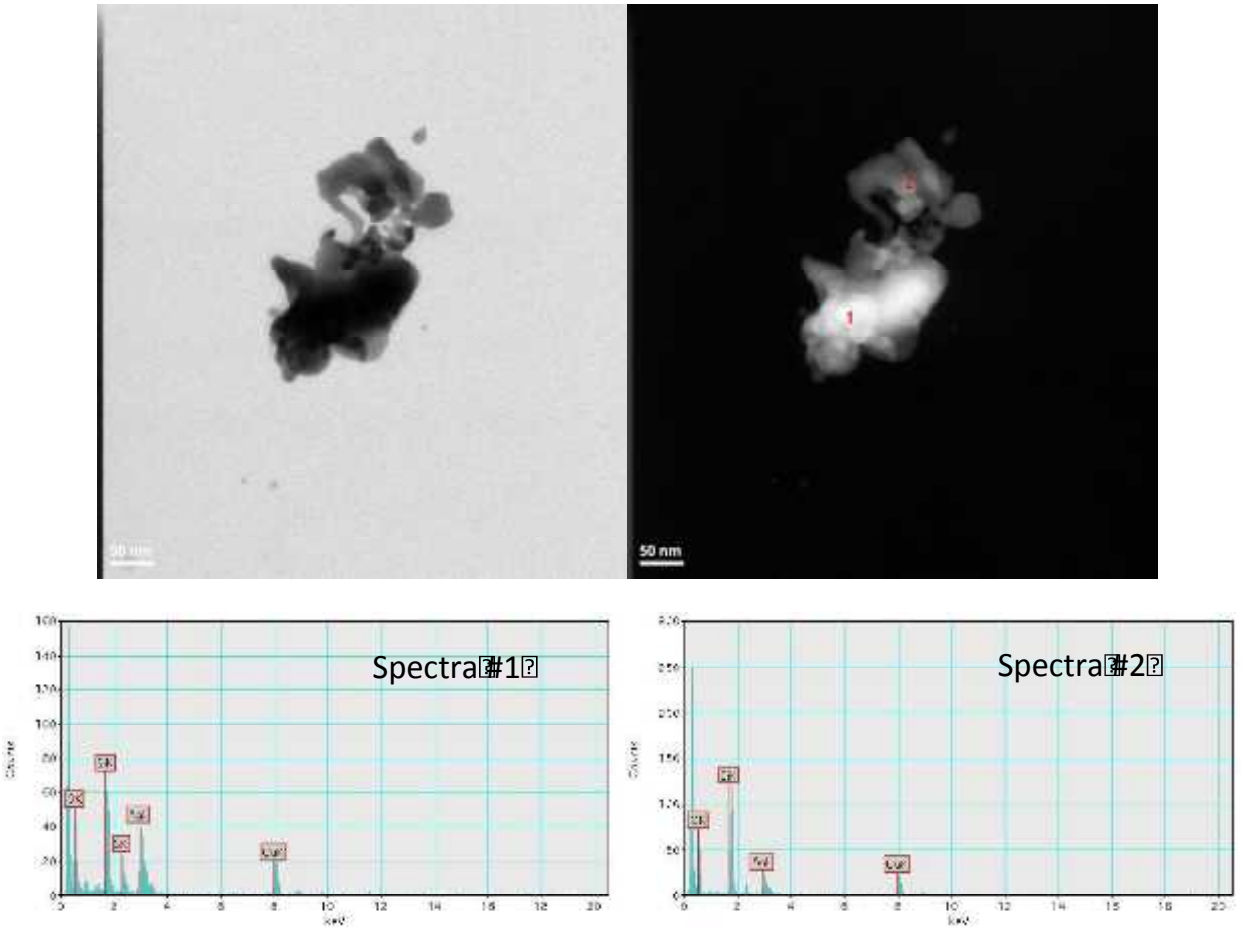

Figure B.4-1: TEM/EDX measurements confirming Ag NPs have been sulfidized.

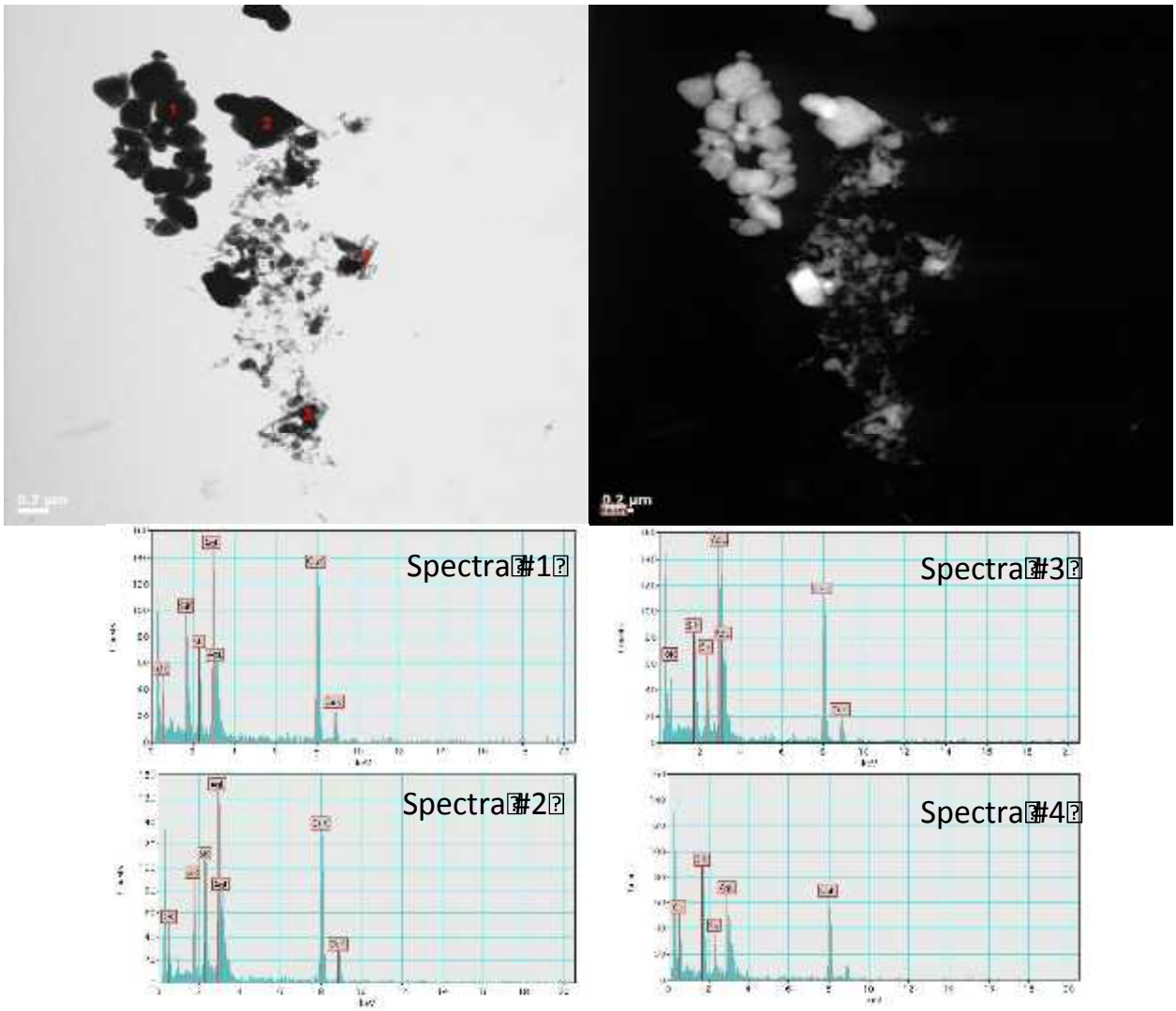

Figure B.4-2: TEM/EDX measurements confirming Ag NPs have been sulfidized.

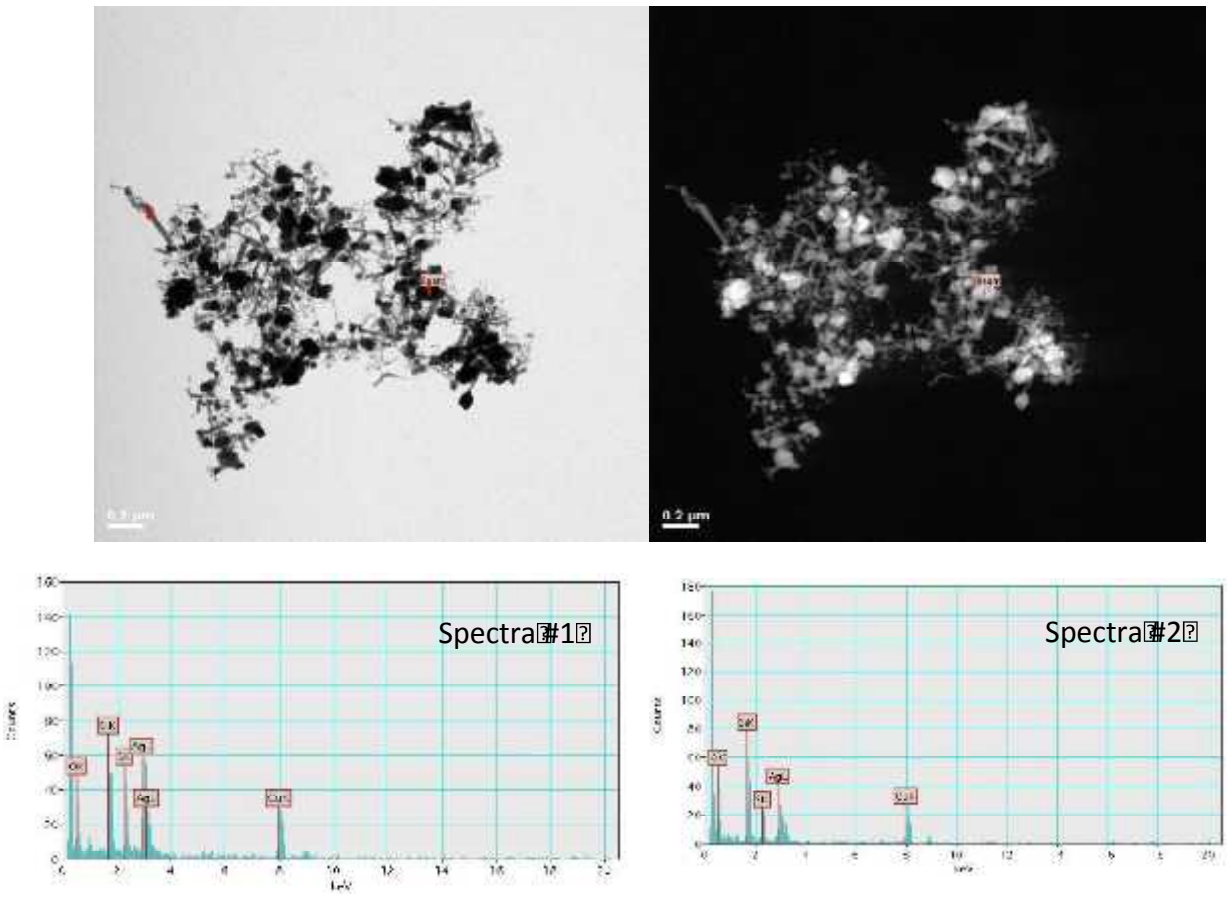

Figure B.4-3: TEM/EDX measurements confirming Ag NPs have been sulfidized.

Conclusions

Characterization of the MNMs from the NanoMILE library

Aging experiments reported herein have shown that the sole exposure to UV/visible light, even in extreme conditions, is not efficient in altering the dry (powder) form of the NPs tested (i.e. TiO_2, CeO_2 and ZnO). The investigations performed did not allow to conclude to a protective effect of the various coatings nor to their degradation by the UV-light exposure. However, it is most probable that, even if not evidenced here, polymer coatings do suffer from chain-breaking and no longer play their initial role, but the metal-oxides were already stable enough not to be affected by the aging protocole.

The most significant morphological and chemical changes were obtained when the MNMs are in colloidal form and come in contact with chemical reagents/chelating agents. Severe appearance changes were thus obtained with phosphate-exposed CeO_2 nano-suspensions with newly-formed sea-urchin structures. Likewise, spherical Ag NPs were modified into spider web-like structures under sulfidation in solution. These Ag nano-suspensions were altered differently when exposed to sunshine-enhanced irradiation in suspension to yield nanoprisms of triangular shape. The extent to which these transformations occur depend on the NP itself (size, capping agent) and physico-chemical parameters such as pH, oxidative agents and temperature. Some may play a protecting role (like citrate for Ag NPs, to some extent compared with PEG or fulvic acid for ceria) while others increase the rate of conversion/dissolution of the NPs (like oxidizers or temperature).

The wide variety of MNMs evolutions described in this report confirms the notion that each form of an MNM (coating, chemical identity, mineralogical form, synthesis methods) in a specific environment (medium, physical and chemical conditions) needs to be evaluated separately for its potential transformations. The different fates of MNMs during relevant processes during their life-cycle are evidence for a necessary grouping strategy in risk assessment that goes beyond the material identity.

Characterization of the MNMs from Milestone 6 (delivered to WP 4-8) Part B:

Complete phosphatization of ceria and sulfidation of Ag-MNM under our aging parameters were achieved, but the chemical composition was not the only physical parameter to be altered during this transformation process. For instance, while the pristine Ag MNMs were generally monodisperse, free particles suspended in solution, the particles significantly agglomerated to form a spider web structure after aging. This may have been due to a few factors, including building sulfide bridges and/or the removal of surfactants and capping agents during the washing process to remove excess sulfidizing agents. Very vigorous sonication was needed to re-release particles to their primary particle size. This makes it clear that the exposure to organisms and fate of these particles, if they remained agglomerated during subsequent exposure tests in the other workpackages, would dose a very different type of material into the system. Under natural conditions, where Ag MNMs are expected to form Ag/S complexes, this extreme aggregation behavior may be avoided since the particles would undergo sulfidation at a more dilute concentration and homo-aggregation would be unlikely to occur. Therefore, when comparing/contrasting the effects of pristine to altered MNM produced under these conditions, it may not necessarily be the chemical transformations alone which are responsible for different biological or ecological effects but also the physical structure may play a role.

Contrary to the chemically (and physically)-modified MNMs that will probably show related modified biological/ecological effects, the mostly unchanged UV-aged MNMs are not expected to behave differently from their pristine forms regarding possible toxicological effects.

References

Appel, C., Ma, L.Q., Rhue, R.D., Kennelley, E., 2003. Point of zero charge determination in soils and minerals via traditional methods and detection of electroacoustic mobility. Geoderma 113, 77-93.

Blok, L., de Bruyn, P.L., 1970. The ionic double layer at the ZnO/solution interface. I. The experimental point of zero charge. J. Colloid Interfac. Sci. 32, 518-526.

Buettner, K.M., Rinciog, C.I., Mylon, S.E., 2010. Aggregation kinetics of cerium oxide nanoparticles in monovalent and divalent electrolytes. Colloids Surf. Physicochem. Eng. Asp. 366, 74–79.

Charanjeet, S., Friedrichs, S., Carlander, D., Levin, M., Jensen, K.A., Goenaga Infante, H., Rasmussen, K., Gibson, N., Ceccone, G., 2014. JRC Repository: NM-Series of Representative Manufactured Nanomaterials Cerium Dioxide, NM-211, NM-212, NM-213. Characterisation and test item preparation. JRC89825, EUR 26649 EN.

Ershov, B. G., Henglein, A., 1998. Reduction of Ag+ on polyacrylate chains in aqueous solution. The J. Phys. Chem. B 102(52), 10663-10666.

Ershov, B. G., Henglein, A., 1998(b). Time-resolved investigation of early processes in the reduction of Ag+ on polyacrylate in aqueous solution. J. Phys. Chem. B 102(52), 10667-10671.

Falletta, E., Bonini, M., Fratini, E., Lo Nostro, A., Pesavento, G., Becheri, A., Lo Nostro, P., Canton, P., Baglioni, P., 2008. Clusters of poly (acrylates) and silver nanoparticles: structure and applications for antimicrobial fabrics. J. Phys. Chem. C 112(31), 11758-11766.

Furtado, L. M., Hoque, M. E., Mitrano, D. F., Ranville, J. F., Cheever, B., Frost, P. C., Xenopoulos, M. A., Hintelmann, H., Metcalfe, C. D., 2014. The persistence and transformation of silver nanoparticles in littoral lake mesocosms monitored using various analytical techniques. Environ. Chem. 11(4), 419-430.

Geranio, L., Heuberger, M., Nowack, B., 2009. The Behavior of Silver Nanotextiles during Washing. Environ. Sci. Technol. 43(21), 8113-8118.

Gregory, J., 2005. Particles in water: properties and processes. CRC Press.

Henglein, A., Mulvaney, P., Linnert, T., 1991. Chemistry of silver aggregates in aqueous solution: non-metallic oligomers and metallic particles. Electrochim. Acta 36, 1743-1745.

Ilić, V., Šaponjić, Z., Vodnik, V., Mihailović, D., Jovančić, P., Nedeljković, J., Radetić, M., 2009. The study of coloration and antibacterial efficiency of corona activated dyed polyamide and polyester fabrics loaded with Ag nanoparticles. Fibers and Polymers 10(5), 650-656.

Jiang, X.C., Chen, C,Y, Chen, W.M., Yu, A.B., 2010. Role of citric acid in the formation of silver nanoplates through a synergistic reduction approach. Langmuir 26, 4400-4408.

Jin, R., Cao, Y., Mirkin, C.A., Kelly, K.L., Schatz, G.C., Zheng J.G., 2001. Photoinduced conversion of silver nanospheres to nanoprisms. Science 294, 1901-1903.

Jin, R., Cao, Y.C., Hao, E., Métraux, G.S., Schatz, G.C., Mirkin, C.A, 2003. Controlling anisotropic nanoparticle growth through plasmon excitation. Nature 425, 487-490.

Jolivet, J.-P., Henry, M., Livage, J., 2000. Metal oxide chemistry and synthesis: from solution to solid state. Wiley-Blackwell.

Kapoor, S., 1998. Preparation, characterization, and surface modification of silver particles. Lagmuir 14, 1021-1025.

Klemenčič, D., Tomšič, B., Kovač, F., Žerjav, M., Simončič, A., Simončič, B., 2013. Antimicrobial wool, polyester and a wool/polyester blend created by silver particles embedded in a silica matrix. Colloids and Surfaces B: Biointerfaces 111, 517-522.

Laborda, F., Jimenez-Lamana, J., Bolea, E., Castillo, J. R., 2011. Selective identification, characterization and determination of dissolved silver (I) and silver nanoparticles based on single particle detection by inductively coupled plasma mass spectrometry. J. Anal. At. Spectrom. 26(7), 1362-1371.

Li, K., Chen, Y., 2012. Effect of natural organic matter on the aggregation kinetics of CeO2 nanoparticles in KCl and CaCl2 solutions: Measurements and modeling. J. Hazard. Mater. 209–210, 264–270.

Li, K., Zhang, W., Huang, Y., Chen, Y., 2011. Aggregation kinetics of CeO2 nanoparticles in KCl and CaCl2 solutions: measurements and modeling. J. Nanoparticle Res. 13, 6483–6491.

Li, X., Lenhart, J.J., Walker, H.W., 2010. Dissolution-accompanied aggregation kinetics of silver nanoparticles. Langmuir 26, 16690-16698.

Lombi, E., Donner, E., Scheckel, K. G., Sekine, R., Lorenz, C., Goetz, N. V., Nowack, B., 2014. Silver speciation and release in commercial antimicrobial textiles as influenced by washing. Chemosphere 111, 352-358.

Loosli, F., Le Coustumer, P., Stoll, S., 2015. Effect of electrolyte valency, alginate concentration and pH on engineered TiO2 nanoparticle stability in aqueous solution. Sci. Total Environ., Special Issue: Engineered nanoparticles in soils and waters 535, 28–34.

Lorenz, C., Windler, L., von Goetz, N., Lehmann, R., Schuppler, M., Hungerbühler, K., Heuberger, M., Nowack, B., 2012. Characterization of silver release from commercially available functional (nano) textiles. Chemosphere 89(7), 817-824.

Merrifield, R. C., Wang, Z. W., Palmer, R. E., Lead, J. R. 2013. Synthesis and Characterization of olyvinylpyrrolidone Coated Cerium Oxide Nanoparticles. Environ. Sci. Technol., 47**,** 12426-12433.

Mitrano, D. M., Lesher, E. K., Bednar, A. J., Monserud, J., Higgins, C. P., Ranville, J. F., 2012. Detection of nano-Ag using single particle inductively coupled plasma mass spectrometry. Environ. Toxicol. Chem. 31, 115-121.

Mitrano, D. M., Barber, A., Bednar, A., Westerhoff, P., Higgins, C., Ranville, J., 2012(b). Silver nanoparticle characterization using single particle ICP-MS (SP-ICP-MS) and asymmetrical flow field flow fractionation ICP-MS (AF4-ICP-MS). J. Anal. At. Spectrom. 27, 1131-1142.

Mitrano, D. M., Rimmele, E., Wichser, A., Erni, R., Height, M., Nowack, B., 2014. Presence of Nanoparticles in Wash Water from Conventional Silver and Nano-silver Textiles. ACS nano 8(7), 7208-7219.

Mitrano, D. M., Ranville, J., Bednar, A., Kazor, K., Hering, A. S., Higgins, C., 2014(b). Tracking dissolution of silver nanoparticles at environmentally relevant concentrations in laboratory, natural and processed waters using single particle ICP-MS (spICP-MS). Environ. Sci.: Nano 1(3), 248-259.

Mitrano, D. M., Arroyo Rojas Dasilva, Y., Nowack, B., 2015. Effect of Variations of Washing Solution Chemistry on Nanomaterial Physicochemical Changes in the Laundry Cycle. Environ. Sci. Technol. 49(16), 9665-9673.

Mohd Omar, F., Abdul Aziz, H., Stoll, S., 2014. Aggregation and disaggregation of ZnO nanoparticles: Influence of pH and adsorption of Suwannee River humic acid. Sci. Total Environ. 468–469, 195–201.

Montazer, M., Alimohammadi, F., Shamei, A., Rahimi, M. K., 2012. Durable antibacterial and cross-linking cotton with colloidal silver nanoparticles and butane tetracarboxylic acid without yellowing. Colloids and Surfaces B: Biointerfaces 89, 196-202.

Oriekhova, O., Stoll, S., 2016. Effects of pH and fulvic acids concentration on the stability of fulvic acids – cerium (IV) oxide nanoparticle complexes. Chemosphere 144, 131–137.

Parks, G.A., de Bruyn, P.L., 1962. The zero point of charge of oxides. J. Phys. Chem. 66, 967-973.

Ravel, B., Newville, M., 2005. ATHENA, ARTEMIS, HEPHAESTUS: Data analysis for X-ray absorption spectroscopy using IFEFIT. J. Synchrotron Rad. 12(4), 537-541.

Reinsch, B., Levard, C., Li, Z., Ma, R., Wise, A., Gregory, K., Brown Jr, G., Lowry, G.,2012. Sulfidation of silver nanoparticles decreases Escherichia coli growth inhibition. Environ. Sci. Technol. 46(13), 6992-7000.

Simončič, B., Klemenčič, D., 2015. Preparation and performance of silver as an antimicrobial agent for textiles: A review. Textile Res. J. , 0040517515586157.

Windler, L., Lorenz, C., von Goetz, N., Hungerbuhler, K., Amberg, M., Heuberger, M., Nowack, B., 2012. Release of Titanium Dioxide from Textiles during Washing. Environ. Sci. Technol. 46(15), 8181-8188.

Windler, L., Height, M., Nowack, B., 2013. Comparative evaluation of antimicrobials for textile applications. Environ. Int. 53, 62-73.

Zhang, X.N, Zhao, A.Z., 1997. Surface charge. In Yu, T.R. (Ed.),Chemistry of variable charge soils. Oxford University Press, 23-26.

Zhang, P.; Ma, Y.; Zhang, Z.; He, X.; Zhang, J.; Guo, Z.; Tai, R.; Zhao, Y.; Chai, Z., 2012. ACS Nano 6 (11), 9943-9950.